MECHANISMS OF BRANCHED ACTIN NETWORK FORMATION THROUGH COORDINATE ACTIVATION OF ARP2/3 COMPLEX

by

LUKE ANDREW HELGESON

A DISSERTATION

Presented to the Department of Biology
and the Graduate School of the University of Oregon
in partial fulfillment of the requirements
for the degree of
Doctor of Philosophy

December 2014

DISSERTATION APPROVAL PAGE

Student: Luke Andrew Helgeson

Title: Mechanisms of Branched Actin Network Formation through Coordinate Activation of Arp2/3 Complex

This dissertation has been accepted and approved in partial fulfillment of the requirements for the Doctor of Philosophy degree in the Department of Biology by:

Bruce Bowerman	Chairperson
Bradley Nolen	Advisor
Alice Barkan	Core Member
J. Andrew Berglund	Core Member
Kenneth Prehoda	Institutional Representative

and

J. Andrew Berglund	Dean of the Graduate School

Original approval signatures are on file with the University of Oregon Graduate School.

Degree awarded December 2014

© 2014 Luke Andrew Helgeson

DISSERTATION ABSTRACT

Luke Andrew Helgeson

Doctor of Philosophy

Department of Biology

December 2014

Title: Mechanisms of Branched Actin Network Formation through Coordinate Activation of Arp2/3 Complex

Fundamental cellular processes such as motility and endocytosis rely on the actin cytoskeleton to translate biochemical protein interactions into mechanical forces. Cells utilize an extensive collection of actin binding proteins to comprehensively regulate actin networks during these dynamic cell operations. Branched actin networks, which are geometrically and functionally disparate from linear networks, are required for numerous cellular actions. Actin-related protein 2/3 complex (Arp2/3 complex) nucleates branched actin filaments upon activation by regulatory proteins known as nucleation promoting factors (NPFs). Often, several biochemically distinct NPFs are required for the same cellular structure, leading us to hypothesize that multiple NPFs can coordinately activate Arp2/3 complex to regulate the nucleation, architecture and assembly of branched networks. We identified and dissected the mechanisms of two sets of NPFs which coordinately activate Arp2/3 complex. Overall, these findings provide a better understanding of how Arp2/3 complex is activated and how cells control branched actin networks.

In chapters II and III, we investigated the mechanism of synergistic activation of Arp2/3 complex by the NPFs cortactin and WASP family proteins. We found that cortactin accelerates the release of WASP family proteins from a branching intermediate, a previously unknown rate limiting step. Further dissection of the mechanism revealed that cortactin is specifically suited to displace WASP family proteins through a unique Arp2/3 complex binding region and target stalled branching intermediates with high affinity. Three different WASP family members were tested for their capacity to synergize with cortactin in Arp2/3 complex activation, establishing a list of cellular structures where cortactin-mediated synergistic activation is likely occurring.

In chapter IV, we investigated the ability of Dip1 and Wsp1 to coordinately activate Arp2/3 complex during branched network formation. We established that Dip1 activation of Arp2/3 complex results in the formation of linear filaments which can template Wsp1 mediated branching. Subsequent kinetic data and modeling revealed that Dip1 and Wsp1 likely increase the rate of network formation by simultaneously binding to and co-activating Arp2/3 complex. These findings suggest that, together, Dip1 and Wsp1 regulate the initiation and rate of branched network assembly.

This dissertation includes previously published and unpublished co-authored material and videos files.

CURRICULUM VITAE

NAME OF AUTHOR: Luke Andrew Helgeson

GRADUATE AND UNDERGRADUATE SCHOOLS ATTENDED:

University of Oregon, Eugene, OR
Iowa State University, Ames, IA

DEGREES AWARDED:

Doctor of Philosophy, Biology, 2014 University of Oregon
Bachelor of Science, Biochemistry, 2009, Iowa State University

AREAS OF SPECIAL INTEREST:

Biochemistry
Biophysics
Microscopy

PROFESSIONAL EXPERIENCE:

Graduate Teaching Assistant, Department of Biology, University of Oregon, Eugene, OR, 2009-2010

GRANTS, AWARDS, AND HONORS:

Pete von Hippel Scholar Award, Institute of Molecular Biology, Department of Biology, University of Oregon, Eugene, OR. 2014.

NIH Training Grant: Molecular Biology and Biophysics. Institute of Molecular Biology, Department of Biology, University of Oregon, Eugene, OR. 2010-2013

Robert Stupka Memorial Scholarship. Department of Biochemistry, Biophysics and Molecular Biology, Iowa State University, Ames, IA. 2009

Dexter Memorial Fund. Department of Biochemistry, Biophysics and Molecular Biology, Iowa State University, Ames, IA. 2005/2006.

Award for Competitive Excellence Scholarship. Iowa State University, Ames, IA. 2005-2009.

PUBLICATIONS:

Helgeson, Luke A, Julianna G Prendergast, Andrew R Wagner, Max Rodnick-Smith, and Brad J Nolen. 2014. “Interactions with Actin Monomers, Actin Filaments and Arp2/3 Complex Define the Roles of WASP Family Proteins and Cortactin in Coordinately Regulating Branched Actin Networks.” *The Journal of Biological Chemistry* 289 (42) (August 26): 28856–28869. doi:10.1074/jbc.M114.587527.

Helgeson, Luke A, and Brad J Nolen. 2013. “Mechanism of Synergistic Activation of Arp2/3 Complex by Cortactin and N-WASP.” *eLife* 2 (September 3): e00884. doi:10.7554/eLife.00884.

Hetrick, Byron, Min Suk Han, **Luke A Helgeson**, and Brad J Nolen. 2013. “Small Molecules CK-666 and CK-869 Inhibit Actin-Related Protein 2/3 Complex by Blocking an Activating Conformational Change.” *Chemistry & Biology* 20 (5) (April): 701–12. doi:10.1016/j.chembiol.2013.03.019.

Liu, Su-Ling, Jordan R May, **Luke A Helgeson**, and Brad J Nolen. 2013. “Insertions within the Actin Core of Actin-Related Protein 3 (Arp3) Modulate Branching Nucleation by Arp2/3 Complex.” *The Journal of Biological Chemistry* 288 (1) (January 4): 487–97. doi:10.1074/jbc.M112.406744.

Leung Daisy W, Dominika Borek, Mina Farahbakhsh, Parameshwaran Ramanan, Jay C Nix, Tianjiao Wang, Kathleen C Prins, Zbyszek Otwinowski, Richard B Honzatko, **Luke A Helgeson**, Christopher F Basler, Gaya K Amarasinghe. 2010. “Crystallization and preliminary X-ray analysis of Ebola VP35 interferon inhibitory domain mutant proteins.” *Acta.Crystallogr. Sect. F Struct. Biol.Cryst.Commun.* 66(6): 689-92.

Leung Daisy W, Kathleen C Prins, Dominika M Borek, Mina Farahbakhsh, JoAnn M Tufariello, Parameshwaran Ramanan, Jay C Nix, **Luke A Helgeson**, Zbyszek Otwinowski, Richard B Honzatko, Christopher F Basler, Gaya K Amarasinghe. 2010. “Structural basis for dsRNA recognition and interferon antagonism by Ebola VP35”. *Nature Structural & Molecular Biology*. 17(2): 165-72.

ACKNOWLEDGMENTS

First and foremost, I would like to express my sincere gratitude to my mentor and thesis advisor, Dr. Brad Nolen. Under Brad's guidance, I developed a strong set of scientific skills which will be fundamental to my success for years to come. I am thankful to all past and present members of the Nolen lab; without them I would not have been able to accomplish my goals. I would especially like to thank Dr. Byron Hetrick for his mentoring and Dr. Su-Ling Liu who was always helpful and full of knowledge. I would like to thank my dissertation advisor committee for their assistance and words of encouragement throughout the years. Additionally, I would like to thank the University of Oregon, Institute of Molecular Biology community for their various means of support. I am thankful to my undergraduate mentor, Dr. Gaya Amarasinghe, for helping me build a solid foundation for performing rigorous scientific research. Successful science requires a clear and refreshed mind. I am especially grateful for my friends who have allowed me to maintain a refreshed mind and have made my graduate school experience memorable. Specifically, I am forever grateful to those friends who ventured into the wilderness with me to experience and explore all the beauty nature has to offer. I would especially like to thank Dr. Alesia McKeown for her invaluable companionship throughout this challenging endeavor. Alesia's love, support and humor constantly sustains me and brings joy to my life. Last but not least, I am forever thankful to my family for their love throughout the years. My parents, Benny and Janice, and sister, Beth, have been constant sources of inspiration, knowledge and encouragement. Without their love and support, I would not be where I am today.

I dedicate this work to my family, past and present.
Thank you for everything.

TABLE OF CONTENTS

Chapter Page

I. INTRODUCTION 1

II. MECHANISM OF SYNERGISTIC ACTIVATION OF ARP2/3 COMPLEX BY CORTACTIN AND N-WASP 15

Introduction 15

Results 19

Discussion 43

Material and Methods 49

Bridge to Chapter III 58

III. INTERACTIONS WITH ACTIN MONOMERS, ACTIN FILAMENTS, AND ARP2/3 COMPLEX DEFINE THE ROLES OF WASP FAMILY PROTEINS AND CORTACTIN IN COORDINATELY REGULATING BRANCHED ACTIN NETWORKS 59

Introduction 59

Results 65

Discussion 84

Experimental Procedures 92

Bridge to Chapter IV 97

IV. DIP1 AND WSP1 CO-ACTIVATE ARP2/3 COMPLEX TO INITATE BRANCHED NETWORK ASSEMBLY 98

Introduction 98

Chapter Page

Results 103

Discussion 118

Materials and Methods 124

Bridge to Chapter V 127

V. DISCUSSION 128

APPENDICES 133

A. SUPPLEMENTAL FIGURES AND VIDEO LEGENDS FOR CHAPTER II 133

B. VIDEO LEGENDS FOR CHAPTER III 138

C. VIDEO LEGENDS FOR CHAPTER IV 139

REFERENCES CITED 140

SUPPLEMENTAL VIDEO FILES

LIST OF FIGURES

Figure Page

CHAPTER I

1. Mechanism of Branched Filament Nucleation by Arp2/3 Complex 5
2. Overview of Known NPFs and Their Mechanisms of Arp2/3 Complex Activation.. 8

CHAPTER II

1. Schematic Overview of Branching Nucleation and the Proteins Involved........... 17
2. Cortactin Synergizes with GST-N-WASP-VCA 20
3. Actin Filament Recruitment Cannot Explain Cortactin-mediated Synergy 22
4. The Oligomerization State of VCA Is an Important Determinant of Synergy 29
5. VCA Affinity for the Nascent Branch Junction Is an Important Determinant of Synergy 31
6. Cortactin Binds Statically to Actin Filaments 34
7. Cortactin Directly Targets Branch Junctions with a Fast On-rate 35
8. Cortactin Remains at the Branch Junction during Daughter Filament Elongation 38
9. Mathematical Model of the Obligatory Displacement Mechanism of Cortactin-mediated Synergy 41

CHAPTER III

1. Overview of Activation of Arp2/3 Complex by Cortactin and N-WASP 61
2. Cortactin Is a Weak NPF Because It Cannot Recruit Actin Monomers to Arp2/3 Complex.. 66

Figure Page

3. Cortactin Bundles Branched Actin Filaments to Form Actin Networks Distinct from N-WASP 67
4. Cortactin Monomers Bundle Parallel and Antiparallel Actin Filaments 70
5. Cortactin NtA Has Unique Biochemical Properties Compared to the CA Region of WASP 74
6. All Regions of the Cortactin NtA Contribute to Synergy 76
7. Cortactin Synergistically Activates Arp2/3 Complex to Different Extents with WAVE, WASP and N-WASP 81

CHAPTER IV

1. Dip1 Activates Arp2/3 Complex and Remains Bound at the Pointed End of the Nucleated Filament 104
2. Dip1 Generated Filaments Serve as Templates for Branching 108
3. Dip1 Bound Arp2/3 Complex Weakly Interacts with Two Actin Monomers Prior to Nucleation 111
4. Dip1 and Wsp1 Compete for Arp2/3 Complex Activation 114
5. Dip1 and Wsp1 Co-activate Arp2/3 Complex 116

LIST OF TABLES

Table Page

CHAPTER II

1. Mathematical Modeling Parameters 25

2. Mathematical Modeling Reaction Sets 27

CHAPTER I

INTRODUCTION

Branched Actin Networks Are Essential for Cellular Function

Cell survival is dependent upon its ability to interact with its environment, primarily, through numerous membrane-mediated processes such as: motility, nutrient uptake through endocytosis, surface adhesion and intracellular vesicle movement. Critical to the completion of these processes is the cell's ability to dynamically manipulate the cellular membrane. Specific and sufficient control over membrane structure is a complex problem that requires the coordinated effort of many different types of proteins. Actin is a cytoskeletal protein that dynamically forms dense networks of protein filaments that are capable of scaffolding reactions, tracking motor proteins and generating mechanical forces sufficient to deform membranes (Pollard and Cooper 2009; Blanchoin et al. 2014). The mechanochemical capability of actin is necessary for the precise function of many vital cellular processes.

Actin is unique because it self assembles into protein polymers called filaments. In the cell there are two populations of actin: monomeric actin and filamentous actin (Pollard and Cooper 2009). *De novo* formation of actin filaments proceeds through a process known as nucleation. During nucleation, actin monomers will interact with one another to form various oligomeric species, however these intermediates are very unstable and often rapidly fall apart (Sept and McCammon 2001). Stochastically, one of these actin oligomers can achieve a favorable thermodynamic state whereby a stable actin nucleus is formed which then elongates by addition of monomers to its ends. Actin filaments are polar and elongation occurs much more rapidly at the barbed end of the filament as opposed to the pointed end (Pollard 1986). Through the process of nucleation multiple actin filaments form and grow into a dense actin network; it is this collective network that performs the desired biological functions.

Generation of actin networks is controlled at the step of nucleation which makes it one of the most regulated aspects of actin structures. To overcome the slow and stochastic rate of actin nucleation, cells utilize special actin interacting proteins known as actin nucleators (Campellone and Welch 2010). Nucleators typically stabilize actin intermediates, thereby driving the reaction towards nucleus formation and subsequent filament elongation. Actin nucleators are often themselves highly regulated through protein activators, post-translational modifications and cellular signaling cascades.

In addition to regulation of network formation; different actin filament interacting proteins can govern the functional architecture of actin networks. Actin filaments can be bundled or crosslinked to form thick linear or meshwork like networks, amongst other structures (Pollard and Cooper 2009). Interestingly, cellular processes such as motility, vesicle movement and endocytosis require the formation of architecturally distinct networks which are composed of branched actin filaments (Svitkina and Borisy 1999; Welch, Iwamatsu, and Mitchison 1997; Rodal et al. 2005). Repeated nucleation of branched actin filaments produces densely branched networks that are highly dendritic, with branches forming from branches. The unique branching geometry of these filamentous networks reinforces a rigid structure that pushes against the membrane or object to generate the necessary functional forces (Svitkina and Borisy 1999; Bernheim-

Groswasser et al. 2002; Blanchoin et al. 2014). Disruption of branched network structure severely affects its mechanical function (Bernheim-Groswasser et al. 2002; Haviv et al. 2006). In order to fully grasp the biology of branched actin based processes critical for cell survival, it is imperative to comprehensively understand branched actin networks and the mechanisms by which they are regulated.

The actin related protein 2/3 complex (Arp2/3 complex) is the only known actin nucleator to nucleate branched actin filaments (Mullins, Heuser, and Pollard 1998; Blanchoin et al. 2000). Arp2/3 complex is a seven subunit protein complex composed of two large subunits, Arp2 and Arp3, which are structurally related to actin monomers, and five smaller non-actin related subunits: ARPC 1-5 (Robinson et al. 2001). Arp2/3 complex is inherently inactive and is activated by a class of proteins known as a nucleation promoting factors (NPFs) (Goley and Welch 2006). Upon activation, the Arp2 and Arp3 subunits rearrange into a more actin filament like conformation within the complex (Rouiller et al. 2008; Hetrick et al. 2013). Through this mechanism of structural mimicry, Arp2 and Arp3 are hypothesized to compose the pointed end of the newly nucleated filament.

Nucleation of branched filaments requires the coordinate effort of multiple proteins (Figure 1). Canonical branched filament nucleation begins with activation of Arp2/3 complex by an NPF (Higgs, Blanchoin, and Pollard 1999). The active complex, still bound by the NPF, binds to the side of a pre-existing filament to form a nascent branch junction (Machesky et al. 1999; Smith, Padrick, et al. 2013). From this nascent branch junction, a new filament is nucleated and elongates away from the pre-existing filament at a ~70° angle (Volkmann et al. 2001). Recent kinetic measurements revealed that the NPF-Arp2/3 complex binds to filaments very dynamically with many association events that are unproductive in branching (Smith, Padrick, et al. 2013). These results suggest that the nascent branch junction is a key control point on the pathway to branched filament nucleation. Importantly, the formation of branched filaments requires pre-existing filaments to serve as templates. Arp2/3 complex nucleated branched filaments can and often serve as substrates for succeeding rounds of branching; creating networks of branches from branches (Mullins, Heuser, and Pollard 1998; Amann and Pollard 2001). However, the initial branching reaction still requires a pre-existing filament. This first filament is called the seed filament and its cellular origins remain unknown. Many details of Arp2/3 complex nucleation and branched network regulation still need to be explored.

Multiple Biochemically Distinct Nucleation Promoting Factors (NPFs) Activate Arp2/3 Complex

Every branched filament is the result of NPF activation of Arp2/3 complex; this activity emphasizes the critical role of NPFs in regulating branched network formation. NPFs are characterized by their ability to bind to and activate Arp2/3 complex. Interestingly, cells contain many different NPFs and most have distinct biochemical properties (Goley and Welch 2006). NPFs have traditionally been subdivided into three different types based on their actin binding ability: type I, type II and WISH/DIP/SPIN90 proteins (Figure 2A). While numerous diverse NPFs have been discovered, their mechanisms of Arp2/3 complex activation and their roles in cellular branched network assembly have not been fully explored.

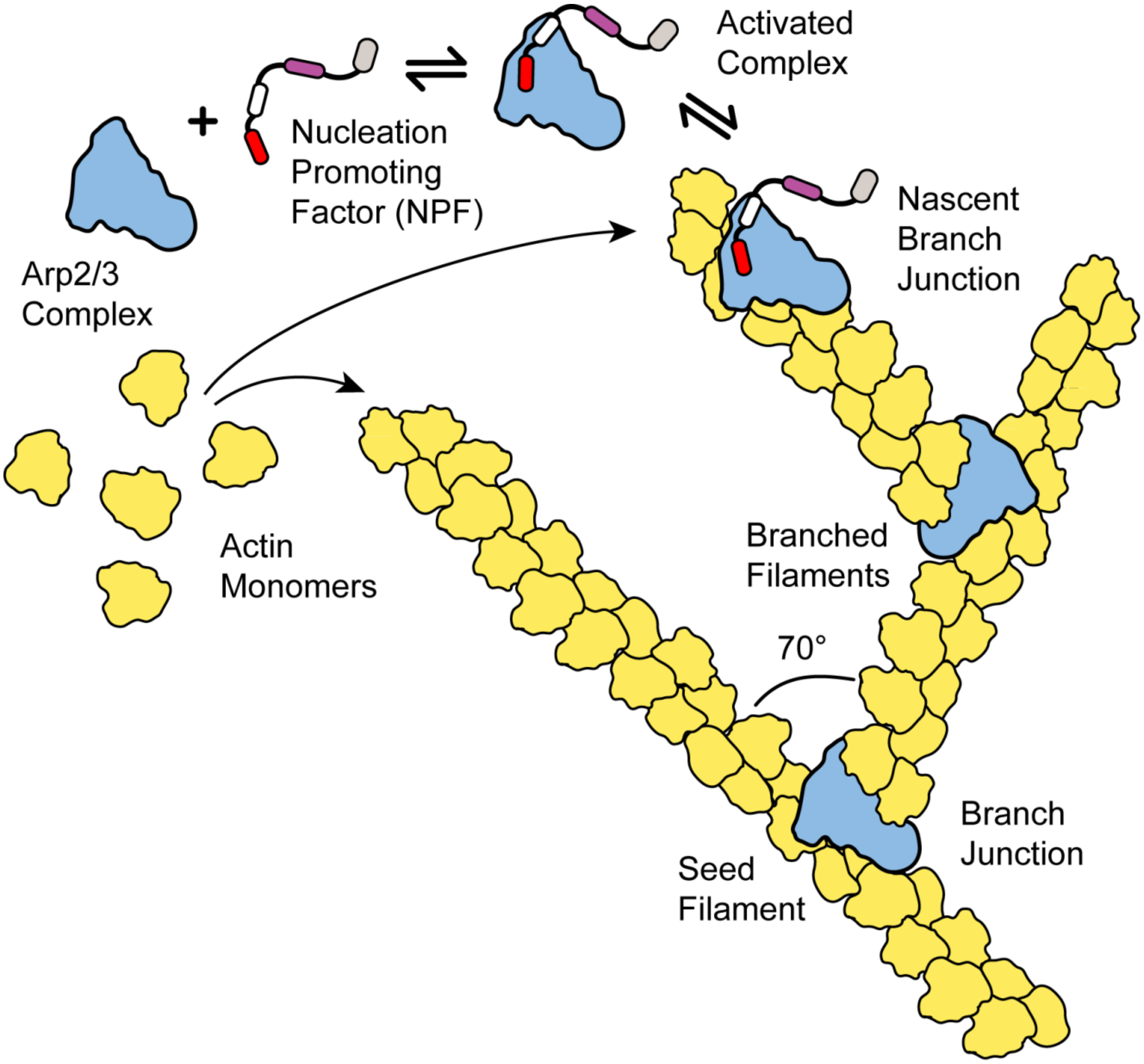
Activated
Complex
Nucleation
Promoting
Factor (NPF)
Arp2/3
Complex
Nascent
Branch
Junction
Actin
Monomers
Branched
Filaments
70°
Branch
Junction
Seed
Filament

Figure 1. Mechanism of Branched Filament Nucleation by Arp2/3 Complex
Arp2/3 complex (blue) is bound and activated by a nucleation promoting factor (NPF, red/white/magenta representation). The activated NPF-Arp2/3 complex then binds to a pre-existing filament side (yellow actin) to form a nascent branch junction. The NPF is released from the nascent branch junction to complete nucleation and allow elongation (yellow actin monomers) of the new branched filament at a ~70° angle away from the pre-existing filament. Arp2/3 complex remains at the branch junction. The pre-existing filament that initiates the first branched filaments is called the seed filament.

Actin monomer binding type I NPFs are the largest and most well understood NPFs. Wiskott-Aldrich syndrome (WASP) family proteins, including WASP, N-WASP and WAVE, are the archetypal type I NPFs and are some of the first discovered and characterized NPFs (Machesky and Insall 1998; Rohatgi et al. 1999). Due to their cellular abundance and necessity for many processes, WASP family proteins are believed to be the primary activators of Arp2/3 complex *in vivo*. At the C-terminal end of WASP family proteins is the VCA domain which is necessary and sufficient for Arp2/3 complex activation (Figure 2A) (Marchand et al. 2001). The VCA domain is composed of three distinct regions: Verpolin-homolog (V) region, central (C) region and acidic (A) region. The V (also called WASP Homolog 2, WH2) region binds to actin monomers through an amphiphilic α-helix that wedges into a barbed end pocket, as well as a highly conserved LKKT/V motif, C-terminal to the α-helix, which interacts with the charged surface of the monomer to confer a majority of the V region binding specificity (Figure 2B) (Chereau et al. 2005; Didry et al. 2011). VCA binds Arp2/3 complex through the combined effort of the CA regions. The acidic (A) region on its own is able to bind Arp2/3 complex, but its affinity is increased 5-10 fold when the C region is included (Marchand et al. 2001). The C region contains an amphiphilic α-helix that is critical for Arp2/3 complex activation in the context of VCA but the C region on its own does not bind the complex (Panchal et al. 2003). Required for A (and CA) region binding to Arp2/3 complex is a highly conserved DDWE motif; mutation of the tryptophan abolishes binding to the complex (Marchand et al. 2001). Recently, two conserved VCA binding sites have been identified on Arp2/3 complex (Ti et al. 2011; Padrick et al. 2011). One site, centered on Arp2, has a ~100 fold higher affinity for VCA than the low affinity site, centered on Arp3. Further investigations suggest that Arp2/3 complex is bound and activated by two VCAs during branching nucleation (Padrick et al. 2008). Although WASP family proteins do not contain dimerization domains, in cells they are believed to behave like oligomers through clustering when bound to membranes and through association with scaffolding proteins like Nck (Padrick et al. 2008; P. Li et al. 2012; Suetsugu 2013; Gohl et al. 2010). From these data, type I NPFs are believed to actively recruit multiple actin monomers to activate Arp2/3 complex for branching nucleation.

Type II NPFs are a diverse set of proteins which are characterized by their ability to bind actin filaments. Cortactin, Abp1 and coronin are well known members of this family. Similar to type I NPFs, most type II NPFs bind to Arp2/3 complex through acidic regions at the same binding sites as VCA (Weaver et al. 2002; Liu et al. 2011; Goode et al. 2001). However, the acidic region of cortactin only binds the Arp3 site whereas the acidic region of coronin preferentially binds the Arp2 site. These binding interactions suggest that subtle differences between acidic regions govern binding specificity of NPFs. Unlike type I NPFs with their monomer binding V regions, there is no common actin filament binding region shared amongst type II NPFs (Figure 2A). Cortactin binds actin filaments using 6.5 novel 37 residue actin binding repeats, whereas coronin proteins using a large β-propeller domain to interact with filaments (Wu and Parsons 1993; Galkin et al. 2008). The biochemical diversity amongst type II NPFs has made determination of their Arp2/3 complex activation mechanism difficult but it is hypothesized that they activate the complex by recruiting it to the side of filaments (Figure 2C) (Weaver et al. 2001; Cai et al. 2008; Goode et al. 2001). Through recruitment these NPFs could increase the affinity of Arp2/3 complex for filament sides, which some lines of evidence suggest is a slow, possibly, rate limiting reaction (Beltzner and Pollard 2008). The activation potency of type II NPFs is more diverse than WASP family proteins. Cortactin weakly activates the complex, whereas coronin weakly activates at low concentrations but at high

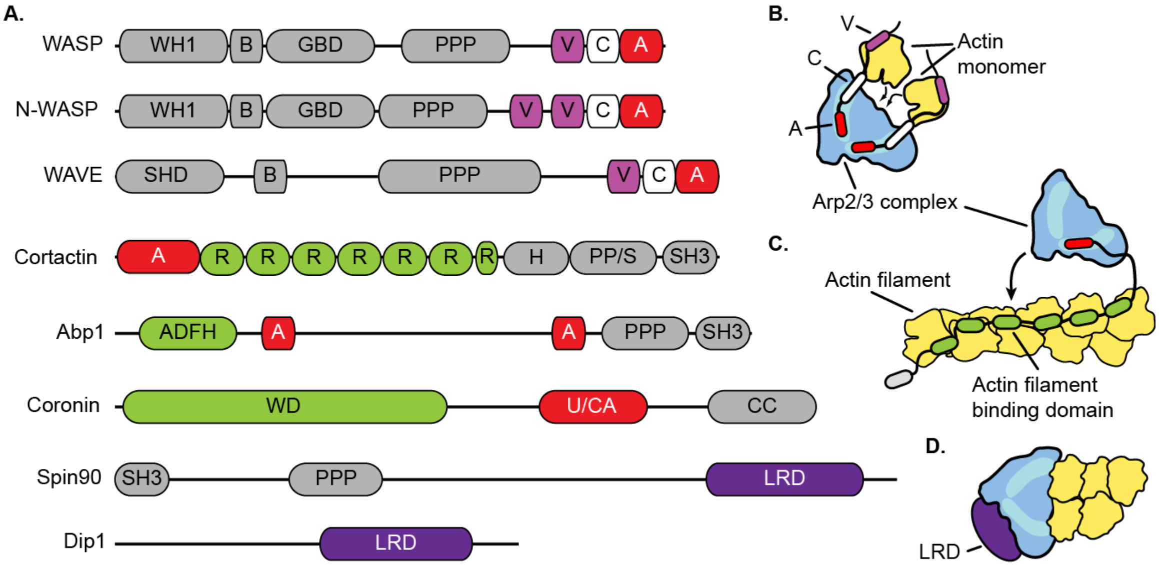
A.
WASP
WH1
B
GBD
PPP
V
C
A
N-WASP
WH1
B
GBD
PPP
V
V
C
A
WAVE
SHD
B
PPP
V
C
A
Cortactin
A
R
R
R
R
R
R
R
H
PP/S
SH3
Abp1
ADFH
A
A
PPP
SH3
Coronin
WD
U/CA
CC
Spin90
SH3
PPP
LRD
Dip1
LRD
B.
V
C
A
Actin monomer
Arp2/3 complex
C.
Actin filament
Actin filament binding domain
D.
LRD

Figure 2. Overview of Known NPFs and Their Mechanisms of Arp2/3 Complex Activation
A. Domain organization of example proteins from each type of NPF: WH1, wasp-homology 1; B, basic region; GBD, GTPase binding domain; PPP, poly-proline rich region; V, verpolin-homology region (also known as WH2, WASP homology 2); C, central region; A, acidic region; SHD, SCAR-homology domain; NtA, N-terminal acidic region; SH3, Src-homology 3 domain; R, actin filament binding repeat; H, helical region; PP/S. poly-proline and serine rich region; ADFH, actin-depolymerizing factor homology domain; WD, WD40 β-propeller domain; U/CA, unique and Arp2/3 complex binding CA region; CC, colied-coil domain; LRD, leucine rich domain. **B.** Activation of Arp2/3 complex by the VCA domain of type I NPFs. Two VCA domains recruit two actin monomers to a single Arp2/3 complex. Light blue shaded areas represent acidic region binding sites. **C.** Activation of Arp2/3 complex by the type II NPF, cortactin. Light blue shaded areas represent acidic region binding sites. **D.** Activation of Arp2/3 complex by the leucine rich domain of WISH/DIP/SPIN90 proteins. Light blue shaded areas represent acidic region binding sites.

concentrations inhibits branching by coating actin filaments and blocking association of Arp2/3 complex with filaments (Uruno et al. 2001; Liu et al. 2011). The reduced activity of type II NPFs could be due to the lack of actin monomer recruitment because enhanced cortactin activity has been observed through association with the monomer binding WASP-Interacting protein (Kinley et al. 2003). Taken together, these findings suggest that each type II NPF possess unique activation properties that will require individual biochemical dissection to understand their role in branched network formation.

Recently identified as NPFs, WISH/DIP/SPIN90 proteins activate Arp2/3 complex without the need of a pre-existing filament (Wagner et al. 2013). Spin90, the mammalian ortholog, was originally reported to activate Arp2/3 complex through a WASP-like mechanism, with an acidic region and actin monomer binding region (Kim et al. 2006). Subsequent studies revealed that Dip1, the fission yeast ortholog, does not bind to either state of actin and does not bind Arp2/3 complex through a DDWE motif (Wagner et al. 2013). Spin90 and Dip1 were both shown to activate Arp2/3 complex without a pre-existing filament, suggesting that both proteins share a conserved activation mechanism that is distinct from type I and II NPFs (Figure 2D). WISH/DIP/SPIN90 proteins appear to use a conserved leucine-rich domain (LRD) to both bind to and activate Arp2/3 complex; possibly by mimicking actin filament interactions with Arp2/3 complex to induce the conformational changes necessary for filament nucleation (Figure 2D) (Rouiller et al. 2008). Interestingly, because their activation is independent of preformed filaments, WISH/DIP/SPIN90 generated networks are linear. Genetic evidence from *S. pombe* endocytosis along with the biochemical data suggests that WISH/DIP/SPIN90 proteins initiate branched network formation (Basu and Chang 2011; Wagner et al. 2013). It remains to be seen if WISH/DIP/SPIN90 generated filaments can support branched filament nucleation and how this new type of NPFs interact with Arp2/3 complex in the presence of type I or II NPFs.

NPFs Are Highly Regulated

Through the integration of multiple cellular signals and intramolecular interactions, NPFs themselves are often strictly regulated to ensure proper spatial and temporal formation of branched networks (Padrick and Rosen 2010). WASP and N-WASP are autoinhibited through N-terminal domains masking the C-terminal VCA domain. This autoinhibition is relieved through interactions with a multitude of factors, such as the SH3 domains of Nck and cortactin, but the primary relief factor is a combination of the GTPase Cdc42 and the phospholipid PIP2 (Prehoda et al. 2000; Higgs and Pollard 2000; Martinez-Quiles et al. 2004; Rohatgi et al. 2001). Disruption in the ability of N-WASP to bind Cdc42 significantly reduces actin polymerization *in vitro* and *in vivo*. In addition to relieving autoinhibition, interactions with Cdc42 and PIP2 spatially regulate N-WASP and WASP by recruiting them to the membrane to nucleated branched filaments with their growing barbed-ends oriented at the membrane (Takenawa and Suetsugu 2007).

Cellular WAVE is part of and regulated by a complex of 4 additional proteins, called the WAVE regulatory complex (Eden et al. 2002). Unlike WASP and N-WASP, WAVE is activated by another GTPase, Rac. Activation of WAVE by Rac and subsequent association with the phospholipid PIP3, localizes the WAVE regulatory complex to the leading edge of the cell for branched network assembly (Miki, Suetsugu, and Takenawa 1998). Knockdown of Rac or the ability of WAVE to activate Arp2/3 complex prevents proper lamellipodia formation and cell motility (Suetsugu et al. 2003).

Whereas WASP family proteins are primarily regulated through intra- and intermolecular interactions; the type II NPF, cortactin is controlled through extensive post-translational modifications. Multiple cortactin phosphorylation events are required for proper invadopodia formation and clathrin-independent endocytosis (Ayala et al. 2008; Grassart et al. 2010). Src and ERK1/2 phosphorylation of cortactin governs branched networks through regulating cortactin's ability to activate N-WASP and inhibit cofillin mediated filament severing (Martinez-Quiles et al. 2004; Oser et al. 2009). Src phosphorylation of cortactin was reported to have no effect on its ability to directly activate Arp2/3 complex, however cortactin phosphorylation increases branched network assembly indirectly through activation of N-WASP (Tehrani et al. 2007; Martinez-Quiles et al. 2004). Due to the multiple pathways of network control, the NPF specific role of cortactin in regulating branched network formation must be carefully teased apart through isolation of individual cortactin activities. NPF activity is tightly regulated through multi-faceted molecular interactions. Dissection of NPF regulation mechanisms will be critical to fully understand cellular control of branched network assembly.

A Cellular Structure May Contain and Require Several NPFs

Multiple biochemically distinct NPFs are often found to function within the same cellular processes. Critical to cell motility and the formation of lamellipodia are the NPFs: WAVE, cortactin and Spin90 (Suetsugu et al. 2003; Bryce et al. 2005; Kim et al. 2006). Abolishing the ability of WAVE to activate Arp2/3 complex prevents cell motility, suggesting WAVE is the primary driver of branched network assembly in lamellipodia (Suetsugu et al. 2003; Z. Chen et al. 2010; Suraneni et al. 2012). However, cortactin was also observed to localize with Arp2/3 complex in lamellipodia and mutations in its Arp2/3 complex binding acidic region reduce lamellipodia protrusion and cell motility (Weed et al. 2000; Bryce et al. 2005). These results suggest that both cortactin and WAVE mediate the assembly of branched networks in lamellipodia. Stimulation of COS-7 cells with PDGF targets Spin90 to the lamellipodia where it localizes with Arp2/3 complex and is required for proper lamellipodia formation (Kim et al. 2006). Arp2/3 complex activation by Spin90 remains to be shown during this processes but its biochemical characterization suggests Spin90 also regulates lamellipodia branched networks through NPF activity (Wagner et al. 2013).

N-WASP is the predomenant type I NPF found in endocytosis and is required for invadopodia, which are invasive structures found in cancerous cells (Lorenz et al. 2004; Merrifield et al. 2004). Additionally, both cellular structures also contain the type II NPF cortactin and are dependent upon branched actin networks to function (Kaksonen, Peng, and Rauvala 2000; Artym et al. 2006). Cortactin is a necessary component of invadopodia assembly and for the structure's role in degrading the extracellular matrix. Within invadopodia, cortactin can increase the activity of N-WASP but the Arp2/3 complex binding region of cortactin is still important for matrix degradation (Oser et al. 2009; Ayala et al. 2008). These results suggest that cortactin and N-WASP both activate Arp2/3 complex to generate the branched filaments required for invadopodia formation and function. Like N-WASP, the fission yeast (*S. pombe*) ortholog, WASP1 (Wsp1), is an important regulator of branched networks during endocytosis. In addition to Wsp1, the type I NPFs, Pan1 and class 1 myosin (Myo1), and the WISH/DIP/SPIN90 NPF Dip1 are involved in *S. pombe* endocytosis (Sirotkin et al. 2005; Basu and Chang 2011; Galletta, Chuang, and Cooper 2008). Wsp1 deletion significantly reduces the internalization of endocytic pits and Dip1 deletion results in cortically stalled endocytic pits where internalization eventually occurs but at a stochastic rate (Basu and Chang 2011). These phenotypes are consistent with errors in actin network formation identified in other species and through latrunculin mediated inhibition of actin polymerization (Mooren, Galletta, and Cooper 2012). Importantly, the double deletion strains of Wsp1 and Dip1 were less viable then the single mutants, indicating that both proteins are important for functional branched actin assembly (Basu and Chang 2011).

Numerous lines of evidence suggest that cells utilize a diverse arsenal of NPFs to regulate the formation of branched actin network for proper biological function. Why are multiple biochemically distinct NPFs required for the assembly of cellular branched networks? The requirement for many different NPFs indicates that simply increasing the amount of branching nucleation is not the desired effect, but that each NPF plays a specialized role to fine-tune the assembly of the branched network to the particular biological operation. While a significant amount of data establishes the importance of multiple NPFs in the same cellular processes, it remains unknown if the NPFs are activating Arp2/3 complex at the same time or in the same location. Cortactin activation of N-WASP suggests these NPFs are able to simultaneously co-localize with Arp2/3 complex in the same cellular structures and previous evidence suggest these two NPFs can synergistically activate Arp2/3 complex (Weaver et al. 2001). How these NPFs can synergistically activate Arp2/3 complex and whether different pairs of NPFs can also cooperatively activate the complex remains unknown. We hypothesize that multiple NPFs coordinately activate Arp2/3 complex to regulate branched network formation. Understanding why multiple distinct NPFs are necessary for cellular branched network regulation starts with biochemically dissecting Arp2/3 complex activation in the presence of one or more NPFs. Determining the mechanisms of how individual and multiple NPFs synergistically or coordinately activate Arp2/3 complex will identify if activating NPFs uniquely assemble networks and will provide valuable insight into how Arp2/3 complex is regulated during numerous cellular processes. Information obtained from these detailed studies has the potential to improve our basic understanding of Arp2/3 complex alone and establish NPF specific interactions or pathways which can be probed during the cellular investigation of coordinate branched actin network assembly.

The work presented in chapter II was published in the journal Elife and was coauthored with Brad J. Nolen. The work presented in chapter III was published in The Journal of Biological Chemistry and was coauthored with Julianna G. Prendergast, Andrew R. Wagner, Max Rodnick-Smith and Brad J. Nolen. The work presented in chapter IV is unpublished and was coauthored with Brad J. Nolen.

CHAPTER II

MECHANISM OF SYNERGISTIC ACITVATION OF ARP2/3 COMPLEX BY CORTACTIN AND N-WASP

Reproduced with permission from Helgeson, L.A. and Nolen B.J. 2013 *ELife* 2:e00884.

Copyright 2013, ELife.

INTRODUCTION

Orchestration of many complex cellular processes, including cellular motility, endocytosis, and cytokinesis, requires tight control of the assembly and disassembly of actin filament networks (Chhabra and Higgs 2007; Pollard and Cooper 2009). Actin-related protein (Arp)-2/3 complex is an important actin cytoskeletal regulator that mediates the assembly of branched actin filament networks by nucleating new (daughter) filaments from the sides of pre-existing (mother) filaments (Figure 1A) (Goley and Welch 2006; Rotty, Wu, and Bear 2013). When isolated from most species, the complex is inactive, and activation requires binding to the side of a preformed actin filament and association with a nucleation promoting factor (NPF) protein (Figure 1A) (Achard et al. 2010; Pollard 2007). In addition to binding Arp2/3 complex, NPFs discovered to date bind either actin monomers (Type I NPFs) or filaments (Type II NPFs) (Goley and Welch 2006) (Figure 1B,C). Cellular branched actin structures contain multiple NPFs, including representatives from both classes, which frequently have non-redundant roles in actin network assembly (Galletta, Chuang, and Cooper 2008; Yamaguchi et al. 2005; Ayala et al. 2008). However, the mechanism by which multiple NPFs coordinately regulate Arp2/3 complex activity is poorly understood.

WASP (Wiskot-Aldrich syndrome) and Scar (suppressor of cAR) family proteins, the best studied Type I NPFs, have a minimal Arp2/3-activation region called VCA (verprolin homology, central, acidic, Figure 1B) (Goley and Welch 2006). The V and C regions of VCA bind actin monomers (Kelly et al. 2006), and CA binds two sites on Arp2/3 complex (Padrick et al. 2011; Ti et al. 2011). Chemical crosslinking assays demonstrate that one CA site is on Arp3 and the other spans Arp2 and ARPC1 (Padrick et al. 2011). Using two CA binding sites, VCA is thought to recruit actin monomers to the Arp2 and Arp3 subunits, stimulating a conformational rearrangement to create an Arp2-Arp3-actin hetero-oligomer that mimics a stable actin filament nucleus (Padrick et al. 2011; Hetrick et al. 2013). Monomeric versus oligomeric VCA regions activate the complex with distinct kinetics, presumably due to differential engagement of the two sites (Padrick et al. 2008). Oligomerization of WASP/Scar proteins is thought to tune NPF activity *in vivo* (Padrick et al. 2008; Gohl et al. 2010; Footer, Lyo, and Theriot 2008) , so dissecting biochemical differences between monomeric and oligomeric NPFs is an important challenge.

Cortactin, the prototypical type II NPF, was initially discovered as a Src kinase substrate and actin binding protein (Wu and Parsons 1993), and was later found to directly bind and activate Arp2/3 complex (Weed et al. 2000). Cortactin contains an N-terminal acidic region (NtA), which interacts with Arp2/3 complex, 6.5 actin filament binding repeat sequences, and a C-terminal SH3 domain (Figure 1B). Mutations in the NtA that block its interaction with Arp2/3 complex prevent assembly of actin in protrusive structures in

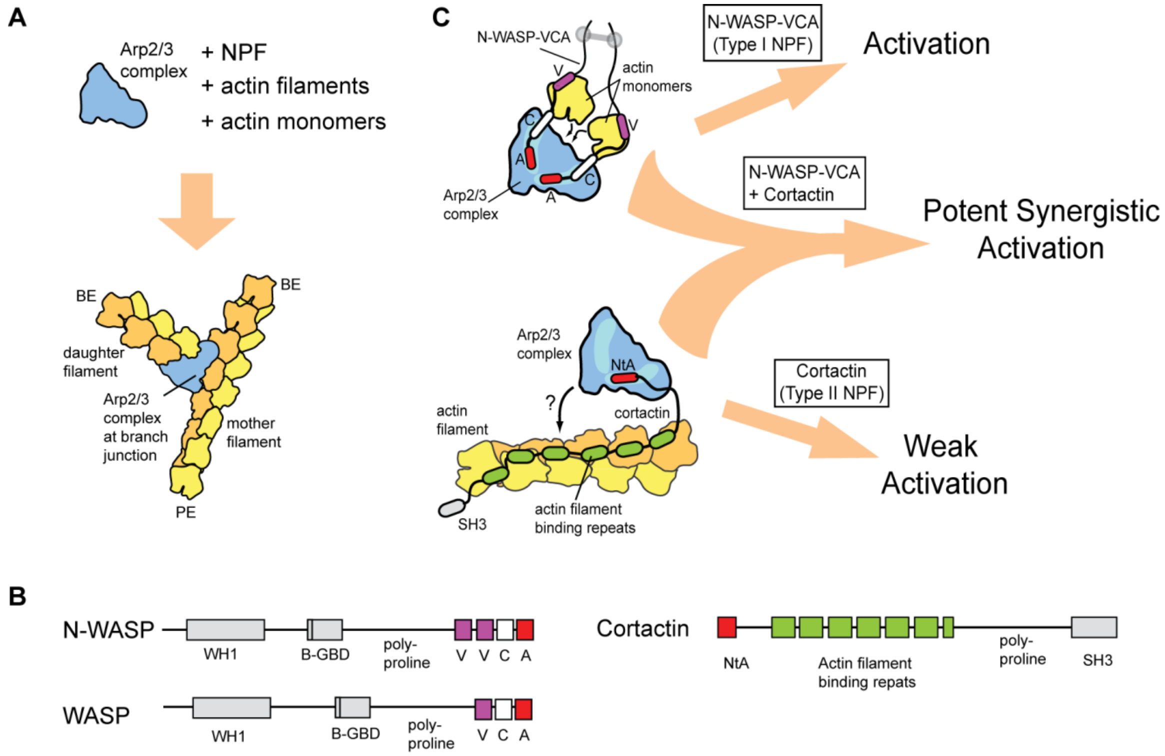
A
Arp2/3 complex
+ NPF
+ actin filaments
+ actin monomers
BE
BE
daughter filament
Arp2/3 complex at branch junction
mother filament
PE
C
N-WASP-VCA
V
actin monomers
V
C
A
C
A
Arp2/3 complex
N-WASP-VCA (Type I NPF)
Activation
N-WASP-VCA + Cortactin
Potent Synergistic Activation
Arp2/3 complex
NtA
?
actin filament
cortactin
SH3
actin filament binding repeats
Cortactin (Type II NPF)
Weak Activation
B
N-WASP
WH1
B-GBD
poly-proline
V
V
C
A
WASP
WH1
B-GBD
poly-proline
V
C
A
Cortactin
NtA
Actin filament binding repats
poly-proline
SH3

Figure 1. Schematic Overview of Branching Nucleation and the Proteins Involved (A) Overview of branching nucleation depicting the required reaction components (Arp2/3 complex, NPF, actin monomers and actin filaments) and the resultant Y-shaped branches. The barbed and pointed ends of the actin filaments are labeled BE and PE, respectively. (B) Domain organization of prototypical Type I (WASP/N-WASP) and Type II (Cortactin) NPFs. WH1, WASP homology 1; B-GBD, Basic region and GTPase binding domain; V, verprolin homology (also known as WH2, WASP homology 2); C, central; A, acidic; NtA, N-terminal acidic region; SH3, Src homology 3. (C) Schematic overview of activation of Arp2/3 complex by two classes of nucleation promoting factors. See text for details. Grey barbell indicates a generic N-WASP dimerization mechanism. Small black arrows indicate either recruitment of actin monomers to Arp2/3 complex by VCA, or recruitment of Arp2/3 complex to actin filaments by cortactin. Light blue areas on Arp2/3 complex indicate the two proposed CA binding sites. The SH3 domain of cortactin is shown here but is omitted in other figures for clarity.

transformed cells called invadopodia, and hinder actin-dependent vesicle trafficking required for lamellipodial protrusion and cellular motility (Ayala et al. 2008; Bryce et al. 2005). These observations demonstrate that cortactin plays an important role in regulating Arp2/3 complex *in vivo*, yet the precise mechanism of Arp2/3 complex activation is unclear. Because the actin filament-binding repeats are required for activation, it has been hypothesized that cortactin recruits Arp2/3 complex to filaments to stimulate nucleation (Uruno et al. 2001) (Figure 1C). However, whether filament recruitment can explain the acceleration of branching nucleation is unknown. In addition, cortactin on its own is a weak activator of Arp2/3 complex *in vitro* (Weed et al. 2000), making it uncertain how cortactin can contribute to branching nucleation *in vivo*.

Importantly, in the presence of WASP/Scar proteins, cortactin potently activates Arp2/3 complex (Weaver et al. 2001; Uruno et al. 2001), suggesting these NPFs synergize to assemble branched actin structures *in vivo* (see Fig 1C for schematic). Consistent with this hypothesis, WASP/Scar proteins and cortactin co-localize in many branched networks *in vivo*, including at the leading edge of motile cells, podosomes and invadopodia, and at sites of endocytosis (Martinez-Quiles et al. 2004; Desmarais et al. 2009; Grassart et al. 2010). Previous data showed that N-WASP and cortactin compete for binding to Arp3 (Weaver et al. 2002), and cortactin competes more strongly when Arp2/3 complex is bound to filaments (Uruno et al. 2003), but the precise mechanism of synergy is unknown. Previously proposed models include scenarios in which cortactin recruits Arp2/3 complex to the mother filament, where it cooperates with VCA to activate nucleation or induces release of VCA from branch-incorporated Arp2/3 complex to stabilize the nucleus (Weaver et al. 2002; Uruno et al. 2003). In another model, VCA becomes sequestered at branch junctions, so the concentration of VCA available to activate Arp2/3 complex limits the rate of branching nucleation (Siton et al. 2011). In this model, called the recycling model, cortactin binding displaces VCA from branch junctions, recycling it back into solution for more activation.

Here we dissect the mechanism of synergy between N-WASP and cortactin. Using single-molecule total internal reflection fluorescence (smTIRF) microscopy along with biochemical assays and mathematical modeling, we show that neither a filament recruitment nor a VCA recycling model can explain synergy. Our data instead support an obligatory displacement model, in which cortactin directly targets nascent branch junctions to accelerate the release of VCA. A key concept of the model is that VCA release is required for nucleation, either with or without cortactin, and the VCA release rate modulates the rate of nucleation. We dissect the biochemical requirements for synergy in cortactin and N-WASP to show that oligomerization of N-WASP VCA is required for significant synergy, but the actin filament binding repeats of cortactin are not. In addition, we provide evidence that slow release of N-WASP at nascent branch junctions limits nucleation rates, and that synergy is dependent on the ability of cortactin to accelerate this step. Our data provide important mechanistic insights into the regulation of Arp2/3 complex by cortactin, and lay the foundation for a molecular understanding of how NPFs work together to regulate branching nucleation.

RESULTS

Cortactin-mediated Synergy Follows a Hyperbolic Activity Curve

Previous experiments showed that cortactin activates Arp2/3 complex weakly on its own, but potently synergizes with WASP/N-WASP (Weed et al. 2000; Weaver et al. 2001; Uruno et al. 2001). To quantify synergy, we added a range of concentrations of cortactin to a reaction with GST-N-WASP-VCA (GST-VCA) and Arp2/3 complex (Figure 2A). Cortactin dramatically increased the polymerization rate, and the

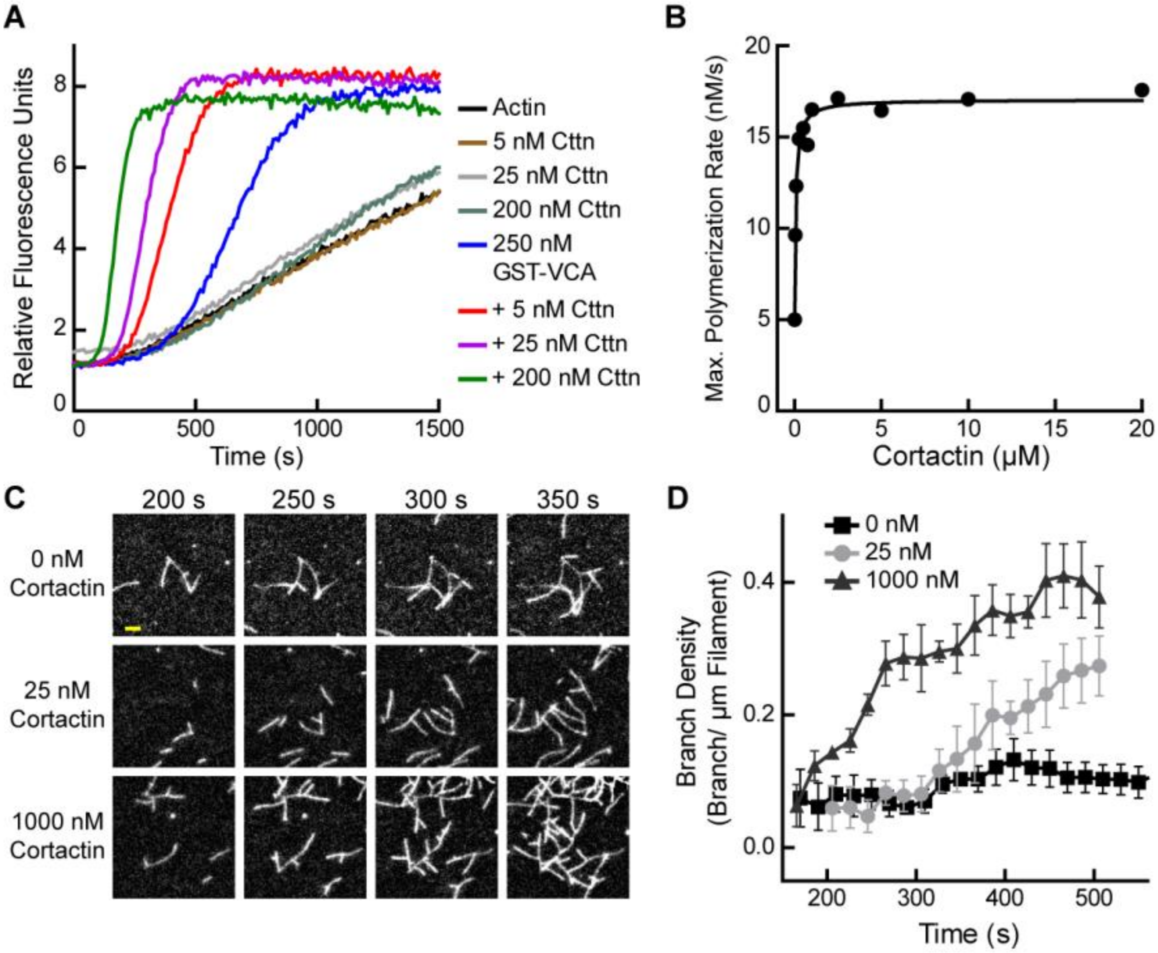

Figure 2. Cortactin Synergizes with GST-N-WASP-VCA
(A) Time course of pyrene-actin polymerization showing synergistic activation of Arp2/3 complex by cortactin and GST-VCA. Reactions contain 2 μM 15% pyrene-actin, 20 nM Arp2/3 complex and cortactin and/or 250 nM GST-VCA as indicated. (B) Plot of maximum polymerization rate versus cortactin concentration for reactions conditions as in panel A with 150 nM GST-VCA. Data were fit as described in methods. (C) TIRF microscopy images of reactions containing 1 μM 33% Oregon-Green actin, 10 nM Arp2/3 complex, 50 nM GST-VCA and indicated concentrations of cortactin. (D) Branch density time versus time for TIRF data from panel C. Error bars are the standard error of the mean for at least three regions of interest from an acquisition period. Scale bar: 2 μm.

concentration dependence of synergy followed a hyperbolic trend (Figure 2B). The concentration of cortactin required for half-maximal synergy was 72 nM and saturating cortactin increased the maximum polymerization rate 3.5-3.8-fold over GST-VCA alone. In contrast to a previous report, cortactin did not inhibit Arp2/3 complex at any concentration we tested, up to 20 μM in pyrene-actin polymerization assays or 1 μM in TIRF microscopy branching assays (Siton et al. 2011) (Figure 2B-D and Video 1; see the Appendices for all videos descriptions and the Supplemental File for all videos).

Actin Filament Recruitment Cannot Account for Synergistic Activation

Several lines of evidence suggest cortactin might synergize with GST-VCA by recruiting Arp2/3 complex to actin filament sides. First, Arp2/3 complex must bind to the side of a pre-existing filament to be activated (Achard et al. 2010), and kinetic measurements of pyrene-labeled *S. pombe* Arp2/3 complex indicated this binding step is slow (Beltzner and Pollard 2008). Second, deletion of the actin filament binding domain of cortactin abolished its weak intrinsic nucleation activity (Uruno et al. 2001). Finally, cortactin increases copelleting of Arp2/3 complex with actin filaments (Cai et al. 2008). To determine if filament recruitment can explain synergistic activation, we first constructed a mathematical model to describe branching nucleation in the presence of GST-VCA and Arp2/3 complex without cortactin (Figure 3A, Supplemental Figure 1; see Appendix A for all supplemental figures). Our goal was to determine how the rate constants for actin filament binding by Arp2/3 complex influence polymerization time courses, and if recruitment of Arp2/3 complex by cortactin could account for the increased rates we measured in our bulk polymerization assays containing cortactin.

We fit pyrene-actin polymerization time courses of reactions containing 50 nM Arp2/3 complex with increasing concentrations of GST-VCA to a mathematical model similar to that of Beltzner, *et. al* (Beltzner and Pollard 2008). The final activation step (k_{nuc}) was optimized by globally fitting the data from time courses at a range of concentrations of GST-VCA, while fixing all other kinetic parameters (Figure 3A, Table 1 and 2). The off rate of Arp2/3 complex bound to a mother filament (k_{fil_off}) was constrained based on the measured K_d, 0.9 µM (Hetrick et al. 2013). The model assumes that the final activation step (k_{nuc}) occurs after two actin monomers have been recruited by GST-VCA (Padrick et al. 2011). The model fit the experimental data well, showing a good visual fit to the time courses and a low residual sum of squares (1.3 x 10^{-11}) (Figure 3B). Optimization of the mother filament on rate showed that k_{fil_on} approaches a minimum threshold (2.7 x 10^3 M^{-1} s^{-1}), beyond which, increases in the on rate do not improve the fit (Figure 3C). We fixed the on rate at 1.4 x 10^6 M^{-1} s^{-1} based on modeling of reactions containing cortactin (see below and supplemental methods), and determined

Figure 3 (next page). Actin Filament Recruitment Cannot Explain Cortactin-mediated Synergy
(A) Cartoon pathway of steps optimized in the kinetic model of branching nucleation. (B) Representative pyrene-actin polymerization time courses of Arp2/3 complex activated by GST-VCA with simulated fits. Dashed lines show experimental data and solid lines show simulated fits after optimization. Residuals are shown below as solid lines. Reactions contained 3 µM 15% pyrene-actin, 50 nM Arp2/3 complex and indicated concentrations of GST-VCA. (C) Plot showing the relationship between the quality of fit (black line) and the optimized value of k_{nuc} (red line) for simulations at a range of fixed values of k_{fil_on}. A range of k_{fil_on} values fit the data well. Dashed purple and blue lines show k_{fil_on} values supported by our analysis in figure 7 (blue line) or by empirically measured k_{off} and K_d values (purple line) (Hetrick et al. 2013; Smith, Daugherty-Clarke, et al. 2013). The dashed green line indicates the minimum value of k_{fil_on} that fits the data with a quality of fit better than 1.3x10^{-11}. Quality of fit was calculated by a mean-weighted residual sum of squares. (D) Simulations showing the effect of increased actin filament side binding sites on the half time to reach equilibrium. Simulations were run using the three different k_{fil_on} values indicated in panel C. Empirical data from actin polymerization time courses with 3 µM 15% pyrene-actin, 20 nM Arp2/3 complex, 100 nM GST-VCA and the indicated concentrations of cortactin are shown as black circles (bottom axis). Initial concentrations of modeled actin filaments in the simulation are indicated on the top axis. (E) Plot of the fold activation over GST-VCA alone for a range of concentrations of full-length cortactin or NtA. Reactions contain 2 µM 15% pyrene-actin, 20 nM Arp2/3 complex, 250 nM GST-VCA and indicated concentrations of cortactin or NtA. Fold activation is calculated as the maximum polymerization rate for each reaction divided by the maximum polymerization rate for the reaction without cortactin. Data were fit (solid lines) as described in methods.

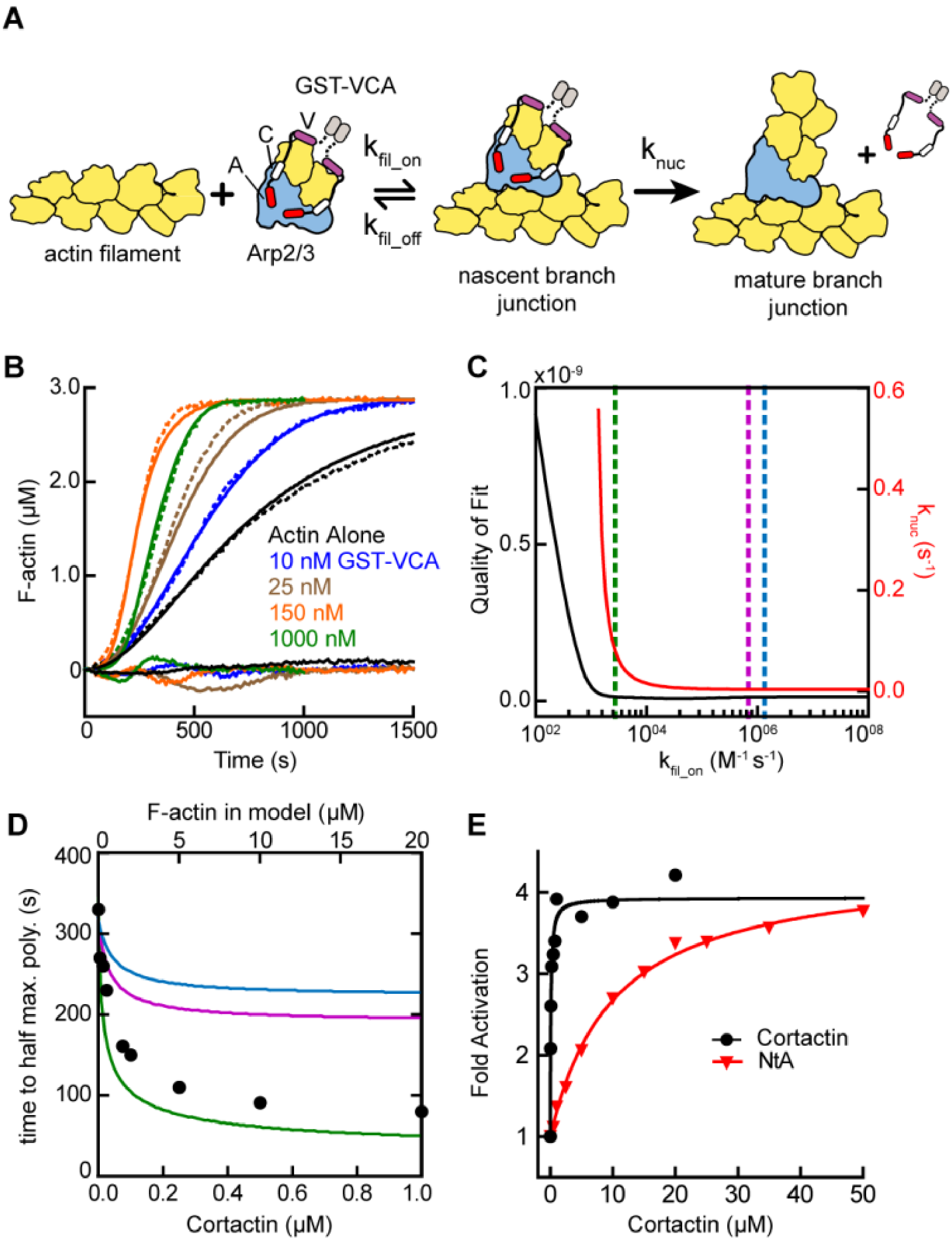
A
GST-VCA
C
V
A
actin filament
Arp2/3
k_fil_on
k_fil_off
nascent branch junction
k_nuc
mature branch junction
B
F-actin (µM)
3.0
2.0
1.0
0
0
500
1000
1500
Time (s)
Actin Alone
10 nM GST-VCA
25 nM
150 nM
1000 nM
C
x10-9
1.0
0.5
0.0
Quality of Fit
0.6
0.4
0.2
0.0
k_nuc (s-1)
10^02
10^04
10^06
10^08
k_fil_on (M-1 s-1)
D
F-actin in model (µM)
0
5
10
15
20
400
300
200
100
0
time to half max. poly. (s)
0.0
0.2
0.4
0.6
0.8
1.0
Cortactin (µM)
E
4
3
2
1
Fold Activation
Cortactin
NtA
0
10
20
30
40
50
Cortactin (µM)

the optimized value for k_{nuc} is 0.0038 s^{-1}. This value is 320-fold smaller than the calculated off rate of the nascent branch complex from filament sides, consistent with smTIRF studies that show Arp2/3 complex binds and is released from filaments many times before nucleating a branch (Smith, Daugherty-Clarke, et al. 2013). We then used the optimized model to determine if recruitment of Arp2/3 complex to the sides of filaments by cortactin can explain synergy. We mimicked the effect of recruitment by simulating an increase in the concentration of actin filaments to saturate Arp2/3 complex side binding. If synergy occurs purely through recruitment, the magnitude of polymerization rate increases caused by adding side-binding sites will be similar to cortactin-induced rate increases. Using k_{fil_on} determined from the experimental data with cortactin (1.4×10^6 M^{-1} s^{-1}, see below, blue line in Figure 3C), we found that increasing side binding sites increased the polymerization rate, but could not account for the dramatic rate increases we observed in experiments containing cortactin (Figure 3D). This suggests that filament recruitment cannot account for cortactin-mediated synergy. Because of the uncertainty in k_{fil_on}, we repeated the simulations at additional k_{fil_on} values. First, we used a k_{fil_on} value (6.9×10^5 M^{-1} s^{-1}, purple line in Fig 3C) calculated from the experimentally determined filament off rate of budding yeast Arp2/3 complex (0.625 s^{-1}) and the affinity of the bovine complex for filaments (Smith, Daugherty-Clarke, et al. 2013; Hetrick et al. 2013). This simulation also failed to account for experimentally observed synergy. However, in a simulation at the minimum threshold on rate (2.7×10^3 M^{-1} s^{-1}, green line in Figure 3C), filament recruitment could fully account for synergy. Therefore, while our best estimates of k_{fil_on} suggest that actin filament recruitment cannot explain synergy, k_{fil_on} is not determined well enough to completely eliminate the possibility that synergy occurs through recruitment.

Therefore, we next asked if the actin filament binding repeats of cortactin are required for synergy. We tested a range of concentrations of full-length cortactin and a construct containing only the NtA (residues 1-84) for their ability to synergize with GST-VCA to activate Arp2/3 complex. We found NtA was synergistic with GST-VCA, demonstrating that actin filament binding is not required for synergy (Figure 3E). The concentration dependence of synergy for both constructs followed a hyperbolic trend, and the concentration of NtA required for half-maximal synergy was 11 μM, 110-fold higher than for full-length cortactin. However, at saturation, NtA was as potent as full-length cortactin, increasing the maximum polymerization rate 3.8 fold over GST-VCA-mediated activation of Arp2/3 complex. These data demonstrate that the NtA is sufficient for synergy, but that the actin filament binding repeats allow cortactin to synergize at lower concentrations.

Table 1: Mathematical modeling parameters

Reaction #	Description	k_{on} ($M^{-1}s^{-1}$)	k_{off} (s^{-1})	K_d (μM)	Reference
1	Actin dimerization	19.8×10^7	5.26×10^7	2.6×10^6	Mullins 1998, This study
2	Actin trimerization	11.6×10^7	4.07×10^5	3.5×10^4	Mullins 1998, This study
3	Spontaneous nucleation	1116 – 1215 [a,b]			This study
4	Barbed end elongation	11.6×10^6	1.4		Pollard 1986
5	Barbed end elongation, actin monomer bound to GST-VCA	11.6×10^6	1.4		Pollard 1986, Higgs 1999
6	Barbed end elongation, two actin monomers bound to	11.6×10^6	1.4		Pollard 1986, Higgs 1999

	GST-VCA				
7	Actin monomer binds GST-VCA	5×10^{6}	3	0.6	Marchand 2001, Beltzner 2008
8	Actin monomer binds GST-VCA with bound actin	5×10^{6}	3	0.6	Marchand 2001, Beltzner 2008
9	Actin monomer binds GST-VCA:actin$_2$	4.2×10^{4}	74.4	1.8×10^{3}	This study
10	Actin monomer binds GST-VCA:actin$_3$	1.5×10^{7}	1.04	0.069	This study
11	Actin monomer binds GST-VCA:actin$_4$	2×10^{7}	0.062	0.003	This study
12	GST-VCA nucleation	6.1×10^{-8} [a]			This study
13	Arp2/3 binds actin filament	1.37×10^{6}	1.23	0.9	Hetrick 2013
14	GST-VCA binds Arp2/3	0.8×10^{6}	0.072	0.009	Padrick 2008
15	GST-VCA:actin binds Arp2/3	0.8×10^{6}	0.0144	0.018	Padrick 2008, Beltzner 2008, Kelly 2006
16	GST-VCA:actin$_2$ binds Arp2/3	0.8×10^{6}	0.029	0.028	Padrick 2008, Beltzner 2008, Kelly 2006
17	Actin monomer binds GST-VCA:Arp2/3	2.5×10^{6}	3	1.2	Marchand 2001, Beltzner 2008
18	Actin monomer binds GST-VCA:actin:Arp2/3	2.5×10^{6}	3	1.2	Marchand 2001, Beltzner 2008
19	GST-VCA:actin$_2$:Arp2/3 binds actin filament **(k_{fil_on})**	1.37×10^{6}	1.23	0.9	Hetrick 2013
20	GST-VCA binds Arp2/3:F-actin	0.8×10^{6}	0.072	0.009	Padrick 2008
21	GST-VCA:Arp2/3 binds F-actin	1.37×10^{6}	1.23	0.9	Hetrick 2013
22	GST-VCA:Arp2/3:actin binds F-actin	1.37×10^{6}	1.23	0.9	Hetrick 2013
23	GST-VCA:Arp2/3:F-actin binds actin monomer	2.5×10^{6}	3	1.2	Marchand 2001, Beltzner 2008
24	GST-VCA:Arp2/3:actin:F-actin binds actin	2.5×10^{6}	3	1.2	Marchand 2001, Beltzner 2008

	monomer				
25	Arp2/3 nucleation **(k_{nuc})**	0.00381 - 0.00594 [a]			This study
26	Cortactin binds actin filament	1.21 x 10^4	0.063	5.21	This study
27	Cortactin binds nascent branch junction	2.0 x 10^6	0.034	0.017	This study
28	Synergy displacement activation of Arp2/3 complex **(k_{dis})**	0.0358 [a]			This study
29	Synergy recycling, cortactin dissociates sequestered GST-VCA	2.0 x 10^6	0.034	0.017	This study

a. Units are s^{-1}. b. This value was adjusted for each full set of reactions. **Underlined values** were allowed to float during some optimizations, see table 2.

Table 2: Mathematical modeling reaction sets

Reaction Set	Reactions	Initial Concentrations	Variable Concentrations (µM)	Floated Parameters	Quality of Fit
1	1-4	-	2.0, 3.0, 4.0, 5.0, 6.0 actin monomers	k_1, k_{-1}, k_2, k_{-2}, k_3	1.75 x 10^{-11}
2	1-12	3 µM actin monomers	0, 0.02, 0. 04, 0.08, 0.1, 0.2, 0.6, 0.8, 1.0 GST-VCA	k_9, k_{-9}, k_{10}, k_{-10}, k_{11}, k_{-11}, k_{12}	2.32 x 10^{-11}
3	1-25	3 µM actin monomers, 50 nM Arp2/3 complex	0, 0.01, 0.025, 0.050, 0.1, 0.15, 0.25, 0.5, 1.0 GST-VCA	k_{25} (k_{nuc})	1.28 x 10^{-11}
4a	1-28	3 µM actin monomers, 20 nM Arp2/3 complex, 100 nM GST-VCA	0, 0.005, 0.025, 0.075, 0.1, 0.25, 1 cortactin	k_{fil_on}(k_{13}=k_{19}=k_{21}=k_{22})[a,b], k_{25}[b], k_{28} (k_{dis})	2.87 x 10^{-11}
4b	1-25, 29	3 µM actin monomers, 20 nM Arp2/3 complex, 100 nM GST-VCA	0, 0.005, 0.025, 0.075, 0.1, 0.25, 1 cortactin	k_{29}, k_{-29}	4.26 x 10^{-10}

a. k_{fil_on} is a single global variable used for the indicated reaction rates. **b**. Only optimized for the 0 µM cortactin reaction.

The Oligomerization State of the Type I NPF Is an Important Determinant of Synergy

To probe further the mechanism of synergy, we next asked if biochemical features of the type I NPF influence synergy. Dimerization of VCA is known to increase its binding affinity for Arp2/3 complex, and some evidence suggests WASP/Scar proteins function as oligomers *in vivo* (Padrick et al. 2008; Gohl et al. 2010; Footer, Lyo, and Theriot 2008). Therefore, we compared cortactin-mediated synergy with monomeric versus GST-tagged N-WASP-VCA in a pyrene-actin polymerization assay. In previous experiments, GST-VCA behaved similarly to WASP dimerized by SH3 domain-containing proteins bound to its polyproline region, so artificial dimerization by GST can mimic physiological dimerization mechanisms (Padrick et al. 2008). Saturating cortactin enhanced the maximum polymerization rate of a reaction containing GST-VCA 3.7-fold over the rate without cortactin, whereas cortactin weakly influenced a reaction containing monomeric VCA, accelerating the reaction only ~1.5-fold over VCA alone (Figure 4A,B, Supplemental Figure 2). Increasing the concentration of monomeric VCA did not increase synergy, suggesting the failure to observe potent synergy is not due to under-saturation of two CA binding sites on the complex (Figure 4B,C, Figure 4-figure supplement 1). VCA dimerized with a leucine zipper (LZ-VCA) behaved identically to GST-VCA, demonstrating that the difference in synergy is due to the oligomerization state of the VCA rather than an artifact caused by GST (Figure 4A).

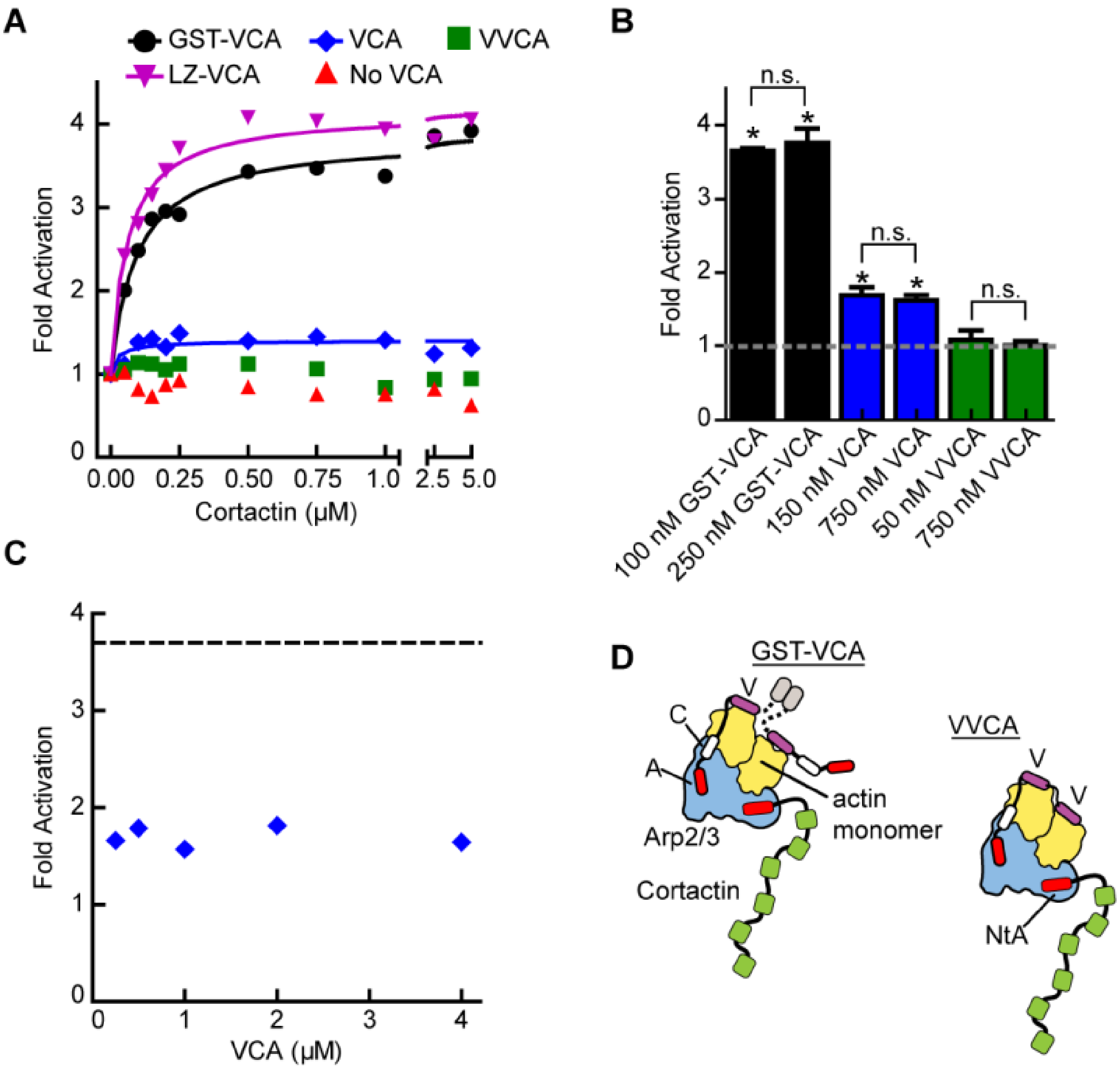

Figure 4. The Oligomerization State of VCA Is an Important Determinant of Synergy

(A) Plot of the fold activation versus cortactin concentration for reactions containing 2 μM 15% pyrene-actin, 20 nM Arp2/3 complex and 250 nM GST-VCA (black), 750 nM VCA (blue), 750 nM VVCA (green), 250 nM Leucine-zipper VCA (LZ-VCA, magenta) or no N-WASP (red). Monomer concentrations are listed. Fold activation is calculated as described in Figure 3E. (B) Plot of the average fold activation for reactions containing 1 μM cortactin and the indicated concentration of GST-VCA, VCA or VVCA. Dashed line indicates no synergy. P-values were calculated by two-tailed Student's t-test. Error bars are s.e.m. n.s. = not significant, $p > 0.05$. Asterisks indicate average fold activation values are significantly different ($p < 0.05$) than a fold activation value of 1 (no synergy) (C) Fold activation versus concentration of monomeric VCA for pyrene-actin polymerization assays containing 0 to 4 μM N-WASP-VCA, 500 nM cortactin and Arp2/3 complex and actin as in panel A. Dashed line shows average fold activation of GST-VCA. (D) Cartoon showing hypothetical branching intermediates with the potential to recruit two actin monomers (G-actin) to Arp2/3 complex with bound cortactin.

The dimerization state of N-WASP could control synergy by influencing the number of actin monomers recruited to the complex. For instance, if NtA and VCA simultaneously interact with Arp2/3 complex during activation, GST-VCA may be able to recruit two actin monomers while engaging only one NPF binding site, while VCA can only recruit one actin monomer (Figure 4D). Unlike WASP and Scar, native N-WASP contains tandem V regions and may be able to recruit two actin monomers to Arp2/3 complex (Rebowski et al. 2010). Therefore, we made a monomeric N-WASP construct with both V regions (VVCA) and tested its ability to synergize with cortactin. We found that VVCA is not synergistic with cortactin at any concentration (Figure 4A,B, Figure 4-figure supplement 1). These data suggest that the ability to recruit two actin monomers to the complex using one NPF binding site is not sufficient for synergy.

Dissociation of N-WASP from Branch Junctions May Limit the Rate of Branching Nucleation

Dimerization increases the affinity of N-WASP for Arp2/3 complex 180-fold, allowing it to saturate both NPF binding sites on the complex at lower concentrations than monomeric VCA (Padrick et al. 2008). We next explored the importance of the affinity of the type I NPF for Arp2/3 complex in synergy. Based on a number of observations, we hypothesized that type I NPF release is required for nucleation, and that tight binding of the type I NPF can slow the final activation step. First, we observed that at saturation, VCA is a better activator of Arp2/3 complex than GST-VCA (Figure 5A). Second, recent single-molecule imaging experiments show that WASP dissociates from the branch junctions before elongation of the daughter filament

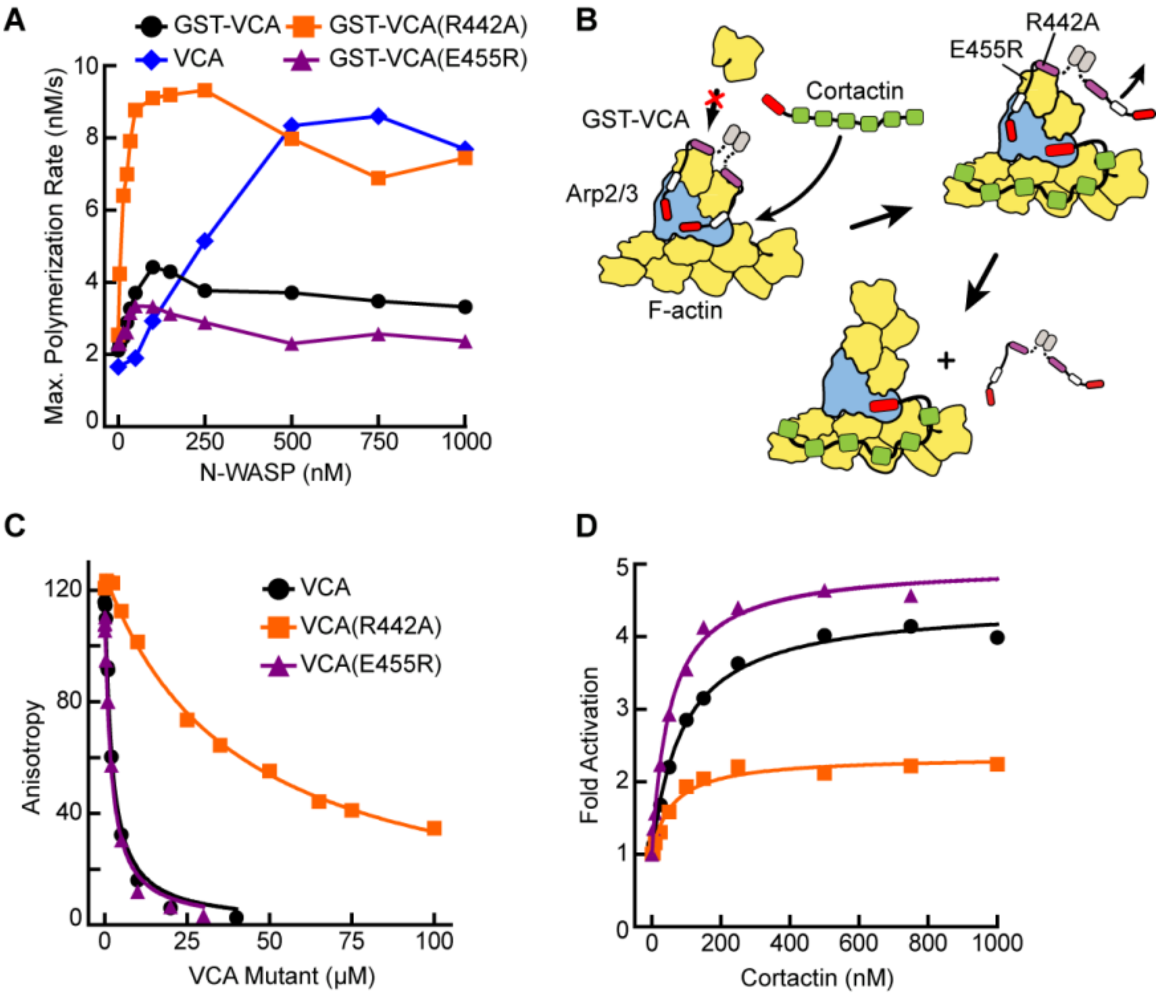

Figure 5. VCA Affinity for the Nascent Branch Junction Is an Important Determinant of Synergy

(A) Maximum polymerization rates verses (monomer) concentration of N-WASP constructs for reactions containing 20 nM Arp2/3 complex and 2 µM 15% pyrene-actin. (B) Cartoon depicting obligatory displacement model of cortactin-mediated synergy. Approximate location of residues (based on 2A41.pdb and 2VCP.pdb)(Chereau et al. 2005; Gaucher et al. 2012) mutated in the V region of GST-VCA are indicated in one V region. (C) Fluorescence anisotropy binding measurements showing competition between wild type rhodamine-VCA and unlabeled VCA constructs for actin monomers. $K_{d,\ WT}$ = 0.56 ± 0.03 µM (black) $K_{d,\ R442A}$ = 11.2 ± 1.3 µM, (orange) $K_{d,\ E455R}$ = 0.63 ± 0.06 µM (purple). (D) Plot of fold activation versus cortactin concentration for reactions containing 20 nM Arp2/3 complex, 2 µM 15% pyrene-actin and 250 nM of a GST-VCA construct, colors as in panel A. Fold activation is calculated as described in Figure 3E.

(Martin, Welch, and Drubin 2006) (Smith et al 2013, in press at eLife). Finally, crystal structures show that the V region may block the barbed end of actin monomers, preventing interactions with incoming actin monomers required for elongation (Chereau et al. 2005). Therefore, we hypothesized that cortactin synergizes with GST-VCA by displacing it from the nascent branch complex, increasing the rate of the final activation step by accelerating the obligatory release of GST-VCA (Figure 5B).

To test this model, we prepared a VCA construct (GST-VCA(R442A)) with a point mutation in V that decreases its affinity for actin monomers 20-fold (Co et al. 2007)(Figure 5B,C). We reasoned that this mutation would decrease the affinity of GST-VCA for the nascent branch junction, but still allow V to recruit actin monomers to the Arp2/3 complex (Co et al. 2007). We predicted that in the absence of cortactin, saturating concentrations of this mutant would have a higher maximal polymerization rate, because it would release from the nascent branch junction faster than wild-type GST-VCA. Consistent with this prediction, the maximal polymerization rate at saturation was increased 2.5-fold in the R442A mutant compared to wild type (Figure 5A). The obligatory displacement model predicts that cortactin will be less synergistic with the GST-VCA(R442A) mutant because of its higher intrinsic off rate from the nascent branch complex. Our data are also consistent with this prediction. In the presence of the R442A mutant, cortactin showed approximately 2-fold less synergy compared to the wild-type GST-VCA (Figure 5D). To provide further evidence of the model, we made an additional V region mutation, E455R, which we predicted would bind more tightly to actin monomers and the nascent branch junction. Based on mutational data and a crystal structure of the V region of WIP bound to actin, an E455R mutation was predicted to interact favorably with Glu93 on the surface of actin (Didry et al. 2011) (Figure 5 and Supplemental Figure 3). Interestingly, this mutation had no influence on the affinity of N-WASP-VCA for actin monomers (Figure 5C). However, it decreased the maximal polymerization rate at saturation (Figure 5A) and increased synergy with cortactin (Figure 5D). This suggests that the E455R/E93 interaction may occur only in the context of the nascent branch junction. Together, these data support an obligatory displacement model for synergistic activation of the complex.

Cortactin Binds Statically to Actin Filaments

Our data suggest that cortactin may displace GST-VCA from branch junctions to activate the complex synergistically. This model requires that cortactin bind to nascent branch junctions and avoid being nonproductively sequestered along the sides of filaments. The actin filament-binding region of cortactin is composed of 6.5 tandem 37-amino acid repeats, which are unstructured (Shvetsov et al. 2009). The multivalent architecture of its actin binding domain led us to hypothesize that cortactin may find branch junctions by diffusing along actin filaments through multiple weak and dynamic interactions, similar to the actin binding protein VASP (Hansen and Mullins 2010). To test this, we labeled cortactin (residues 1-336) with Alexa-568 and actin monomers with Oregon-Green 488 and visualized their interactions using TIRF microscopy. Single-molecules of cortactin bound to and dissociated from actin filaments during the time courses of the movies (Figure 6A, Supplemental Figure 4, Video 2). The cortactin molecules bound statically, eliminating the possibility that cortactin targets nascent branch junctions by diffusing along filaments (Figure 6B). We measured the lifetimes of

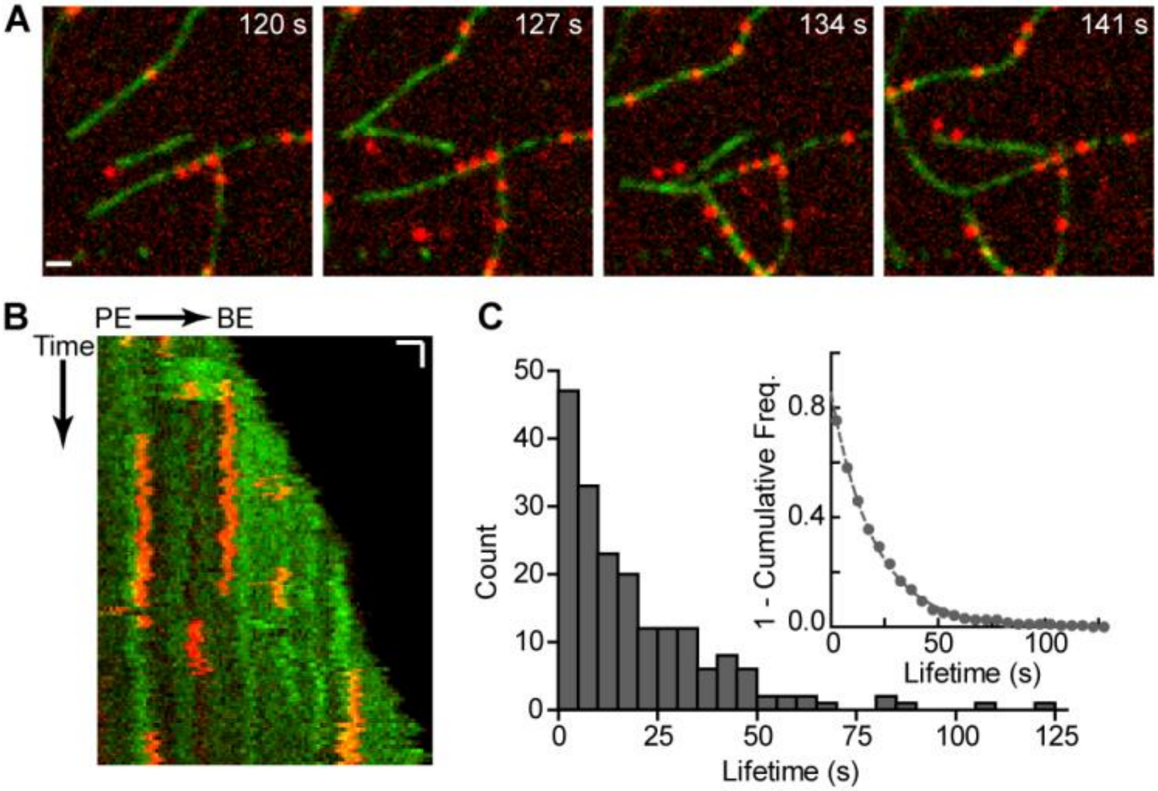

Figure 6. Cortactin Binds Statically to Actin Filaments
(A) smTIRF microscopy images of single cortactin molecules (red) bound to polymerizing actin filaments (green). TIRF reactions contained 1 µM 33% Oregon-Green actin and 2 nM Alexa568-cortactin (residues 1-336). Scale bar: 1 µm. (B) Kymograph showing cortactin molecules bound statically to a polymerizing filament. The barbed end (BE) and pointed end are indicated. Vertical scale bar: 10 s, horizontal scale bar: 1 µm. (C) Histogram showing binned lifetimes of single molecules of cortactin on actin filament sides. Counts were transformed into 1 – cumulative frequency plot (inset) and fit with a single-exponential decay equation to determine the off rate, 0.050 s^{-1}. n = 191.

bound cortactin molecules and fit the cumulative lifetime data to a single exponential decay equation and determined an off rate (k_{off}) of 0.050 s^{-1} (Figure 6C).

Cortactin Specifically Targets Preformed Branch Junctions

Because cortactin does not diffuse along filaments to find branch junctions, we hypothesized that cortactin may target junctions simply by preferentially binding junctions over filament sides. To test this, we visualized single molecules of cortactin with preformed branch junctions. Cortactin added to a TIRF chamber with preformed branches bound to both filament sides and branch junctions (Figure 7A, Video 3). The off rate of cortactin for branch junctions was 0.034 s^{-1}, almost two-fold slower than the off rate for preformed filament sides measured from the same reaction (0.063 s^{-1}) (Figure 7B). Interestingly, 30% of the 270 tracked cortactin molecules were bound to branch junctions even though branches made up only ~0.13% (68 branch junctions versus ~53,000 filament side binding sites) of total cortactin binding sites (Figure 7C,D). This suggests that cortactin binds with a significantly higher affinity to branch junctions than filament sides. A two-fold change in the off rate is unlikely to account for this difference. To determine if cortactin binds to branch junctions with a higher on rate than filament sides, we first measured the affinity of cortactin for branch junctions and filament sides using the single-molecule data. We counted the total number of bound cortactin molecules, branch junctions and side binding sites in each frame and calculated the average fraction of cortactin bound over hundreds of frames.

Figure 7 (next page). Cortactin Directly Targets Branch Junctions with a Fast On-rate

(A) smTIRF microscopy images showing interaction of cortactin with preformed branched networks. Reactions were initiated using 1 µM 33% Oregon-Green actin, 5 nM Arp2/3 complex and 30 nM VCA and allowed to proceed for ~ 6 min before flushing a solution containing 1.5 nM Alexa568-cortactin and 0.1 µM actin monomers into the reaction chamber. Single cortactin molecules (red) bound actin filament sides (gray arrows) and branch junctions (blue arrowhead). Large images show a single region of interest with both side and branch binding events. Time after cortactin addition is indicated. Smaller images show examples of complete filament side and branch junction binding events. Scale bars: 1 µm. (B) Frequency plot of tracked cortactin lifetimes for molecules bound to filament sides (gray) or branch junctions (blue) and fit with a single exponential decay function. (C) Plot of the total number of tracked cortactin molecules on filament sides (FS) or branch junctions (BJ) (D) Plot of the average number of cortactin filament side or branch binding sites across all analyzed frames. (E) Summary of kinetic and thermodynamic binding constants for each class of binding event.

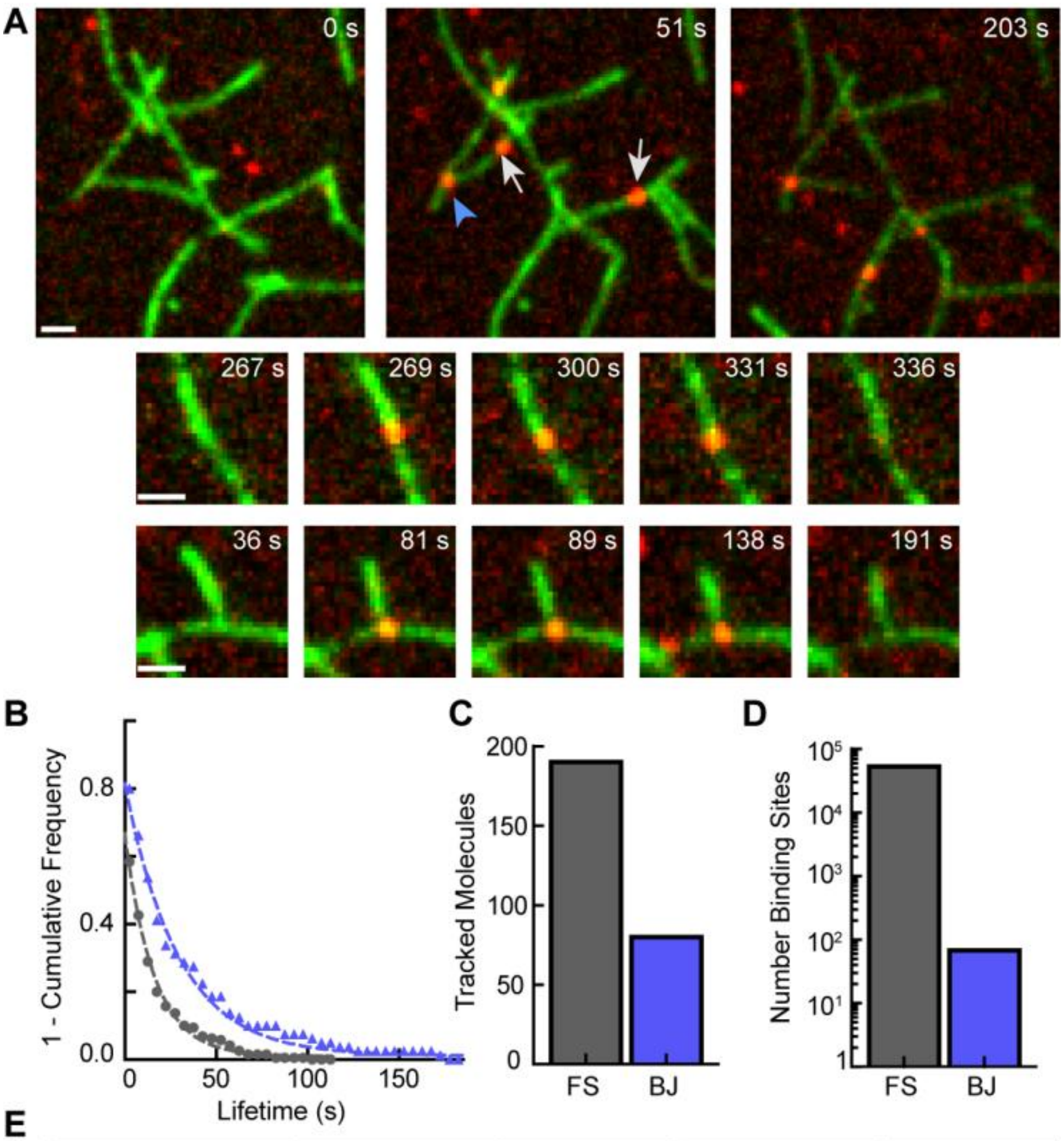

E

Reaction	Lifetime (s)	k_{off} (s^{-1})	k_{on} ($M^{-1} s^{-1}$)	K_d (μM)
Filament Side	15.8	0.063	12100	5.2
Branch Junction	29.2	0.034	2.0×10^6	0.017

Using the average fraction bound, we determined that the affinity of cortactin for branch junctions is ~300-fold greater than for filament sides: 17 nM versus 5.2 μM, respectively (Figure 7E). Using these equilibrium constants and our previously measured off rates, the calculated on rates of cortactin for branch junctions and filament sides are 2.0×10^{6} M^{-1} s^{-1} and 1.2×10^{4} M^{-1} s^{-1}, respectively. Our data show that cortactin targets branch junctions by binding over two orders of magnitude more tightly to junctions than filament sides. High affinity binding to branch junctions is accomplished through a ~160-fold increase in the on rate and further amplified by a ~2-fold decrease in the off rate. These data explain how cortactin can specifically target nascent branch junctions to displace N-WASP.

Cortactin Remains at the Branch Junction during Daughter Filament Elongation

The obligatory displacement model predicts that cortactin can target nascent branch junctions, displace N-WASP, and remain bound to the branch junction without blocking elongation of the new (daughter) filament (Figure 5B). To test this prediction, we visualized single-molecules of cortactin in a reaction during active branching nucleation. We observed multiple instances (n=66) in which cortactin bound to the side of a filament where a daughter filament was later nucleated (Figure 8A,B; Video 4 and 5). In each instance, cortactin remained bound to the branch junction after nucleation, consistent with the predictions of the obligatory displacement model. The average lifetime at the junction after nucleation was 62 s, 2.1-fold longer than the average lifetime of cortactin binding to a preformed branch junction (Figure 8C). The average lifetime before nucleation was 6.5 s. While the accuracy of pre- and post-nucleation lifetime measurements is limited by our ability to resolve newly formed daughter filaments, the data clearly indicate that cortactin stays bound to the junctions long after nucleation. We note that in a TIRF chamber with active branching, cortactin bound existing branch junctions with an average lifetime of 29.5 s, the same lifetime found using preformed filament reactions (29.1 s). Interestingly, the lifetime of cortactin molecules on filament sides was 2.0-2.5-fold lower (8.0 s) than with preformed filaments or polymerizing filaments in the absence of Arp2/3 complex. We cannot currently explain this result, but speculate that it may be due to conformational changes in the filament caused by Arp2/3 complex binding.

These data show that cortactin remains at the branch junction during and after nucleation, but do not allow us to eliminate the possibility that NtA disengages from Arp2/3 complex during elongation while the actin filament binding repeats hold cortactin at the junction. To test this, we labeled an NtA fragment (residues 1-48) with Alexa-568 and visualized it during branching reactions. Single-molecules of NtA were observed bound to existing branch junctions and to nascent branches from which new daughter filaments nucleated (Figure 8C and Video 6). These data indicate that NtA can directly

---

Figure 8 (next page). Cortactin Remains at the Branch Junction during Daughter Filament Elongation
(A) smTIRF microscopy images of polymerizing branch networks containing 1 µM 33% Oregon-Green actin, 5 nM Arp2/3 complex, 50 nM VCA and 2 nM Alexa568-cortactin (red). Images show filament side (gray arrow), existing branch junction (blue arrowhead) and nascent branch junction (yellow arrow) cortactin binding events. (B) Montage from reaction described in panel A showing a single event in which cortactin binds to a filament side, a new branch is nucleated, and cortactin remains bound during elongation. (C) Average lifetimes for each binding class from reaction described in panel A. Error bars represent error of the fit. (D) Image montage showing NtA (yellow arrow) remains bound for ~4.5 s after daughter filament nucleation before dissociating. The reaction contained 1 µM 33% Oregon-Green actin, 10 nM Arp2/3 complex, 350 nM VCA and 10 nM Alexa568-NtA(1-48). Scale bars: 1 µm.

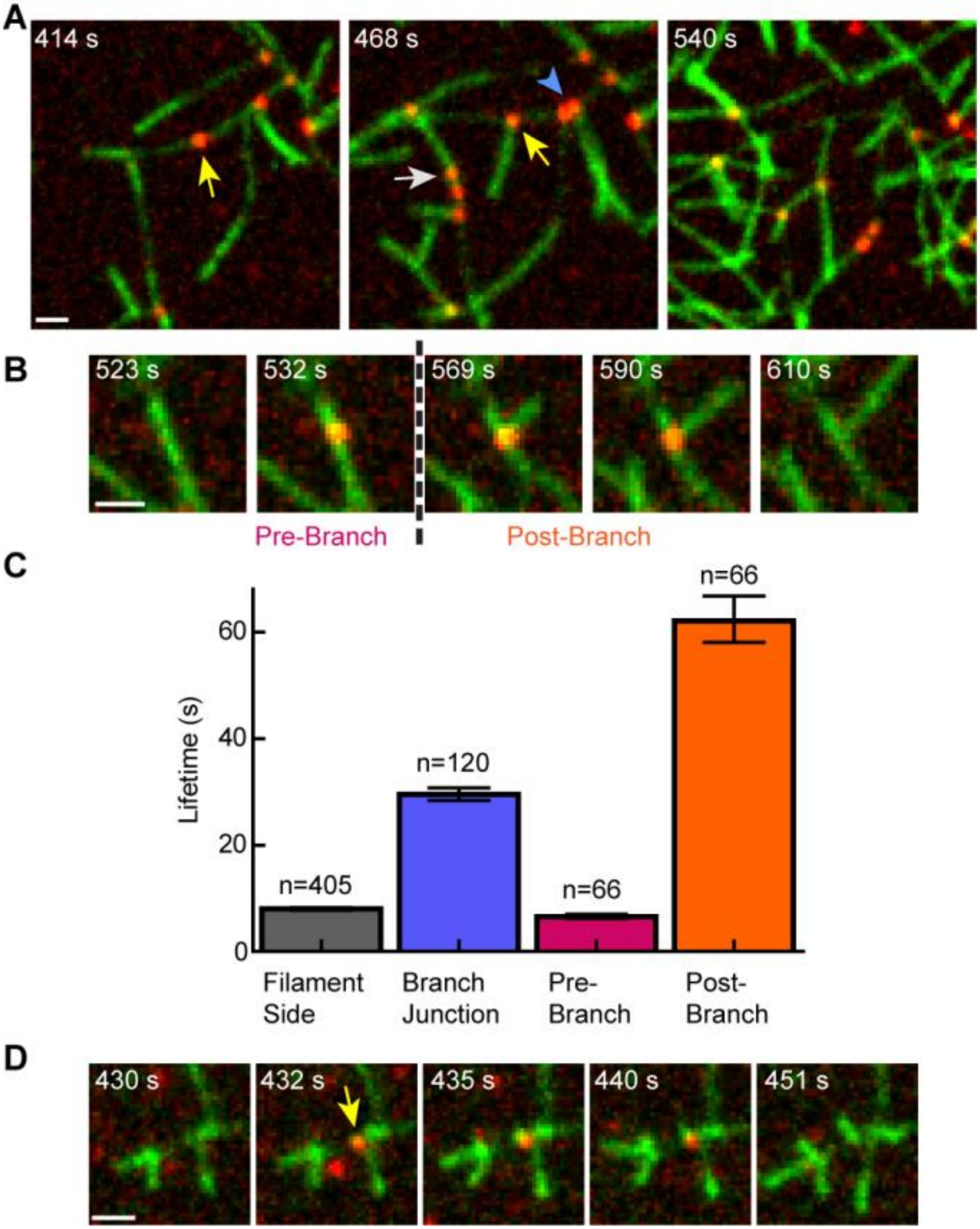
A
414 s
468 s
540 s
B
523 s
532 s
569 s
590 s
610 s
Pre-Branch
Post-Branch
C
Lifetime (s)
0
20
40
60
n=405
n=120
n=66
n=66
Filament Side
Branch Junction
Pre-Branch
Post-Branch
D
430 s
432 s
435 s
440 s
451 s

engage Arp2/3 complex after and during branch nucleation and that it does not block daughter filament elongation. This observation is consistent with pyrene-actin polymerization assays showing NtA does not inhibit nucleation even at high micromolar concentrations (Figure 3E) (Weaver et al. 2002).

An Obligatory Displacement Model Can Account for the Influence of Cortactin in Pyrene-actin Polymerization Assays

Given the biochemical evidence in support of the displacement mechanism, we next built a mathematical model to determine if obligatory displacement could account for the synergy we observed in our bulk polymerization assays. This model was similar to the recruitment model described above, but included additional reactions to account for cortactin interactions with filament sides and at nascent branch junctions (Figure 9A and Supplemental Figure 1). We used the kinetic rate constants determined from our single-molecule experiments to describe these reactions, and assumed that cortactin binds to the nascent branch junction with the same rate constants as mature branch junctions. Following cortactin binding to the nascent branch junction, we added a cortactin-mediated displacement activation step (k_{dis}) analogous to the GST-VCA-dependent activation step (k_{nuc}). Full time courses of pyrene-actin polymerization at a range of cortactin concentrations were fit with the new model, allowing only k_{dis} and k_{fil_on} to float while k_{fil_off} was constrained by the previously measured K_d value (Figure 9B). This model fit the experimental data well (Figure 9B,C). A plot of the half time to reach equilibrium ($t_{1/2}$) versus cortactin concentration indicated that $t_{1/2}$ decreased identically in both the model and the experimental data, and both showed a $t_{1/2}$ of about 80 s at

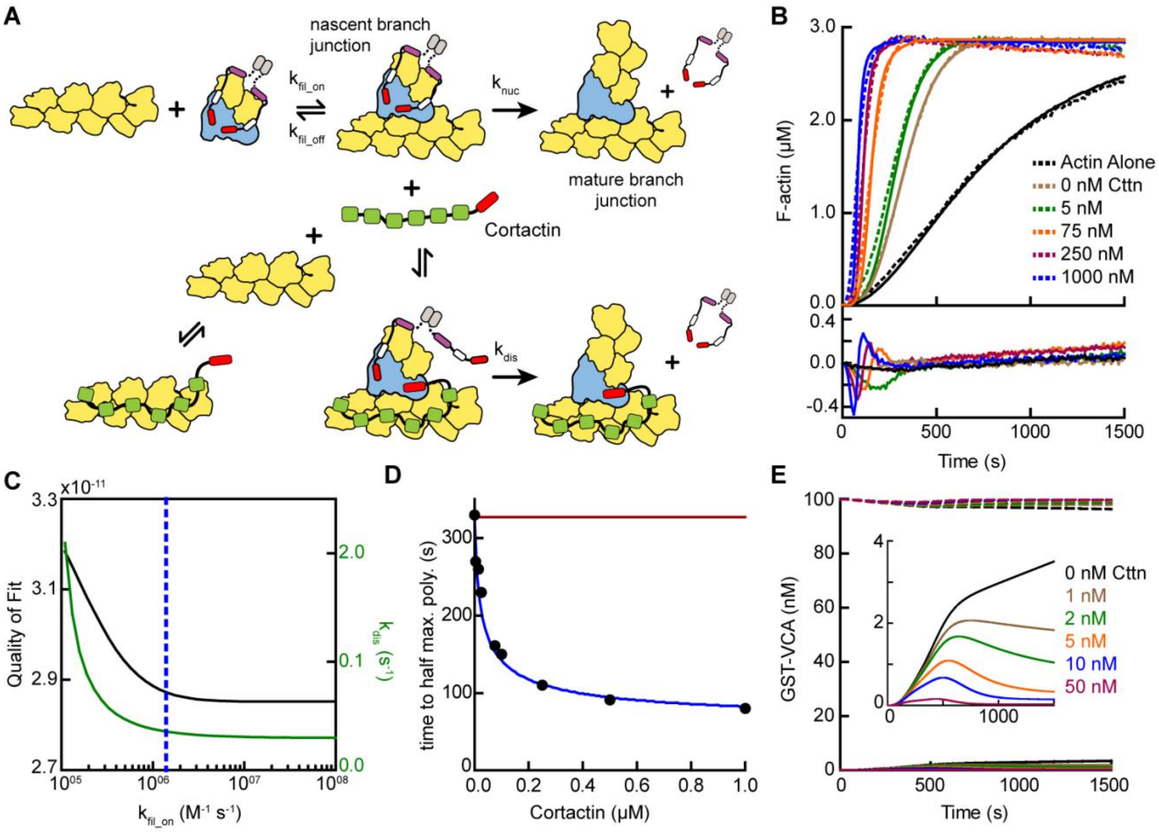

Figure 9. Mathematical Model of the Obligatory Displacement Mechanism of Cortactin-mediated Synergy

(A) Cartoon pathway of key reactions describing cortactin-mediated displacement of GST-VCA. (See supplemental materials for full model) (B) Pyrene-actin polymerization time courses of Arp2/3 complex activated by GST-VCA and cortactin with simulated fits based on an obligatory displacement mechanism of synergy. Dashed lines show experimental data and solid lines show simulated fits after optimization of the two floating parameters, k_{fil_on} and k_{disp}. Residuals are shown in lower panel. Reactions contained 3 µM 15% pyrene-actin, 20 nM Arp2/3 complex, 100 nM GST-VCA and indicated concentrations of cortactin. (C) Plot of quality of fit (black) and resulting optimized k_{disp} (green) versus k_{fil_on}. Blue dashed line indicates minimum threshold k_{fil_on} value of 1.4×10^6 M^{-1} s^{-1}. Quality of fit was calculated by a mean-weighted residual sum of squares. (D) Plot of half time to equilibrium for reactions in panel A (black circles) versus a simulation of the obligatory displacement model (blue line) or the recycling model (red line). (E) Plot showing concentration of free GST-VCA (dashed lines, includes any species of GST-VCA not bound to a branch junction) and sequestered GST-VCA (solid lines, includes any species bound at nascent or mature branch junction) versus time in simulations of the recycling model run at a range of cortactin concentrations. Insert shows magnification of a section of the plot, highlighting the concentration of sequestered GST-VCA as a function of cortactin concentration.

saturating cortactin (Figure 9D). As in the simulations of reactions without cortactin, k_{fil_on} had a minimal threshold value, but in these simulations the minimum value was ~500-fold greater, 1.4 x 10^6 M^{-1} s^{-1} (Figure 9C). Above the threshold, the optimized value for displacement activation (k_{dis}) was 0.036 s^{-1}, ten-fold higher than the activation step in the absence of cortactin, k_{nuc} (Figure 9C). The simplifications and assumptions made in the construction of the model limit the precision of the optimized values in representing the true microscopic rate constants. Nevertheless, the kinetic pathway of the obligatory displacement model fits the experimental data well, indicating that this model can explain synergy.

A previously proposed model for cortactin-mediated synergy hypothesized that cortactin displaces GST-VCA from the Arp2/3 complex during elongation of the daughter filament instead of before or during nucleation (Siton et al. 2011). In this model, called the recycling model, cortactin is hypothesized to prevent GST-VCA from being sequestered at branches, which could slow polymerization by limiting the concentration of GST-VCA in solution available to activate Arp2/3 complex. A key prediction of this model is that the concentration of free GST-VCA limits branching nucleation rates. To test this mechanism, we simulated recycling by forcing GST-VCA to remain bound after nucleation and introducing a single binding reaction whereby cortactin returns the branch junction-bound GST-VCA to the pool of non-sequestered GST-VCA (Figure 3-figure supplement 1). We attempted to use this model to fit time courses of pyrene-actin polymerization containing Arp2/3 complex, GST-VCA and a range of concentrations of cortactin. The recycling displacement model could not fit the data because increasing concentrations of cortactin had no influence on modeled polymerization rates. To determine why, we plotted the concentration of sequestered GST-VCA during the modeled time courses at various concentrations of cortactin. In the absence of cortactin, only 3.8% of the total GST-VCA was sequestered at the end of the reaction (Figure 9E). Addition of cortactin reduced the concentration of sequestered GST-VCA, but did not influence the polymerization rate because the free GST-VCA concentration did not limit the rate of the reaction. Therefore, the recycling model cannot account for the synergistic activation of Arp2/3 complex we observe in our assays.

DISCUSSION

Here we dissect the mechanism of synergistic activation of Arp2/3 complex by cortactin and N-WASP. Our data support an obligatory displacement model in which cortactin specifically targets nascent branch junctions to displace GST-VCA, thereby accelerating nucleation (Figure 9). In this model, GST-VCA, two actin monomers and Arp2/3 complex assemble on the side of a filament, creating a nascent branch junction. Cortactin targets the junction, making a multivalent interaction with Arp2/3 complex and the adjacent mother filament. At the nascent branch junction, NtA can compete with CA at the Arp3 binding site on the complex, as previously reported (Weaver et al. 2002; Padrick et al. 2008). Release of one CA speeds release of the GST-VCA, allowing nucleation and elongation to proceed. Importantly, NtA does not block elongation, as we demonstrate by visualizing labeled NtA at nascent branch junctions during nucleation/elongation. Rather, NtA stays engaged with Arp2/3 complex and the repeats stay bound to the mother filament after elongation, allowing cortactin to remain tightly bound to the mature branch junction. Our smTIRF measurements are consistent with immuno-gold-labeled electron micrographs and three-dimensional EM reconstructions that show cortactin remains at the mature branch junction (Cai et al. 2008; Egile et al. 2005). The obligatory displacement model is also consistent with the observation that cortactin competes weakly with GST-VCA in the absence of filaments, but strongly in their presence (Uruno et al. 2003).

A key aspect of the obligatory displacement model is that GST-VCA must be released before nucleation. Our mutational analyses support this requirement, since a mutation in the V region that decreased its affinity for actin increased the rate of nucleation at saturating GST-VCA, suggesting weakened interactions with the nascent branch junction can increase nucleation rates. Additional evidence comes from recent single-molecule TIRF experiments, which show that VCA release precedes elongation of the daughter filament (Martin, Welch, and Drubin 2006) (Smith et al 2013, in press at eLife). Why release of the type I NPF is programmed into the branching nucleation mechanism, at least in the case of dimerized N-WASP-VCA, is not clear. One possibility is that because WASP/Scar proteins are attached to membranes (Higgs and Pollard 2000), incorporation of the release step into the nucleation mechanism ensures branches are not strongly tethered to the membrane as the growing actin network pushes outward on it. In support of this hypothesis, Akin *et. al.* showed that increasing transient connections between bead-immobilized NPFs and nascent branch junctions decreased bead motility (Akin and Mullins 2008). Our data suggest cortactin could stimulate release of a membrane bound NPF from Arp2/3 complex to regulate network-substrate connections, providing an additional mode by which cortactin can control the dynamics of branched actin networks. Recent experiments showed that addition of cortactin to a solution of

GST-VCA coated beads increased the bead motility to an extent unlikely to be accounted for simply by an increased nucleation rate (Siton et al. 2011). Therefore, cortactin may stimulate branched network dynamics both by increasing nucleation rates and by preventing stalling caused by tight membrane-network attachments.

A second key aspect of the displacement model is that cortactin must be able to target nascent branch junctions and avoid being non-productively sequestered along filament sides. Our single-molecule experiments revealed the kinetic basis for targeting. Instead of diffusing along filament sides to find branch junctions, cortactin targets branches using a ~300-fold increased affinity over filament sides. Most of the binding preference arises from an unusually slow on rate (12100 M^{-1} s^{-1}) of cortactin for filament sides. This on rate is 200-2000-fold slower than for most other actin filament binding proteins, and is unlikely to be diffusion limited (Kovács et al. 2004; De La Cruz et al. 1999; Wegner and Ruhnau 1988). Binding may be slow because it requires a conformational change in filaments, in agreement with an electron microscopy reconstruction showing that cortactin binding widens the gap between protofilaments (Pant et al. 2006). Our mathematical model of obligatory displacement did not include reactions in which cortactin binds filament sides before Arp2/3 complex rather than targeting an existing nascent branch junction. While these pathways can be inserted into the model, we note that in the case of the NtA construct, synergy must occur completely through nascent branch targeting, suggesting nascent branch targeting may be the dominant displacement pathway for the full-length protein. Additional multi-color smTIRF experiments will be required to fully map out the kinetic pathways.

We showed the actin filament binding repeats of cortactin are not required for synergy, eliminating an actin filament recruitment mechanism. While it is possible that recruitment operates simultaneously with displacement in full-length cortactin, we observed that saturating concentrations of NtA activated nucleation to the same extent as saturating full-length cortactin, so there is no recruitment component of synergy that cannot be mimicked by NtA. The high concentrations of NtA required for saturation likely reflect the decreased affinity of NtA for the nascent branch junction caused by removal of the actin filament binding repeats. Importantly, cortactin can weakly activate Arp2/3 complex on its own (Weed et al. 2000), and in contrast to synergy, this intrinsic activity requires the filament binding repeats (Uruno et al. 2001). Therefore, filament recruitment may explain the weak intrinsic activity of cortactin observed *in vitro*. Our data are inconsistent with a previously proposed recycling model of synergy, in which cortactin indirectly increases nucleation rates by recycling WASP sequestered at mature branch junctions, freeing it to activate Arp2/3 complex (Siton et al. 2011). Instead, our data indicate that cortactin directly influences nucleation at nascent branch junctions. These biochemical distinctions will have important implications in understanding the influence of cortactin on the regulation of Arp2/3 complex *in vivo*.

In addition to activating Arp2/3 complex, cortactin has been shown to stabilize branch junctions *in vitro (*Weaver 2001*)*. The average lifetime of cortactin at branch junctions was 29.2 s, whereas the lifetime of branches has been reported to be between 8-27 min (Martin, Welch, and Drubin 2006; Mahaffy and Pollard 2006). Given these data, cortactin dissociates from branches much more rapidly than branches disassemble. However, cortactin has a high affinity for junctions (K_D = 17 nM), so it likely dissociates and rebinds branches many times during the life of a branch, even when present at low (nanomolar) concentrations. Therefore, cortactin dynamically stabilizes branch junctions. This mechanism is consistent with FRAP experiments that show cortactin is incorporated into treadmilling networks not just at the leading edge but also throughout the entire network, and exchanges rapidly (Lai et al. 2008). Importantly, *in vivo* treadmilling networks turn over on much shorter timescales than *in vitro* branch lifetimes (Lai et al. 2008; Martin, Welch, and Drubin 2006). In cells, the competition of cortactin with branch disassembly factors like GMF, coronin1B, and cofilin may be more important than the intrinsic branch stabilizing activity of cortactin (Gandhi et al. 2010; Cai et al. 2008; Blanchoin, Pollard, and Mullins 2000).

The mathematical models we present show how rate constants for filament binding by the complex influence the potential of filament recruitment to contribute to activation. Measuring filament on rates has been technically challenging, and a range of values has been reported. Experiments using pyrenyl-Arp2/3 complex from fission yeast yielded a k_{on} of 150 $M^{-1}s^{-1}$ (Beltzner and Pollard 2008), while a k_{on} value of 3×10^3 M^{-1} s^{-1} was calculated for budding yeast Arp2/3 complex from smTIRF experiments, (Smith, Daugherty-Clarke, et al. 2013). Our optimized k_{on} value for bovine Arp2/3 complex was ~1×10^6 $M^{-1}s^{-1}$. Species-specific differences may account for some of the differences in these values, but are unlikely to fully explain them. In single-molecule studies, complications arise from the lack of simple methods to directly measure on rates for filaments (van Oijen 2011). Off rates can generally be determined directly from the lifetimes of the on state, but difficulties arise from the complexity of interactions of Arp2/3 complex with filaments. For example, budding yeast Arp2/3 complex dissociated from filaments with three distinct off rates, indicating a heterogeneous population of dissociating species (Smith, Daugherty-Clarke, et al. 2013). Filament binding rate constants are important for not only understanding how Arp2/3 complex works with type I NPFs like WASP/N-WASP, but also how other regulators control Arp2/3 complex activity by mediating its interactions with filaments. The advent of three-color smTIRF experiments will be critical in allowing us to dissect these interactions.

An important finding of this work is that potent synergy occurs only when the type I NPF is dimerized. We hypothesize that this is because dimerized type I NPFs engage both Arp2/3 complex binding sites to bind tightly to nascent branch junctions, thereby slowing the nucleation step. In our assays, we artificially oligomerized N-WASP, but *in vivo*, N-WASP can oligomerize by association with scaffolding proteins like Nck or BAR domain proteins (P. Li et al. 2012; Suetsugu 2013; Padrick et al. 2008). SCAR/WAVE, another widely expressed type I NPF, has also been shown to oligomerize or cluster on membranes, suggesting it can also act as a higher order oligomer (Gohl et al. 2010). These observations suggest the potential for cortactin-mediated synergy to activate Arp2/3 complex in multiple distinct branched networks in *vivo.* We note that in addition to Arp2/3 complex, cortactin has dozens of other binding partners, including some that influence its ability to regulate branched networks (Kirkbride et al. 2011). For instance, cortactin binding to WIP, an actin momomer binding protein, greatly enhances cortactin-mediated activation of Arp2/3 complex (Kinley et al. 2003). In addition, the SH3 of cortactin binds N-WASP to relieve its autoinhibition, providing an indirect mechanism for cortactin to upregulate branching nucleation (Kowalski et al. 2005). Biochemical dissection of these reactions will allow us to understand precisely how cortactin coordinates branched networks *in vivo*.

MATERIALS AND METHODS

Protein Purification and Labeling

GST-tagged mouse cortactin and cortactin NtA (residues 1-84 or 1-48) (gifts from John Cooper) were overexpressed in BL21(DE3)-RIL *E. coli* and purified using glutathione sepharose, Resource Q ion exchange and size exclusion chromatography columns, in that order. The GST tag was cleaved using TEV protease prior to ion exchange chromatography. Cortactin (residues 1-336) or NtA (1-48) used in smTIRF were prepared for dye labeling by mutating all endogenous cysteines to serine and adding a KCK (Lys-Cys-Lys) tag at the C-terminus. Purified fractions from size exclusion chromatography were reacted with Alexa Fluor 568 maleimide (Molecular Probes) at a molar ratio of 15-20:1 (dye:cortactin) overnight at 4 °C. Free dye was removed by extensive dialysis and a HiTrap desalting column (GE). The concentration of labeled cortactin (1-336) was determined using absorbance at 280 nm with the dye signal subtracted using the 280:575 nm absorbance ratio of free dye. Labeled NtA concentration was estimated by measuring the dye absorbance at 575 nm and assuming that all free dye was removed and 100% of the protein was labeled. LZ-VCA was constructed by inserting the leucine zipper domain of *S. cerevisiae* Gcn4 (residues 250-281, a gift from Alan Hinnebush) and a 21 residue Gly-Ser linker between the TEV protease site and the N-terminus of VCA. All N-WASP-VCA constructs, including N-WASP-VVCA (residues 392-505), were purified as described previously (Hetrick et al. 2013). Bovine Arp2/3 complex, Oregon-Green actin, rabbit muscle actin and pyrene-labeled actin were prepared as previously described (Hetrick et al. 2013).

Pyrene-actin Polymerization Assays

Pyrene-actin polymerization assays were performed and analyzed as described previously (Liu et al. 2011). Fold activation due to cortactin-mediated synergy was calculated by dividing the maximum polymerization rate at a given cortactin concentration by the maximum polymerization rate of the equivalent reaction containing no cortactin. Synergistic activation versus cortactin concentration data were fit to a saturating hyperbolic equation with an added background factor equal to the activity at no cortactin.

Competition Binding Assays

The anisotropy of a solution containing 50 nM Rhodamine-VCA, 150 nM G-actin, 10 mM Hepes pH 7.0, 50 mM KCl, 1 mM $MgCl_2$, 1 mM EGTA, 1 mM DTT, 0.2 mM ATP, 350 nM Latrunculin B and increasing concentrations of VCA or VCA mutants was measured using excitation and emission wavelengths of 530-nm and 574-nm, respectively. Plots of anisotropy versus VCA concentration were fit with a previously described equation (Wang 1995). Binding assays were repeated at least three times. The final reported K_ds are the mean of the individual fits.

TIRF Buffers

The TIRF reaction buffer contained 50 mM KCl, 1 mM $MgCl_2$, 1 mM EGTA, 10 mM Imidazole pH 7.0, 0.5% methyl cellulose cP 400, 1 mM DTT, 0.2 mM ATP, 25 mM glucose, 1 mM Trolox (Sigma-Aldrich), 0.02 mg/mL catalase (Sigma-Aldrich), 0.1 mg/mL glucose oxidase (MP Biomedicals) and 2 mg/mL BSA. Methyl cellulose (2% cP 400) stock was prepared by overnight mixing at 4 °C and then centrifuged for 1 hour at

245,070xg in a table-top ultracentrifuge (Beckman). A stock solution of 5 mg/mL glucose oxidase and 1 mg/mL catalase (GODCAT) was prepared according to manufacturer's instructions in water and stored at -20 °C. A 2x stock of TIRF buffer was prepared by mixing KMEI (50 mM KCl, 1 mM $MgCl_2$, 1 mM EGTA, 10 mM Imidazole pH 7.0), glucose and Trolox and incubating overnight at room temperature to allow for formation of the Trolox quinone derivative (Cordes, Vogelsang, and Tinnefeld 2009). ATP, DTT and the clarified methyl cellulose were added before filtering the mixture through a 0.22 μm filter and storing at -20 °C. Just before use, GODCAT and BSA were added to make the final 2x TIRF buffer stock.

PEGylated TIRF Chamber Assembly and Preparation for Reaction Imaging

Cover slips (no. 1.5) were sonicated for 20-25 minutes in acetone, then 1 M KOH with extensive water rinsing between sonication steps. Cover slips were then briefly washed in methanol before incubating for 30 minutes in a 1% APTES ((3-Aminopropyl)triethoxysilane, Sigma-Aldrich), 5 % acetic acid methanol solution. Aminosilanized cover slips were rinsed with methanol then water and allowed to completely dry. TIRF chambers were assembled by adhering two strips of double-sided tape, separated by 5 mm, along the long axis of an aminosilanized cover slip. A 24 mm wide, 1 mm thick microscope slide was rinsed briefly with ethanol and placed perpendicular across the cover slip such that the middle of the slide and cover slip were aligned. Firm, even pressure was applied to the slide to secure it to the cover slip tape. The resulting assembly contains a 5 mm x 24 mm x 0.1 mm (tape height) reaction chamber with openings on two sides for reaction solution addition and exchange. Solution exchange was performed by using Whatman paper to wick out the chamber solution from one end resulting in the uptake of the new solution into the chamber, from the opposite end.

TIRF reaction chambers were then treated with biotinylated-PEG to create a low binding surface to which actin filaments could be tethered through streptavadin and biotinylated-myosin. A single-use solution of 250-300 mg/mL methoxy PEG succinimidyl succinate (JenKem USA) ~0.1% Biotin PEG NHS Ester was prepared in 0.22 µm filtered 0.1 M $NaHCO_3$ pH 8.3. TIRF chambers were prepared for PEGylation by flowing in 0.1 M $NaHCO_3$ pH 8.3 twice. The PEG solution was then wicked into the reaction chamber and allowed to incubate for 4-5 hours at room temperature, protected from light and in a humidity chamber to prevent the reaction chamber from drying. After PEGylation, filtered water was flowed through the reaction chamber 3-5 times to remove all the unbound PEGs. PEGylated chambers were stored at 4 °C in a light protected humidity chamber for up to one week.

Immediately before imaging, individual TIRF reaction chamber surfaces were prepared by flowing in 50-100 µM streptavidin followed by 0.5 µM biotinylated myosin, which was previously prepared by reacting maleimide-biotin (Thermo Scientific) with full length rabbit myosin II (Cytoskeleton Inc) on ice for 2-4 hours and stored at 4 °C. The chamber was then washed with high then low salt buffer solutions (20 mg/mL BSA, 50 mM Tris pH 7.5 and 600/150 mM NaCl, respectively), followed by two washes with 1x TIRF buffer with GODCAT and BSA (see above). Each solution was allowed to incubate in the TIRF chamber for 5-10 minutes. TIRF actin polymerization reactions were initiated by adding a protein solution containing the protein(s) of interest (Arp2/3 complex, Alexa568-cortactin, VCA) in 1x TIRF buffer to a solution of 6 µM 33%

Oregon-Green actin, pretreated for 60 s with 50 µM $MgCl_2$ and 200 µM EGTA, to give a final reaction solution of 1 µM 33% Oregon-Green actin and the correct concentration of the proteins of interest (see below). The reaction was then wicked into the prepared reaction chamber and imaged as described below.

smTIRF Microscopy

Dual wavelength TIRF images were collected on a Nikon TE2000-U microscope outfitted with a Nikon 100x NA 1.49 TIRF objective, 1.5x auxiliary lens and an EM-CCD camera (iXon3, Andor or Image-EM, Hamamatsu). Argon 488-nm (Dynamic Laser) and solid-state 561 nm (Coherent) lasers were used to excite Oregon-Green and Alexa-568 fluorophores, respectively. Laser beam selection and intensity was controlled using an AOTF (Gooch & Housego) and each beam passed through dual-band (488/561) excitation and dichroic filters (Chroma) before entering the objective. Prior to collection at the EM-CCD, emission signals passed through dual-band dichroic and emission filters (Chroma). Images were acquired using the open source microscopy software, Micro-Manager (Edelstein et al. 2010). Image processing was performed in ImageJ, where each raw image was background subtracted using the rolling ball algorithm with a rolling ball radius of 10 pixels and subsequently smoothed using a Gaussian blur filter with a sigma of 0.5. Unless noted otherwise, TIRF reactions were imaged at a final magnification of 150x with 50 ms and 30-50 ms 561- and 488-channel exposures, respectively. Images were acquired at 561:488 image channel ratios of 5-15:1 and at calculated frame rates of 1-11 frames per second. Specific imaging parameters are indicated in figure or video legends.

Lifetime Analysis

Single molecules were tracked and lifetimes measured using a custom Matlab script (MathWorks). Single cortactin molecules were identified in each 561-channel image using thresholding image segmentation after removal of noise using a band pass filter. Single-molecule trajectories were created by identifying and linking identical molecules between frames using a nearest neighbor algorithm. An assembled trajectory represents a single-molecule and contains a preliminary frame-based lifetime. All identified molecules were filtered based on the following criteria: Molecule cannot be present in the first or last frame of the image acquisition period, molecule cannot have a lifetime of 1 frame, molecule average intensity must be within a standard deviation of the overall molecular average intensity and the molecule must be associated with an actin filament based on filament identification statistics performed on the corresponding 488-channel images. The molecules that passed the filter were manually tracked to verify the initially determined frame lifetime and to identify the binding class (filament side, branch junction, nascent branch). We identified branches manually by visually inspecting movies. Potential branches were examined in multiple frames to verify that they were not overlapping linear actin filaments. Lifetimes were converted from frames to seconds based on calculated frame rates from image time stamps, and binned into 5 second intervals. The cumulative frequency across all bins was calculated and a plot of 1-cumulative frequency versus lifetime (bin) was fit with a single-exponential decay equation to determine the average off rate from which the average lifetime is the reciprocal.

Single-molecule Affinity Determination

Single-molecules of cortactin were identified (see above) and classified into filament side or branch junction binding from 1000 randomly chosen frames of the preformed branch network image acquisition. Start of equilibrium binding was determined from a plot of number of particles versus frame. Number of filament binding sites was calculated for each frame at equilibrium (829 frames) by a custom image processing script run in Matlab, described as follows. For each frame, pixels corresponding to filament fluorescence were identified using image segmentation followed by morphological area opening to remove non-filamentous small fluorescent objects. Pixels corresponding to branch junctions (5 pixels per junction) were subtracted from the total number of pixels and this new number of pixels was divided by 3 (average filament width in pixels) to remove pixels corresponding to the PSF of the filament fluorescence. The final pixel number value was converted to micrometers (1px = 106.7 nm) to yield the total length of actin filaments in the image frame, and further converted to number of subunits using 370 subunits μm^{-1} (Kuhn and Pollard 2005). A 4% error in total filament length was found between using the above algorithm and manual filament tracing on a small subsection of filaments; therefore, the described length calculation algorithm works well for the extensive length measurements needed. The total number of cortactin filament side binding sites was calculated by assuming a cortactin to F-actin subunit stoichiometry of 1:6. The total number of branch junctions was visually counted in each frame. For each frame, the fraction bound of actin for each binding group was calculated by dividing the total number of counted molecules by the total number of binding sites. The affinity for each binding group was calculated, assuming excess ligand conditions (see below), using the equation: $Kd = \frac{[cortactin]}{fraction\ bound} - [cortactin]$, where fraction bound is the average across all analyzed frames and concentration of cortactin is 1.5 nM.

Excess ligand conditions were established using the following calculations. The average area of a reaction chamber is 120 mm^2 and the area of a single image is 2.98 x 10^{-3} mm^2 (512 x 512 pixels at 106.7 nm per pixel), indicating that, in two dimensions, a single image composes 0.00248% of the total chamber area. The average number of cortactin molecules bound to junctions or filaments sides per image frame was 20. Because unbound actin filaments were washed out of the chamber, all binding events occurred on the surface, so this number allows us to account for all actin-bound cortactin molecules in the chamber. Using the chamber-to-image ratio (2.48 x 10^{-5}), this gives an average number of cortactin molecules bound per chamber of 8.06 x 10^5. In the reaction chamber there are 1.08 x 10^{10} cortactin molecules (12 µL of 1.5 nM cortactin) indicating that on average 0.0075% (8.06 x 10^5/1.08 x 10^{10}) of the total cortactin molecules are bound to actin, therefore the free cortactin concentration is essentially equal to its total concentration.

Mathematical Modeling of Arp2/3 Complex Nucleation by GST-VCA Activation with and without Cortactin

To limit the number of floating parameters in our kinetic models, we ran four sets of pyrene-actin polymerization assays, and fit each set to an independent model with a limited number of floating variables (Table 2) For example, to determine rate constants for spontaneous actin filament nucleation, we fit time courses of a range of concentrations of actin polymerizing without additional proteins (Figure 3-figure supplement 1A,B). The optimized rate constants from this model were used to fit sets of pyrene-actin polymerization assays containing additional proteins (GST-VCA, Arp2/3 complex, and cortactin, i.e. reaction sets 1-4). To determine a set of reactions and rate constants that can describe decreased nucleation from GST-VCA-bound actin monomers, we modeled a set of reactions containing a constant concentration of actin and a range of GST-VCA concentrations (Figure 3-figure supplement 1A,C). Table 2 shows each of the four sets of reactions and the simulations of their optimized global fits.

While many of the rate constants for interactions in the branching nucleation reaction are known (Table 1 and 2), we made several assumptions to allow construction of the model. Rate constants of GST-VCA binding to actin monomers were assumed to be the same as monomeric VCA (Marchand et al. 2001). Kinetic rate constants for GST-VCA binding to Arp2/3 complex have not been measured, so we used k_{on} values measured for monomeric VCA and adjusted the k_{off} to account for the previously measured tighter binding of GST-VCA to Arp2/3 complex (Padrick et al. 2008). We decreased the k_{on} of actin for GST-VCA bound to Arp2/3 complex and increased the k_{off} of GST-VCA:actin from Arp2/3 complex to account for competition between the complex and C for actin binding (Kelly et al. 2006). We modeled the Arp2/3 complex activating nucleation step (k_{nuc}) by converting the nascent branch junction of two actin monomers bound to GST-VCA bound to Arp2/3 complex at a filament side to a barbed end which subsequently elongated at 11.6 x 10^6 M^{-1} s^{-1} (Pollard 1986). Pointed end elongation was not included in our simulations, because the actin monomer concentration is low and Arp2/3 complex-mediated nucleation does not create free pointed ends. We assumed GST-VCA dissociates from the branch junction during nucleation (k_{nuc}), except in the recycling model (see main text and Figure 3-figure supplement 1A). For simplicity, the k_{on} of Arp2/3 complex for the sides of filaments was assumed to be unaffected by GST-VCA or GST-VCA and actin monomer binding. For reactions with cortactin, the stoichiometry of cortactin:F-actin subunits was set to 1:6. Rate constants for cortactin binding to filament sides and branch junctions were determined from the single-molecules studies.

Mathematical modeling of pyrene-actin polymerization time courses was performed using COPASI (Hoops et al. 2006). Fluorescence values were converted to actin filament concentrations by assuming 0.1 μM actin was unpolymerized at equilibrium. Optimization of parameters was carried out by simultaneously fitting all traces from a reaction set, using the Levenberg-Marquardt algorithm method in the parameter estimation module. To simulate the influence of actin filament recruitment by cortactin (Figure 3D), we increased the initial concentration of actin filament sides but not ends.

BRIDGE TO CHAPTER III

The work presented in this chapter has established the mechanism of synergistic activation of Arp2/3 complex by the NPFs cortactin and N-WASP. We found that cortactin increases the rate of nucleation by actively displacing N-WASP from the nascent branch junction, thereby accelerating a rate limiting step. In the next chapter, we will investigate the specific features of cortactin and WASP family proteins which allow them to potently synergize with each other.

CHAPTER III

INTERACTIONS WITH ACTIN MONOMERS, ACTIN FILAMENTS, AND ARP2/3 COMPLEX DEFINE THE ROLES OF WASP FAMILY PROTEINS AND CORTACTIN IN COORDINATELY REGULATING BRANCHED ACTIN NETWORKS

Reproduced with permission from Helgeson, L.A., Prendergast J.G., Wagner A.R., Rodnick-Smith M., and Nolen B.J. 2014. *The Journal of Biological Chemistry* 289: 28856-28869. Copyright 2014, The Journal of Biological Chemistry.

INTRODUCTION

Control of actin filament network assembly is required for eukaryotic cells to move, divide and differentiate (Pollard and Cooper 2009). The Arp2/3 complex is one of three major classes of actin regulators capable of *de novo* initiation of new actin filaments, and is unique among actin nucleators in that under most circumstances it creates only branched filaments (Blanchoin, Pollard, and Mullins 2000; Wagner et al. 2013). The activity of Arp2/3 complex is tightly controlled *in vivo*, and there are now approximately a dozen known NPF proteins that bind to the complex and switch on its nucleation activity (Higgs and Pollard 2001; Goley and Welch 2006). NPFs are responsible for regulating assembly of branched actin networks that power a broad range of cellular processes, including endocytosis (Kaksonen, Toret, and Drubin 2006) and protrusion of lamellipodia (Stradal et al. 2004) and invadopodia; the latter of which are actin-based protrusions that allow transformed cells to degrade extracellular matrix during metastasis (Nürnberg, Kitzing, and Grosse 2011). Proper assembly of branched actin networks in these cellular structures frequently requires the coordinated action of multiple NPFs. For example, formation of invadopodia requires the activity of two distinct NPFs: cortactin, and N-WASP (Mizutani et al. 2002; Ayala et al. 2008; Oser et al. 2009). Similarly, multiple NPFs, including the WASP-family protein Wsp1, type I myosins, Pan1, Crn1, Abp1, and Dip1 contribute to Arp2/3 complex activation during endocytosis in yeast (Sirotkin et al. 2010; Galletta, Chuang, and Cooper 2008; Basu and Chang 2011; Liu et al. 2011). Understanding how these distinct NPFs collectively control branched actin assembly is critical to understanding how the actin cytoskeleton mediates complex cellular processes.

Recent evidence suggests that the biochemical mechanisms by which different NPFs turn on Arp2/3 complex influence their ability to coordinately regulate the dynamics of branched actin assembly. N-WASP and other WASP family proteins contain an acidic “A” and central “C” region that binds Arp2/3 complex, and a V (verprolin homology, also called wasp-homology 2, WH2) region that binds monomers (Marchand et al. 2001) (Figure 1A,B). Engineered crosslinking experiments show that actin monomer recruitment by N-WASP stimulates a conformational change in Arp2/3 complex that may be important for nucleation (Hetrick et al. 2013). Like WASP-family proteins, cortactin contains an acidic region that interacts with Arp2/3 complex, but unlike WASP proteins, it contains an actin filament binding domain instead of a V region (Weed et al. 2000; Uruno et al. 2001) (Figure 1A,B). The intrinsic NPF activity of

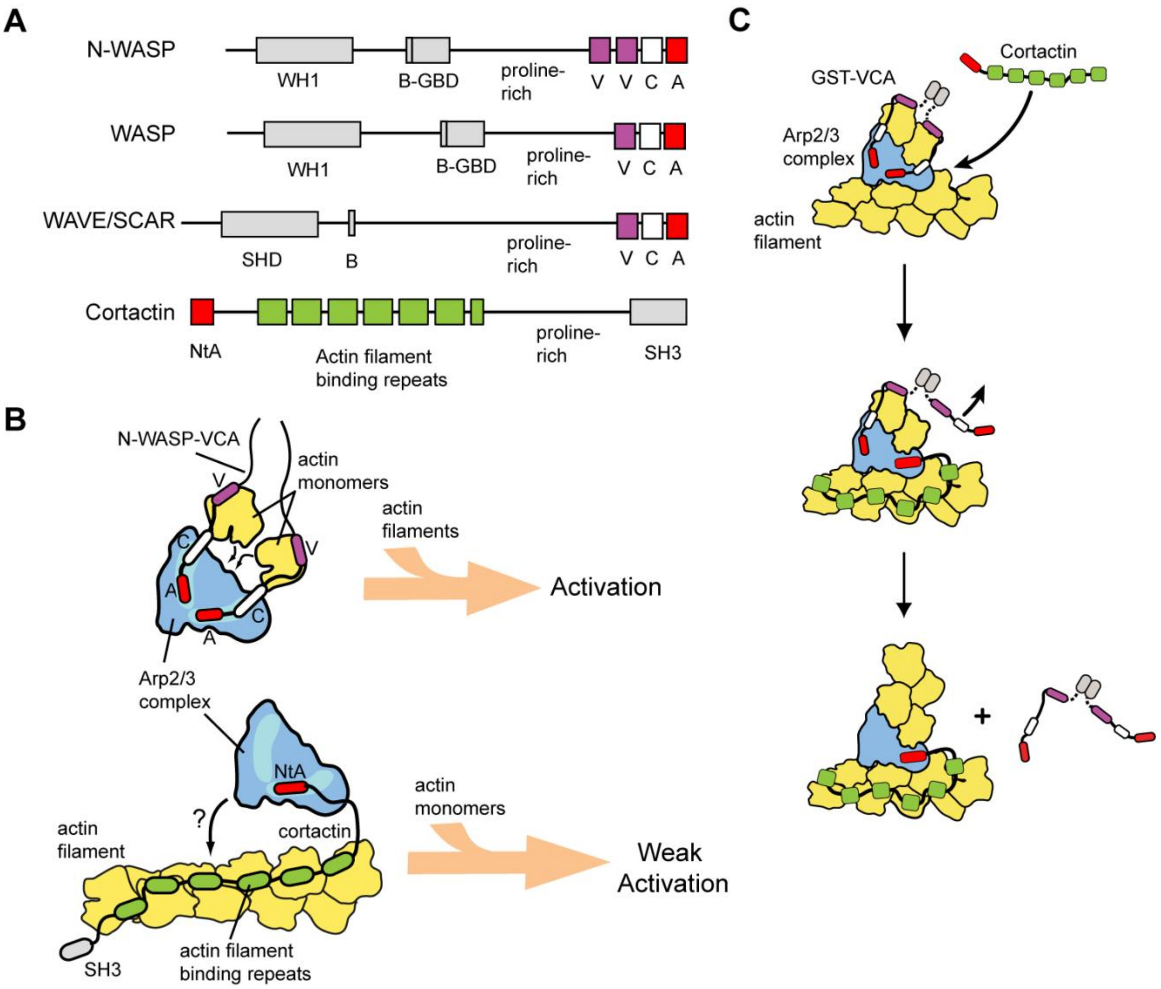
A
N-WASP
WH1
B-GBD
proline-rich
V V C A
WASP
WH1
B-GBD
proline-rich
V C A
WAVE/SCAR
SHD
B
proline-rich
V C A
Cortactin
NtA
Actin filament binding repeats
proline-rich
SH3
B
N-WASP-VCA
V
actin monomers
actin filaments
C
A
V
C
A
Activation
Arp2/3 complex
NtA
?
actin filament
cortactin
actin monomers
Weak Activation
SH3
actin filament binding repeats
C
GST-VCA
Cortactin
Arp2/3 complex
actin filament
+

Figure 1. Overview of Activation of Arp2/3 Complex by Cortactin and N-WASP

A, Domain organization of WASP family proteins and cortactin: WH1, wasp-homology 1; B, basic region; GBD, GTPase binding domain; V, verpolin-homology (also known as WH2, WASP homology 2); C, central region; A, acidic region; SHD, SCAR-homology domain; NtA, N-terminal acidic region; SH3, Src-homology 3. **B**, Schematics of intrinsic NPF activities of N-WASP-VCA and cortactin. Light-blue shaded regions on Arp2/3 complex indicate NPF binding sites. **C**. Schematic of the displacement mechanism of synergistic activation of Arp2/3 complex by cortactin and dimeric N-WASP-VCA (GST-VCA). GST-VCA must be released from the nascent branch for nucleation/elongation to proceed. Cortactin binds to the nascent branch complex at one of the two NPF sites and displaces one CA of the GST-VCA dimer from the Arp2/3 complex (reaction 1), accelerating complete release of GST-VCA (reaction 2) and allowing elongation of the newly nucleated branch filament.

cortactin is weak compared to N-WASP, but importantly, in the presence of N-WASP, it dramatically stimulates branching nucleation (Weaver et al. 2001; Uruno et al. 2003; Siton et al. 2011; Helgeson and Nolen 2013) (Figure 1B,C). The actin filament binding repeats of cortactin potently increase synergy between these two NPFs, and single molecule TIRF microscopy experiments indicate that the repeats allow cortactin to target nascent branch junctions to displace N-WASP and stimulate nucleation (Helgeson and Nolen 2013) (Figure 1C). These observations demonstrate that cortactin and N-WASP have distinct modes of activation of the complex that are controlled by the precise structural mechanism by which each NPF interacts with Arp2/3 complex and actin. Determining how the differences in these interactions tune regulation of the complex by NPFs, alone or in concert, is critical to understanding how branched actin networks are assembled *in vivo*.

The cortactin acidic region (NtA) has generally been posited to be functionally similar to the A region in WASP family proteins. Both A and NtA sequences are characterized by a stretch of multiple acidic residues surrounding a conserved tryptophan which is required for the interaction with Arp2/3 complex (Uruno et al. 2001; Marchand et al. 2001). However, the acidic regions of cortactin and WASP proteins also show several sequence differences, and evidence points to functional implications for these differences. Crosslinking assays showed that the NtA of cortactin competes with N-WASP for binding to Arp3, but unlike N-WASP, it does not bind to the Arp2 subunit (Weaver et al. 2002). It is not known if these differences tailor each NPF for its specific function in activating the complex. For instance, it is not clear if specific structural properties of NtA are required for cortactin to synergize with N-WASP, nor if sequence differences in NtA versus A prevent cortactin (on its own) from activating Arp2/3 complex as potently as N-WASP. Furthermore, while it is known that N-WASP can synergize with cortactin in activating Arp2/3 complex, the precise biochemical properties of N-WASP, including its oligomerization state and affinity for actin monomers, were shown to play critical roles in determining the potency of synergy (Helgeson and Nolen 2013). Therefore, it is unclear if potent synergy with cortactin is a general feature of WASP family proteins and if so, whether the mechanism is conserved. Cortactin colocalizes with WASP family proteins such as N-WASP, WASP, and WAVE in multiple branched actin networks, including in podosomes (Tehrani et al. 2006), at the leading edge of lamellipodia (Martinez-Quiles et al. 2004), and at sites of endocytosis (Taylor, Perrais, and Merrifield 2011). Determining how branched actin is assembled in each of these structures will require an understanding of how each WASP family protein coordinately regulates Arp2/3 complex with cortactin.

A key biochemical difference between cortactin and WASP family proteins is that cortactin binds filamentous actin and WASP proteins bind monomeric actin (Wu and Parsons 1993; Machesky and Insall 1998). Because the actin monomer-binding region of WASP family proteins is required for potent Arp2/3 complex activation (Marchand et al. 2001), its replacement in cortactin with a filament binding domain could explain why cortactin on its own is a weak NPF, but this has not been tested. In fact, the precise role of the actin filament binding region, which consists of 6.5 repeats of a 37 amino acid repeat sequence, is not completely understood, partially due to its multiple biochemical functions. For instance, it increases the potency of cortactin in synergizing with N-WASP and is required for the intrinsic NPF activity of cortactin (Uruno et al. 2001; Helgeson and Nolen 2013). In some studies, the actin filament binding repeats of cortactin have also been also reported to bundle actin filaments (Huang et al. 1997; Cowieson et al. 2008; Yamada et al. 2013). However, bundling has not been studied in the presence of branching, despite the observation that *in vivo*, cortactin colocalizes with Arp2/3 complex within branched actin networks (Kaksonen, Peng, and Rauvala 2000; Weed et al. 2000). Therefore, the influence of cortactin's actin filament binding repeats on the architecture of Arp2/3 complex-nucleated filament networks is not known.

Here we use a combination of biochemical studies and TIRF microscopy to dissect how the Arp2/3 complex- and actin-interacting segments of WASP proteins and cortactin influence their roles in regulating branched actin networks. Our results show that the NtA of cortactin is tailored to synergistically activate the complex with WASP family VCAs, and is biochemically and functionally distinct from the A region of WASP family proteins. The actin filament binding repeats of cortactin allow it to bundle the branched actin filaments it initiates, but bundling is antagonized by N-WASP. In addition, our data show that the intrinsic NPF activity of cortactin is weak because it lacks an actin monomer binding region. Finally, we show that synergy with cortactin is not unique to N-WASP, and that other WASP family proteins, including WASP and WAVE, can cooperate with cortactin to potently activate Arp2/3 complex. Potent synergy requires dimerization of the WASP protein in all cases, suggesting that cortactin displaces each of these WASP proteins from nascent branch junctions to accelerate branching nucleation. These observations have important implications for understanding how cortactin and WASP family proteins independently and coordinately regulate the dynamics of branched actin networks.

RESULTS

Cortactin Is a Weak NPF Because It Cannot Recruit Actin Monomers to Arp2/3 Complex

A critical difference between WASP family proteins and cortactin is that WASP proteins recruit actin monomers to the Arp2/3 complex through their V regions, whereas cortactin lacks a V region and does not bind actin monomers (Uruno et al. 2001). Actin monomer recruitment by WASP is required for NPF activity, and has been shown to stimulate movement of Arp2 and Arp3 into a filament-like (short pitch) conformation that may template nucleation (Marchand et al. 2001; Hetrick et al. 2013; Boczkowska et al. 2008). Therefore, we hypothesized that the weak NPF activity of cortactin is due to its inability to recruit actin monomers to Arp2/3 complex. We tested this hypothesis by creating a chimeric cortactin construct in which the second V region of N-WASP was fused to the N-terminus of cortactin with a 16 amino acid linker (V-cortactin, Figure 2A). Fusion of the V region dramatically increased the activity of cortactin, increasing the maximum polymerization rate 3.1- fold compared to wild type cortactin, demonstrating that cortactin is a weak NPF because it is unable to recruit actin monomers to the Arp2/3 complex (Figure 2B,C). Despite its increased intrinsic NPF activity, the V-cortactin chimera had a 1.4-fold reduced maximum polymerization rate compared to N-WASP-VCA. Recent experiments show that VCA binds to two NPF binding sites on the Arp2/3 complex to recruit two actin monomers and maximally stimulate nucleation (Padrick et al. 2011; Ti et al. 2011; Boczkowska et al. 2014). Cortactin NtA binds to only one of these two sites, so we hypothesized that V-cortactin may be less active than N-WASP

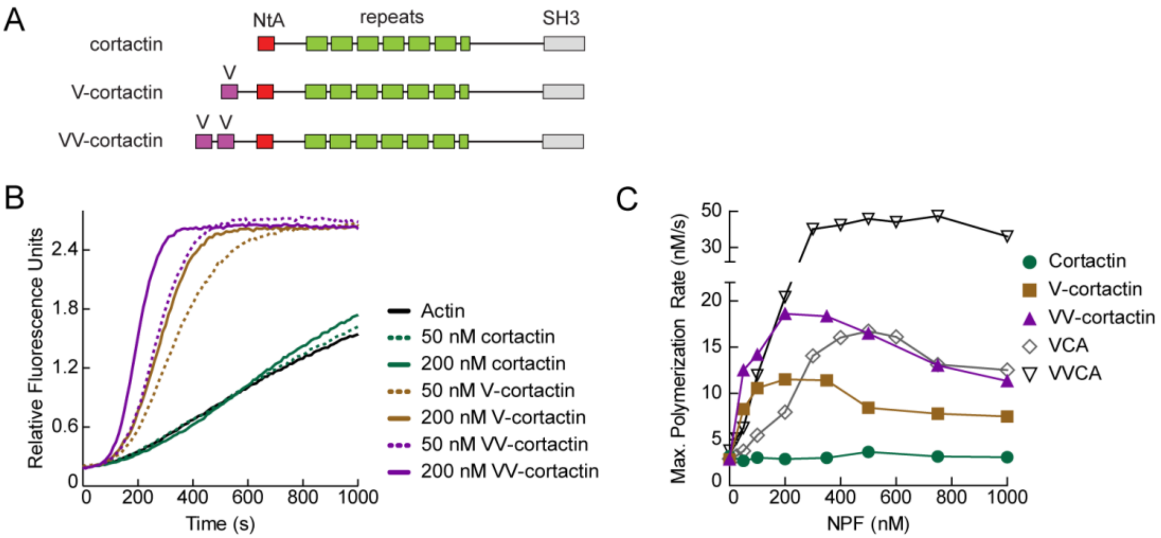

Figure 2. Cortactin Is a Weak NPF Because It Cannot Recruit Actin Monomers to Arp2/3 Complex

A, Domain organization of wild type cortactin and N-terminal V-region fusions. **B**, Pyrene-actin polymerization time courses showing Arp2/3 complex activation by cortactin, V-cortactin or VV-cortactin. Reactions contain 3 µM 15% pyrene-actin, 40 nM Arp2/3 complex and indicated concentrations of cortactin constructs. **C**, Maximum polymerization rate versus NPF concentration for N-WASP VVCA, N-WASP VCA, cortactin, V-cortactin and VV-cortactin. Reactions conditions were as described in B. Maximum polymerization rates were calculated as previously described (Liu et al. 2011).

because it cannot simultaneously recruit two monomers to the complex (Weaver et al. 2002). To test this hypothesis, we prepared a VV-cortactin fusion, in which the tandem V region of N-WASP was appended to the N-terminus of cortactin (Figure 2A). VV-cortactin activated the Arp2/3 complex 1.6-fold more potently than V-cortactin, and to a similar extent as N-WASP-VCA, with a maximum polymerization rate at saturation of 19 nM/s (Figure 2C). Together, these data demonstrate that differences in the actin binding properties and not the Arp2/3 complex interacting regions of cortactin and N-WASP explain their intrinsic potency as NPFs. An important question will be to determine how, in both NPFs, increasing the number of monomer binding regions from one to two increases potency, a property previously reported for N-WASP (Yamaguchi et al. 2000).

Cortactin Bundles Branched Actin Filaments to Create Actin Networks Distinct from N-WASP-activated Arp2/3 Complex

Low speed copelleting assays, negative staining electron microscopy, and small angle X-ray scattering showed that cortactin bundles spontaneously nucleated (unbranched) actin filaments (Huang et al. 1997; Cowieson et al. 2008; Yamada et al. 2013). Cortactin localizes with Arp2/3 complex in branched actin networks *in vivo* (Kaksonen, Peng, and Rauvala 2000) and specifically targets branch junctions *in vitro* (Helgeson and Nolen 2013), but it is uncertain if cortactin can bundle branched actin filaments, or how its nucleation-promoting and bundling activities might together influence branched actin filament architectures. Therefore, we used TIRF microscopy to directly visualize GST-N-WASP-VCA- or cortactin-mediated branching nucleation. GST-N-WASP-VCA activated Arp2/3 complex created both primary branches that grew from spontaneously nucleated filaments and secondary or higher order branches from Arp2/3-nucleated filaments, creating dense dendritic networks (Figure 3A top panel, Video 1). In contrast, cortactin-mediated branching formed dramatically different networks, in which branching was less dendritic, and instead consisted of a few daughter filaments elongating from mother filaments that were frequently bundled. In many instances, daughter filaments growing away from the mother filament (or mother filament bundle) collided with a nearby

---

Figure 3 (next page). Cortactin Bundles Branched Actin Filaments to Form Actin Networks Distinct from N-WASP
A, Time lapse TIRF microscopy images of branched networks assembled by Arp2/3 complex activated by either GST-N-WASP-VCA (top panels) or cortactin (residues 1-336) (bottom panel) at the indicated concentrations. Arrowheads indicate an example of daughter filament bundling. **B**, Time lapse TIRF microscopy images of branched networks assembled by Arp2/3 complex activated by cortactin alone (residues 1-336) (top panel) or cortactin and GST-N-WASP-VCA (bottom panel). **C**, Quantification of the fraction of actin filaments in bundles from reactions in B as a function of time. All TIRF reactions contain 1.5 µM 33% Oregon-Green actin. Scale bars are 2 µm.

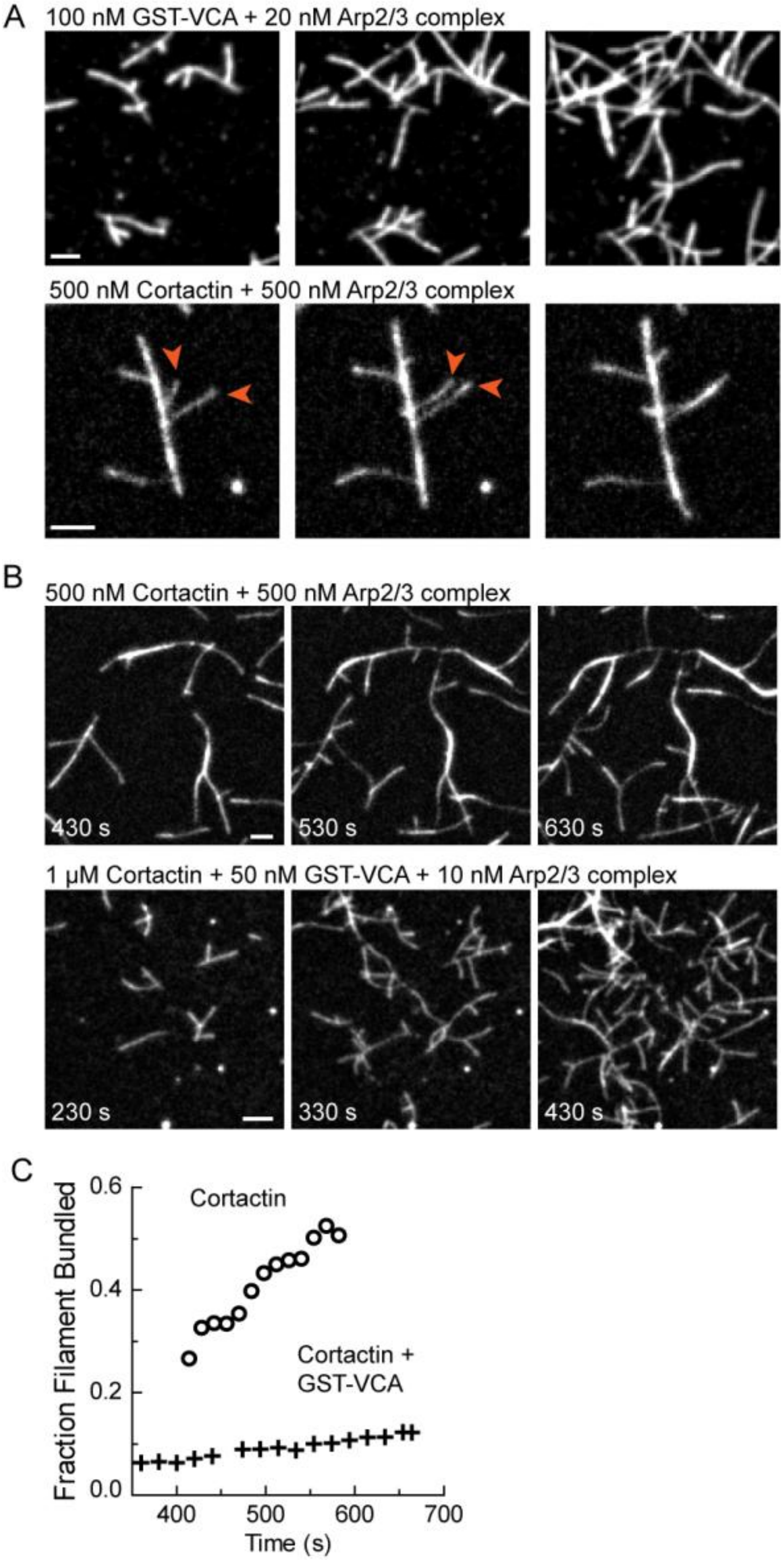
A
100 nM GST-VCA + 20 nM Arp2/3 complex
500 nM Cortactin + 500 nM Arp2/3 complex
B
500 nM Cortactin + 500 nM Arp2/3 complex
430 s
530 s
630 s
1 μM Cortactin + 50 nM GST-VCA + 10 nM Arp2/3 complex
230 s
330 s
430 s
C
Fraction Filament Bundled
0.0
0.2
0.4
0.6
Cortactin
Cortactin +
GST-VCA
400
500
600
700
Time (s)

“sister filament” to form daughter filament bundles (Figure 3A bottom panel, Video 2). These data show that the bundling and branching activation activities of cortactin together create a network of interconnected bundles distinct from N-WASP-mediated branching.

Electron micrographs show actin filaments in lamellipodia and at sites of endocytosis are dendritic, and more similar to the N-WASP-initiated networks we observed in our TIRF images than the bundled cortactin-mediated networks (Svitkina and Borisy 1999; Collins et al. 2011). This presents an apparent discrepancy, as cortactin localizes to both of these actin-based structures (Wu and Parsons 1993; Cao et al. 2003). To resolve this apparent discrepancy, we examined the architecture of branched networks created in the presence of both N-WASP (GST-N-WASP-VCA) and cortactin. Reactions containing both NPFs showed highly dendritic networks, similar to those created with N-WASP-VCA alone (Figure 3B). Even at high concentrations of cortactin, which normally cause dramatic bundling (video 3), very little bundling was observed when GST-N-WASP-VCA was present (Figure 3B,C, video 4). These data suggest that high rates of branching nucleation antagonize bundling, and that the architectures of cortactin-containing actin networks *in vivo* will be modulated by the activities of the other NPFs present.

Cortactin Monomers Bundle Parallel and Antiparallel Actin Filaments

To better understand the bundling mechanism, we directly observed bundling of unbranched elongating filaments by cortactin using two color TIRF microscopy. For these assays, we used an Alexa-568-labelled C-terminally truncated construct of cortactin that lacks the proline-rich region and the SH3 domain. This construct has the same NPF activity as full-length cortactin (Helgeson and Nolen 2013). Multiple pathways to bundling were observed. In some events, actin filaments with bound fluorescent cortactin puncta collided at an acute angle with a second filament (Figure 4A, video 5). The two filaments then either zippered together, or the shorter end of the Y-shaped structure bound to the side of the longer filament, creating a gap that closed from each side. In other cases, filaments aligned along their lengths collided and immediately snapped together, and in others, two filaments attached to the surface elongated into each other (Figure 4A, video 6,7). Using fiduciary marks to identify barbed ends, we observed both parallel and anti-parallel bundling events (Figure 4A). We hypothesized that bundling could occur by cortactin oligomerization, which would allow the actin filament binding region from each cortactin molecule to contact a separate filament. Alternatively, a cortactin monomer could utilize a single set of filament binding repeats to bridge two

---

Figure 4 (next page). Cortactin Monomers Bundle Parallel and Antiparallel Actin Filaments

A, Two-color time lapse TIRF microscopy images of cortactin molecules (magenta) bundling actin filaments (green) in either parallel (top panels) or antiparallel (bottom panels) orientations with respect to their barbed ends (arrowheads). Colocalized signals are white. Reaction contains 1.5 µM 33% Oregon-Green actin and 10 nM Alexa568-cortactin (1-336). **B**, Graphic representation of proposed cortactin bundling mechanism. **C**, Count of fluorescent puncta corresponding to the indicated number of observed photobleaching steps from a reaction of 1 nM biotinylated Alexa568-cortactin attached to a streptavidin coated cover slip. Inset, plot of fluorescence intensity versus time for three different monomeric Alexa568-cortactin molecules during photobleaching experiment. **D**, Frequency plot of tracked cortactin lifetimes for molecules bound to single (gray circles, n=99) or bundled (black crosses, n=49) filaments from the reaction in panel A. Data were fit with a single exponential decay function to yield off-rates of 0.09 ± 0.01 s^{-1} and 0.07 ± 0.01 s^{-1} for single and bundled filaments, respectively, errors are 95% confidence interval from fit. **E**, Number of cortactin molecules bound per micrometer of actin filament for molecules bound to either single (circles, n=99) or bundled (crosses, n=48) filaments from reaction in panel A. Black bars represent mean; single=0.85 ± 0.28 and bundled =0.62 ± 0.17 cortactin molecules per micrometer of actin filament, errors are S.D..

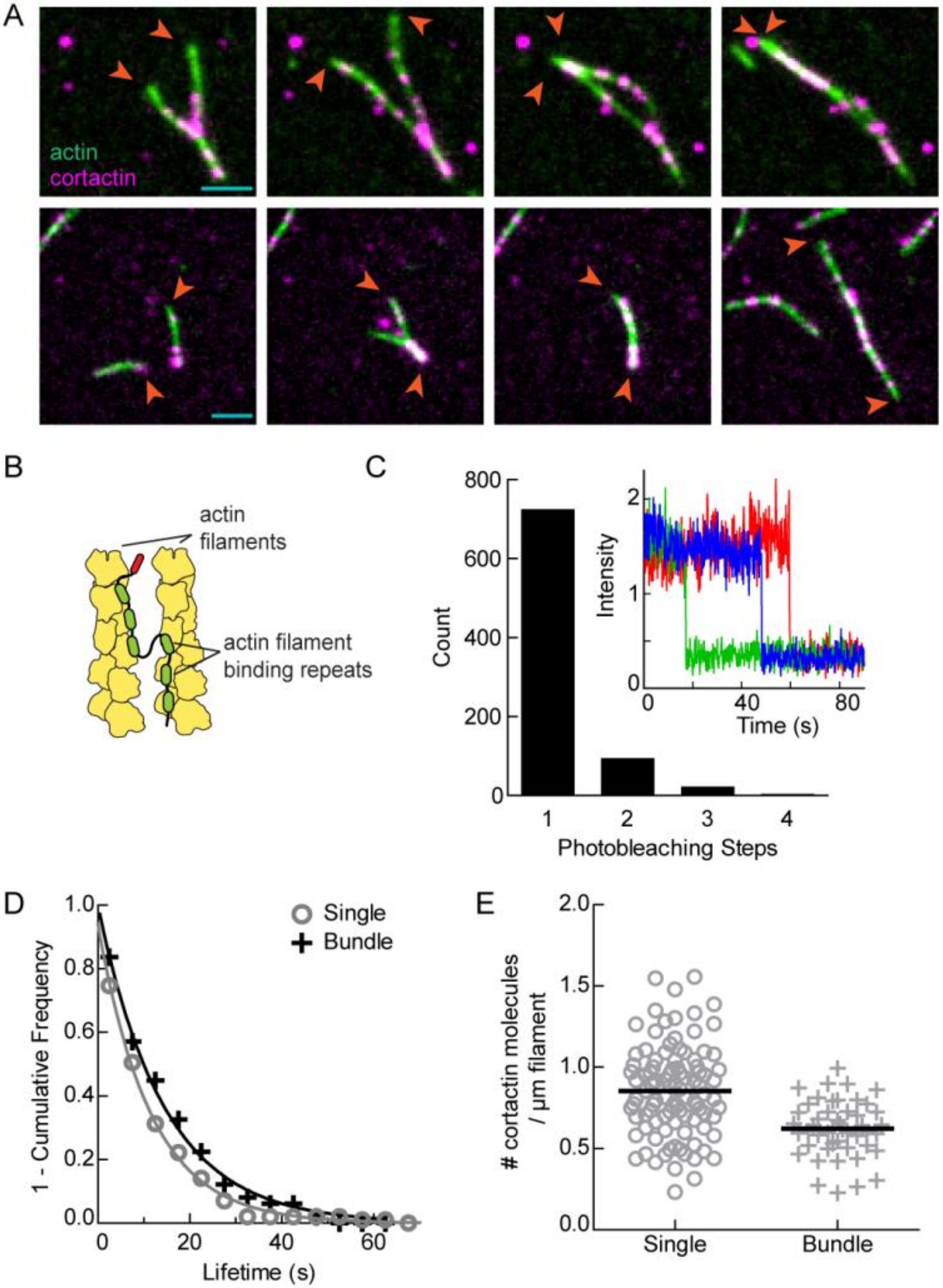
A
actin
cortactin
B
actin filaments
actin filament binding repeats
C
Count
800
600
400
200
0
1
2
3
4
Photobleaching Steps
Intensity
2
1
0
0
40
80
Time (s)
D
1 - Cumulative Frequency
1.0
0.8
0.6
0.4
0.2
0.0
0
20
40
60
Lifetime (s)
Single
Bundle
E
# cortactin molecules / µm filament
2.0
1.5
1.0
0.5
0.0
Single
Bundle

actin filaments (Figure 4B). To distinguish between these possibilities, we measured the oligomerization state of cortactin by attaching it to the imaging surface through biotinylation and observing its photobleaching behavior. The vast majority of fluorescent puncta bleached in a single step, demonstrating that cortactin is a monomer, and supporting a model in which monomers of cortactin mediate bundling using a single set of repeats to bridge two filaments (Figure 4C). To determine how bundling influences the interactions of cortactin with actin, we measured the lifetimes of cortactin bound to single filaments versus bundles. The off rate of cortactin for filaments was nearly identical in each scenario (Figure 4D). In addition, the number of cortactin molecules bound per filament length was nearly identical for cortactin bound to single versus bundled filaments (Figure 4E). These observations indicate that bundling does not dramatically alter the interactions between cortactin and actin filaments.

The Arp2/3 Complex Binding Region of Cortactin Has Unique Biochemical Properties Required for Synergistic Activation

To better understand how functional segments of Arp2/3 complex activators influence branching nucleation, we next focused on the Arp2/3 complex interacting regions of N-WASP and cortactin. Specifically, we asked if features of the Arp2/3 complex binding regions in these NPFs influenced their ability to coordinately regulate the complex. Cortactin and N-WASP have been shown to synergistically activate the complex using a displacement mechanism, in which cortactin increases the nucleation rate by binding to the complex at nascent branch junctions and displacing N-WASP-VCA (Helgeson and Nolen 2013) (Figure 1C). This model is consistent with the observation that the NtA region of cortactin is sufficient for synergy with N-WASP and competes with N-WASP-CA for binding to the Arp3 subunit (Weaver et al. 2002; Helgeson and Nolen 2013). It is also consistent with the observation that N-WASP must be released from the complex at nascent branch junctions before nucleation, while cortactin can remain bound throughout nucleation and elongation (Smith, Padrick, et al. 2013; Helgeson and Nolen 2013). Structural modeling suggests the V region in WASP-VCA blocks the barbed ends of recruited actin monomers from interacting with actin monomers, explaining why VCA must be released (Chereau et al. 2005). These results suggest that any interaction that can promote displacement of VCA from the nascent branch junction without blocking incoming actin monomers might synergistically activate the Arp2/3 complex. Therefore, we asked whether the A region of WASP, which can compete with VCA for binding to the Arp2/3 complex (Marchand et al. 2001), can synergistically activate the complex with GST-N-WASP-VCA. Unexpectedly, the A region of WASP was not synergistic with GST-N-WASP-VCA, even at concentrations where NtA-mediated synergy was saturated (Figure 5A). These data demonstrate that NtA is functionally distinct from A, and harbors unique structural features required for synergy. The failure of A to synergize with GST-N-WASP-VCA cannot be explained by its relatively low affinity (K_D=~9 μM) compared to NtA (K_D=1.6 μM), because neither WASP-CA nor N-WASP-CA (K_D=~1 μM) synergistically activated the complex with GST-N-WASP-VCA (Marchand et al. 2001; Padrick et al. 2008) (Figure 5A). Consistent with this observation, the WASP C region also failed to synergize with GST-N-WASP-VCA (Figure 5A).

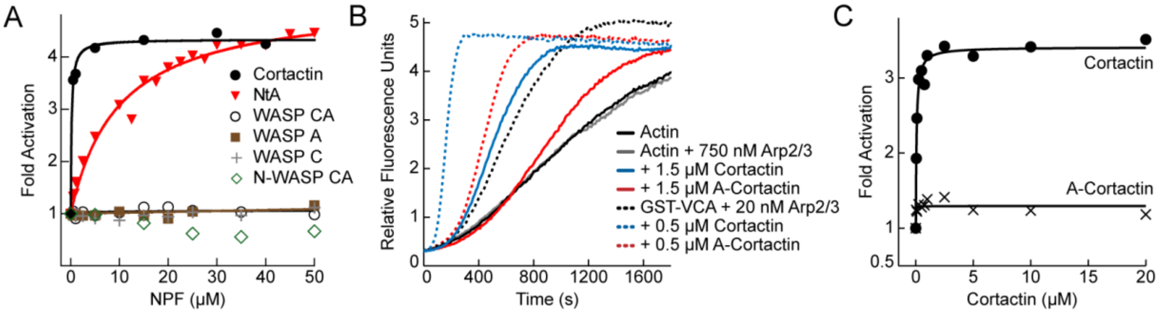

Figure 5. Cortactin NtA Has Unique Biochemical Properties Compared to the CA Region of WASP
A, Fold Arp2/3 complex activation versus NPF concentration for pyrene-actin polymerization reactions containing either cortactin, NtA, WASP CA, WASP A, WASP C or N-WASP CA. All reactions contained 2 μM 15% pyrene-actin, 20 nM Arp2/3, 250 nM GST-N-WASP-VCA and the indicated NPF. Fold activation is defined as the maximum polymerization rate from a reaction with both GST-N-WASP-VCA and either cortactin or WASP proteins divided by the maximum polymerization rate of the reaction with just GST-N-WASP-VCA. **B**, Pyrene-actin polymerization time courses showing intrinsic NPF activity and synergy with 150 nM GST-N-WASP-VCA (GST-VCA) by cortactin and N-WASP acidic cortactin (A-cortactin) for reactions containing 3 μM 15% pyrene-actin and the indicated protein concentrations. **C**, Plot of fold activation versus cortactin concentration for cortactin and A-cortactin. Reactions include 2 μM 15% pyrene-actin, 20 nM Arp2/3 complex and 150 nM GST-N-WASP-VCA.

In some contexts CA inhibits WASP-mediated activation of the complex (Rohatgi et al. 1999; Hüfner et al. 2001). Our data here show that monomeric CA constructs are not effective inhibitors of GST-N-WASP-VCA. While we cannot eliminate the possibility that CA-mediated inhibition is masked by weak synergy between CA and GST-N-WASP-VCA, the observation that WASP proteins do not bind to branch junctions indicates CA lacks a key biochemical property for displacement-mediated synergy (Smith, Padrick, et al. 2013; Helgeson and Nolen 2013). Therefore, we speculate the weak inhibitory potency of CA we measured is due to its weak binding to isolated Arp2/3 complex compared to dimeric N-WASP constructs (Marchand et al. 2001; Padrick et al. 2008).

Because the actin filament binding domain of cortactin increases its potency in synergizing with N-WASP (Figure 5A), we next replaced the NtA region of cortactin with the acidic (A) region of N-WASP and asked if this chimeric construct (A-cortactin) could synergize with GST-N-WASP-VCA. A-cortactin showed dramatically reduced synergy with GST-N-WASP-VCA compared to wild type cortactin (Figure 5B,C). The chimeric construct increased the maximum polymerization rate 1.4-fold over the rate with GST-N-WASP-VCA alone, compared to the 3.5-fold increase of wild type cortactin. These data show that even in the context of actin filament binding, NtA is functionally distinct from WASP family A regions.

NtA Harbors non-WASP-like Sequences that Contribute to Synergy

To determine the basis of functional differences between cortactin NtA and N-WASP A, we aligned cortactin sequences from multiple species to the A region of WASP family proteins. This analysis revealed that the acidic motif of cortactin (the DDWE motif) is embedded within a ~60 amino acid stretch of residues highly conserved among cortactin sequences, but not present in WASP family proteins (Figure 6A). To determine the importance of each of these conserved NtA segments, we tested the influence of truncations of NtA on its ability to synergistically activate the complex. We first asked if the conserved region C-terminal to the DDWE motif is required for synergy. We made a construct (NtA(1-27)) that contains the short conserved stretch N-terminal to the DDWE motif plus the DDWE motif, but lacks the C-terminal region of NtA. NtA(1-27) showed a dramatic reduction in synergy with GST-N-WASP-VCA. The maximum polymerization rate at 50 µM NtA(1-27) was 2.2-fold less than the full-length NtA construct (NtA(1-

84)). A construct lacking only the C-terminal 36 amino acids of the NtA (NtA(1-48)) was 1.6-fold defective compared to NtA(1-84), while one lacking 14-residues at the N-terminus (NtA(15-79)) showed a 1.3-fold decrease in synergy (Figure 6B). These data indicate that the conserved non-WASP-like sequences in NtA region contribute to the ability of cortactin to synergistically activate Arp2/3 complex with N-WASP.

To determine how regions outside the DDWE motif contribute to synergy, we asked if the NtA truncations influenced interactions with Arp2/3 complex. We measured the affinity of the NtA constructs for free Arp2/3 complex using a fluorescence anisotropy competition binding assay (Figure 6C). Unexpectedly, all NtA constructs bound Arp2/3 complex with a similar affinity to the full-length NtA. The displacement model of synergistic activation predicts that cortactin binds Arp2/3 complex at nascent branch

---

Figure 6 (next page). All Regions of the Cortactin NtA Contribute to Synergy
A, Sequence alignment of cortactin NtA and WASP family acidic regions. WASP family proteins are human (Hs) N-WASP (482-505), WASP (481-502) and WAVE1 (540-559). Gray and green shaded NtA residues are 100% and 80% conserved, respectively. Red shaded residues represent the WASP-like DDWE motif. Residue numbering is based on *Mus musculus* cortactin. Vertical black lines indicate truncations of the NtA. **B**, Plot of fold activation versus concentrations of cortactin (black dashed line), NtA(1-84) (red dashed line), NtA(15-79), NtA(1-48) and NtA(1-27). Dashed lines indicate previously published data (Helgeson and Nolen 2013). **C**, Fluorescence anisotropy binding assay showing competition between 100 nM Alexa-546 labeled NtA(1-48) and unlabeled NtA constructs for 750 nM Arp2/3 complex. Plot shows representative competition binding titration data for each construct with accompanying fit. Reported affinities (table) are average of three separate titrations. Errors are S.D.. **D**, Plot of fold Arp2/3 complex activation for a range of concentrations of cortactin in pyrene-actin polymerization reactions containing the indicated cortactin construct and 250 nM GST-N-WASP-VCA, 2 µM 15% pyrene-actin, and 20 nM Arp2/3 complex. Table contains best fit values with 95% confidence intervals of concentration to half maximum saturation of synergistic activation. Fits were performed as described in the experimental procedures. **E**, Plot of maximum polymerization rate versus cortactin concentration for actin polymerization reactions containing 3 µM 15% pyrene-actin and 0.5 µM Arp2/3 complex, but no GST-N-WASP-VCA. **F**, Plot of maximum polymerization rate versus cortactin concentration for actin polymerization reactions containing 3 µM 15% pyrene-actin, 40 nM Arp2/3 complex and the indicated cortactin construct.

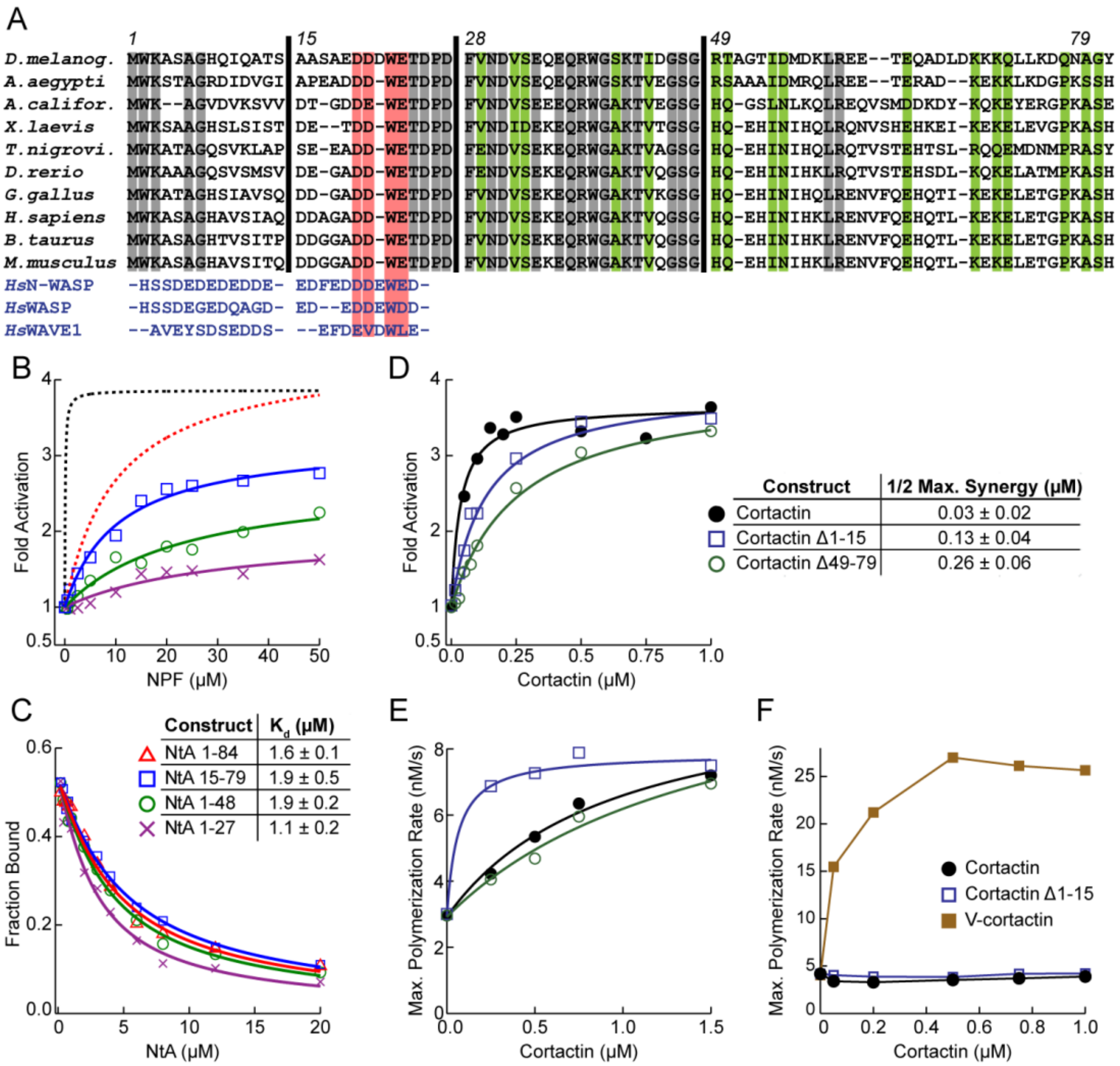

junctions, where interactions of the complex with N-WASP, actin monomers and actin filaments could influence the NtA binding surface (Figure 1C). Therefore, the mutations in NtA might decrease interactions with Arp2/3 complex specifically at nascent branch junctions. To test this, we measured the concentrations of mutant NtA constructs required to saturate synergy with GST-N-WASP-VCA. For these assays, we introduced the NtA mutations in the context of full-length cortactin to enable us to saturate the reactions. The concentrations required for half maximal synergy for the full-length NtA mutants were 4 to 8 fold greater than wild type cortactin, whereas the potency of each mutant at saturation was identical to wild type cortactin (Figure 6D). These results are consistent with a model in which mutations in the NtA decrease the affinity of cortactin for the nascent branch junctions rather than slowing a post-binding first order reaction rate.

The Distinct Modes of Activation of Arp2/3 Complex by Cortactin Are Partially Separable and Encoded within the NtA

The intrinsic NPF activity of cortactin requires both the DDWE motif of the NtA and the actin filament binding repeats, leading to the hypothesis that cortactin recruits free Arp2/3 complex to a pre-existing filament to activate nucleation (Weaver et al. 2002) (Figure 1B). In the recruitment pathway to activation, the interactions of NtA with the free Arp2/3 complex could influence rates of activation. This is in contrast to the displacement mechanism of synergistic activation, in which interaction of NtA with nascent branch junctions (and not the isolated Arp2/3 complex) defines activation rates. Therefore, we hypothesized that NtA residues outside of the DDWE motif, which are important for synergistic activation but not for binding to the isolated complex, might be dispensable for the intrinsic NPF activity of cortactin. Consistent with this hypothesis, we found that deleting the C-terminal portion of NtA had no effect on the intrinsic NPF activity of cortactin (Figure 6E). Similarly, truncating the N-terminus of NtA also failed to reduce cortactin’s intrinsic NPF activity. Instead, this mutant showed increased activity compared to wild type cortactin, indicating that the N-terminus of NtA antagonizes the intrinsic NPF activity of cortactin (Figure 6E). The stimulatory effect of the N-terminal truncation was insignificant when directly compared to potent stimulation caused by the

N-terminal V-cortactin fusions (Figure 6F). Together, these observations indicate that the intrinsic versus synergistic activation activities of cortactin are mechanistically distinct, and that mutations in the NtA allow functional separation of these activities.

Cortactin Synergistically Activates Arp2/3 Complex to Different Extents with WAVE, WASP and N-WASP

Cortactin regulates branched actin assembly in multiple cellular structures, including podosomes (Destaing et al. 2003), invadopodia (Bowden et al. 1999), sites of endocytosis (Cao et al. 2003) and at the leading edge of the cell (Kaksonen, Peng, and Rauvala 2000). Each of these structures contains both cortactin and a WASP family protein, suggesting these two NPFs might synergize to assemble the branched actin filaments in each of these structures. However, N-WASP is the only WASP family protein demonstrated to potently synergize with cortactin, and few experiments have explored synergy with other WASP family proteins (Weaver et al. 2001; Uruno et al. 2003; Siton et al. 2011; Helgeson and Nolen 2013). Dissection of the mechanism revealed strict biochemical requirements for N-WASP, making it uncertain if potent synergy with cortactin is a general feature of WASP family proteins. To answer this question, we tested combinations of cortactin and different WASP family proteins for their ability to synergistically activate Arp2/3 complex.

Cortactin and N-WASP colocalize in ventral actin-based protrusions in transformed cells called invadopodia (Desmarais et al. 2009). We previously showed that GST-N-WASP-VCA and cortactin synergistically activate Arp2/3 complex *in vitro* (Helgeson and Nolen 2013), potentially explaining why both NPFs are required for assembly of actin filaments in invadopodia (Ayala et al. 2008). Potent synergy required dimerization of N-WASP-VCA; monomeric N-WASP-VCA containing either one or both of the two native V regions (N-WASP-VCA or N-WASP-VVCA) showed little or no synergy, respectively (Helgeson and Nolen 2013). This does not rule out the possibility that N-WASP synergizes with cortactin in invadopodia, as there is building evidence that WASP family proteins act as oligomers *in vivo* (Padrick et al. 2008; P. Li et al. 2012; Suetsugu 2013; Gohl et al. 2010). However, experiments to measure synergy of dimerized N-WASP have all used a construct of N-WASP that includes only one of its two native V regions (Weaver et al. 2001; Uruno et al. 2003). Because the additional V-region increases the intrinsic NPF activity of N-WASP (Figure 7H), and we observed that intrinsic and synergistic activity are inversely correlated (Yamaguchi et al. 2000; Helgeson and Nolen 2013) (see discussion) we reasoned that the additional V region may influence synergy with cortactin. Therefore, we tested the ability of GST-N-WASP-VVCA to synergize with cortactin. Addition of cortactin to GST-N-WASP-VVCA increased the maximum polymerization only 1.3-fold over GST-N-WASP-VVCA alone, while its addition to GST-N-WASP-VCA increased the polymerization rate 3.8 fold (Figure 7A,B,G). These data demonstrate that the presence of an additional V region in N-WASP significantly decreases synergy with cortactin. Therefore, synergy between these two NPFs may not contribute significantly to nucleation of branched filaments in invadopodia.

WASP is a haematopoietic cell-specific WASP family protein required for the assembly of actin filaments in podosomes, protrusive structures similar to invadopodia that occur in non-transformed cells (Murphy and Courtneidge 2011). WASP has a single V region and has increased intrinsic dimeric NPF activity compared to GST-N-WASP-

VCA (Figure 7H). Dimeric WASP-VCA was recently shown by TIRF microscopy to increase Arp2/3 complex-mediated branching in the presence of cortactin (Siton et al. 2011). However, it is unknown whether the biochemical differences between WASP and N-WASP influence the potency or mechanism of synergy. To test this, we added cortactin to reactions containing Arp2/3 complex and dimeric or monomeric WASP-VCA. We found that dimeric WASP (GST-WASP-VCA), but not monomeric WASP

Figure 7 (next page). Cortactin Synergistically Activates Arp2/3 Complex to Different Extents with WAVE, WASP and N-WASP
A,**C**,**E** Time courses of pyrene-actin polymerization for reactions containing indicated WASP family proteins with or without 1 µM cortactin, plus 20 nM Arp2/3 complex, 2 µM 15% pyrene-actin and either: 750 nM N-WASP-VVCA, 100 nM GST-N-WASP-VVCA, 750 nM WASP-VCA, 250 nM GST-WASP-VCA, 750 nM WAVE-VCA or 250 nM GST-WAVE-VCA. **B**,**D**,**F** Fold activation for cortactin-mediated synergistic activation of the Arp2/3 complex with either monomeric or dimeric WASP family proteins. Reactions conditions are the same as above but with varying concentrations of cortactin. Data were fit as described in experimental procedures. Dashed lines indicate previous published data (Helgeson and Nolen 2013). **G**, Average fold activation of Arp2/3 complex by cortactin for reactions containing 1 µM cortactin, 20 nM Arp2/3 complex, 2 µM 15% pyrene-actin and a WASP family protein at concentrations listed above. Dimeric N-WASP VCA, monomeric N-WASP VCA and monomeric N-WASP VVCA were previously published (Helgeson and Nolen 2013). Dashed gray line indicates no synergy. P-values were calculated by two-tailed student’s t-test. Error bars S.E.M. n.s. = not significant. **H**, Plot of maximum polymerization rate versus dimeric NPF concentration for actin polymerization reactions performed with 3 µM 15% pyrene-actin, 20 nM Arp2/3 complex and the indicated concentrations of either: GST-N-WASP-VCA (black dashed line, previously published (Helgeson and Nolen 2013)), GST-N-WASP-VVCA, GST-WAVE-VCA or GST-WASP-VCA. **I**, Plot of lag phase lifetime versus cortactin concentration for actin polymerization reactions containing 2 µM 15% pyrene-actin, 20 nM Arp2/3 complex, indicated concentrations of cortactin and either: 250 nM GST-N-WASP-VCA, 100 nM GST-N-WASP-VVCA, 250 nM GST-WAVE-VCA or 250 nM GST-WASP-VCA. **K**, Plot of lag phase lifetime versus cortactin concentration for either actin polymerization reactions performed with 3 µM 15% pyrene-actin, 50 nM Arp2/3 complex, 100 nM GST-N-WASP-VCA and the indicated concentrations of cortactin (black closed circle) or simulations of actin polymerization reactions (black line) from a kinetic model of cortactin mediated synergistic displacement. Kinetic model fits and parameter optimization were published previously (Helgeson and Nolen 2013). **L**, Schematic indicating the actin based cellular structures were cortactin and a corresponding WASP family protein have been observed to colocalize.

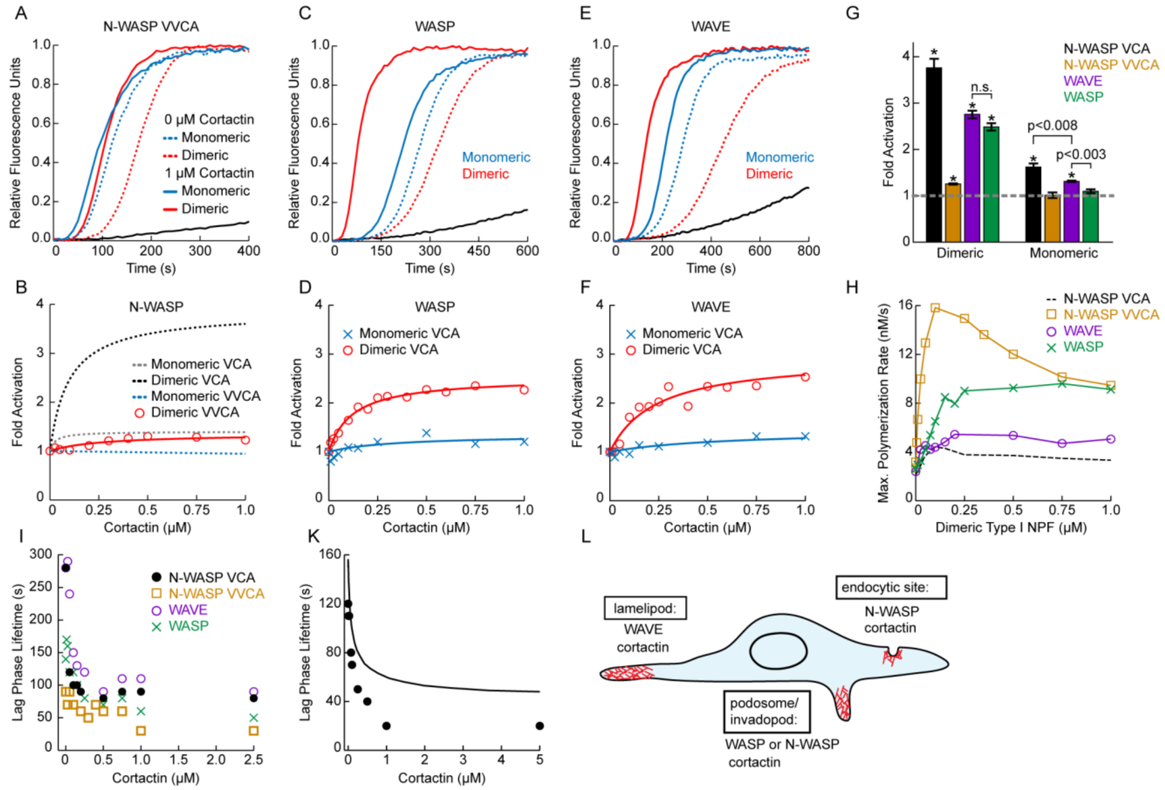

(WASP-VCA), synergistically activated Arp2/3 complex with cortactin (Figure 7C,D,G). Therefore, like N-WASP, the oligomerization state of WASP-VCA is a critical determinant of synergy, suggesting N-WASP and WASP use a similar mechanism to synergize with cortactin. Addition of cortactin to GST-WASP-VCA increased the maximum polymerization rate 2.6 fold over GST-WASP-VCA alone. This value was significantly less than dimeric N-WASP-VCA, indicating that sequence differences in the VCA of distinct WASP proteins tune the potency of their synergy with cortactin (Figure 7G).

WAVE and cortactin colocalize with Arp2/3 complex in lamellipodia and RNAi knockdown experiments indicate that both NPFs contribute to nucleation of actin filaments in these structures (Martinez-Quiles et al. 2004; Bryce et al. 2005; Rogers et al.

2003). WAVE contains one V region and as a dimer was found to have slightly higher activity than dimeric N-WASP-VCA but less activity than dimeric WASP VCA (Figure 7H). Dimeric WAVE-VCA (GST-WAVE-VCA) showed a similar potency as dimeric WASP-VCA in cortactin mediated synergistic activation of the Arp2/3 complex (Figure 7E,F,G).

In addition to increasing the polymerization rate, synergistic activation of the Arp2/3 complex by WASP family VCAs and cortactin significantly decreased the lag phase of the polymerization time courses (Figure 7I). To determine if the displacement mechanism can account for the decreased lag phase, we simulated time courses of reactions of cortactin, GST-N-WASP-VCA, and Arp2/3 complex using a previously optimized kinetic model of cortactin-mediated displacement (Helgeson and Nolen 2013). In our simulations, increasing cortactin concentrations decreased the length of the lag phase almost three-fold, similar to the decreases measured in the reactions (Figure 7K). While the duration of the lag phase simulated at saturating cortactin was greater than the observed value, it was also overestimated at 0 μM cortactin. This indicates that that the reactions describing spontaneous and/or GST-N-WASP-VCA-activated nucleation may be oversimplified, creating the observed differences between predicted and measured lag phase in reactions containing cortactin.

Together, these results show that the ability to synergize with cortactin is a general feature of WASP family proteins. Therefore, synergistic activation of Arp2/3 complex by cortactin and a WASP family protein may be important for assembly of branched actin filaments in diverse actin-based structures, including podosomes, endocytic sites, and lamellipodia (Figure 7L).

DISCUSSION

Cortactin Is a Weak NPF Because It Cannot Recruit Actin Monomers to Arp2/3 Complex

Here we showed that differences between the cortactin NtA and the WASP A region cannot explain the weak intrinsic NPF activity of cortactin. Instead, we showed that cortactin is a weak NPF because it cannot recruit actin monomers to Arp2/3 complex. The absence of an actin monomer binding domain may ensure the NPF activity of cortactin is suppressed until a WASP family protein is activated and branched networks can be assembled by the two NPFs synergistically. Alternatively, the NPF activity of cortactin may be stimulated when it binds proteins that allow it to indirectly tether monomers to Arp2/3 complex. For instance, WIP (WASP interacting protein) contains both a proline-rich region that binds to the SH3 domain of cortactin, and two V regions that bind actin monomers. *In vitro,* WIP increases cortactin-mediated activation of Arp2/3 complex, and co-expression of WIP and cortactin stimulates membrane protrusion (Kinley et al. 2003). Several other NPFs, including type I myosins and Abp1 (actin binding protein 1) (Goley and Welch 2006), share the sequence characteristics of cortactin, in that they contain Arp2/3 complex interacting and actin filament binding regions, but no actin monomer binding segments. Indirect recruitment of actin monomers by these NPFs may be a general mechanism to control their activity. Indeed, myosin 1, like cortactin, shows weak intrinsic Arp2/3 activation, but its NPF activity is potently stimulated by a direct interaction with WIP (Sirotkin et al. 2005).

The observation that fusing a V region onto the N-terminus of cortactin potently activated its NPF activity was unexpected given that cortactin lacks a canonical C region

(Figure 6A). The C region of WASP VCA is thought to be critical for stimulating an activating conformational change in Arp2/3 complex (Panchal et al. 2003). Why the C-region is required for activation in the context of VCA but not in V-cortactin is unclear. One possibility is that the cortactin NtA harbors sequences unique from the WASP C region that stimulate conformational changes in the complex. In support of this, single particle reconstructions of electron microscopy images of cortactin-bound Arp2/3 complex show Arp2 and Arp3 in a filament-like conformation distinct from the splayed conformation observed in crystal structures of inactive Arp2/3 complex (X.-P. Xu et al. 2011). FRET experiments by Goley *et. al*. showed that unlike CA, an NtA construct containing residues 1-39 does not stimulate conformation changes in the complex, indicating that NtA residues important for these changes may be C-terminal to residue 39 (Goley et al. 2004). Determining precisely how V-cortactin and WIP-bound cortactin activate Arp2/3 complex without a C-region will be critical for understanding the structural mechanisms by which NPFs activate the complex.

The activity of V-cortactin was also unexpected because NtA binds to a single NPF site on the complex (Weaver et al. 2002). In contrast, multiple lines of evidence, including analytical ultracentrifugation, isothermal titration calorimetry, and chemical crosslinking indicate that WASP CA binds two sites on the complex, one on Arp3 and the other on ARPC1 and Arp2 (Padrick et al. 2011; Ti et al. 2011; Liu et al. 2011; Boczkowska et al. 2014). Furthermore, mutational studies showed that recruitment of two actin monomers through engagement of VCA to both NPF sites is required for maximal activation (Padrick et al. 2011). Assuming that the conserved tryptophan in NtA binds to the same surface on Arp3 as WASP (Weaver et al. 2002), our structural modeling suggests the V-cortactin construct can deliver an actin monomer to the barbed end of Arp3. V-cortactin could potentially also deliver an actin monomer to the barbed end of Arp2, but the linear distance is much greater (107 versus 50 angstroms) and is unlikely to be spanned by the 43 amino acids between the end of the V to the tryptophan, especially considering that a fully extended conformation of this region would occupy excluded volume in the model. Therefore, these data indicate that V-cortactin activates the complex by recruiting a single actin monomer to Arp3. This is consistent with the results of Padrick, *et. al*., who showed recruitment of actin monomers to Arp3 is more important for activation than monomer recruitment to Arp2 (Padrick et al. 2011). However, as with WASP-VCA, recruitment of actin monomers to both sites may contribute to activation, as we found that fusion of the tandem V of N-WASP to the N-terminus of cortactin (VV-cortactin) further stimulated NPF activity.

Cortactin Bundles Branched Actin Filaments to Create Actin Networks Distinct from N-WASP

Recent observations indicate that filament bundling by fimbrin plays a role in modulating the function of Arp2/3-nucleated branched networks *in vivo* (Skau et al. 2011). These observations suggest other bundlers, including cortactin, may also influence branched filament networks *in vivo*. However, we showed that the bundling potency of cortactin is reduced in the presence of N-WASP, presumably because increased nucleation rates create shorter branches that cannot bundle. Therefore, if cortactin-mediated bundling is important *in vivo*, its bundling activity is likely tuned by the presence of other actin regulators that influence branch density and filament lengths, including capping protein (J. Xu, Casella, and Pollard 1999). During endocytosis, bundling may also be influenced by dynamin, which is thought to oligomerize cortactin, thereby directly regulating its bundling activity (Mooren et al. 2009; Yamada et al. 2013).

Dynamic Multivalent Contacts with Actin Filaments Can Explain Bundling by Cortactin

Our data demonstrate that multiple actin binding regions are harbored within the 6.5 repeats of cortactin. We propose a model in which a cortactin molecule binds to the side of a filament, with individual repeats dynamically binding and releasing the filament. When an adjacent filament collides with the bound cortactin, one or more of the filament binding repeats release from the parent filament and interact with the bundling partner to bridge the filaments, leaving at least one repeat bound to the parent filament (Figure 4B). Several lines of evidence support this model. First, chemical crosslinking and circular dichroism experiments demonstrate that the repeats are dynamic and unstructured in the absence of actin (Shvetsov et al. 2009). Flexibility within the repeat region would allow it to dynamically switch between single and multiple filament binding configurations. Second, the binding stoichiometry of cortactin to actin filaments is approximately 5 actin subunits to one cortactin, consistent with the idea that multiple actin subunits are contacted by a single filament binding repeat region and that each repeat contacts approximately one subunit (MacGrath and Koleske 2012). Third, we showed that the off rate of cortactin for single filaments is identical to its off rate for bundles, and that the apparent affinity of cortactin for single filaments is similar to its apparent affinity for bundles. This suggests that the strength of contacts made by the repeat region is similar whether cortactin is bound to a single or bundled filament. This could occur if repeats act as flexibly connected binding modules, and the total strength of the interaction is additive and tuned by the total number of repeats attached, whether to a single or bundled filaments. This mode of interaction may allow both the actin filament binding and bundling activities of cortactin to be regulated by alternative splicing, which generates isoforms of cortactin that have between 2.5 and 6.5 repeats (Katsube et al. 2004). We note that our data are inconsistent with experiments suggesting that the fourth repeat is entirely responsible for the actin binding affinity of cortactin (Weed et al. 2000), and with small angle x-ray scattering studies and modeling exercises that led to the hypothesis that the repeats fold into a stable globular domain (Cowieson et al. 2008).

The Arp2/3 Complex Binding Regions of Cortactin and WASP Are Functionally Distinct

NtA versus A sequence differences likely contribute to the distinct binding site specificities of NtA versus WASP for the complex, providing one explanation for their functional differences we observed here. Biochemical data suggest that WASP binds more tightly to the NPF site that spans Arp2 and ARPC1, with an approximately 100 fold weaker affinity for the Arp3 NPF site, which is the only site bound by the cortactin NtA (Ti et al. 2011; Weaver et al. 2002; Boczkowska et al. 2014). However, simple competition with dimeric WASP for binding to the Arp3 site cannot explain synergy, since at high concentrations CA and A can bind to both sites, yet we did not observe synergistic activation of the Arp2/3 complex even at very high concentrations of CA or A. Understanding the molecular bases for the functional differences between NtA and A will likely require high resolution structural information showing how both WASP-A and NtA bind to the complex.

Our comparisons of WASP A versus NtA segments have implications for understanding diverse regulators of Arp2/3 complex. In addition to NPFs like WASP and cortactin, the A region is found in several inhibitors of Arp2/3 complex, including PICK1 (Rocca et al. 2008), Gadkin (Maritzen et al. 2012) and Arpin (Dang et al. 2013). These proteins block branching nucleation by competing with WASP family proteins for binding to the complex. However, unlike cortactin, none of these proteins have been observed to synergize with WASP family proteins in activation of Arp2/3 complex. Our data suggest that the A regions of these proteins may lack specific features present in cortactin NtA required for potent synergy.

The Presence of Tandem V Regions in N-WASP Hinders Its Synergy with Cortactin

We showed that the ability to synergistically activate Arp2/3 complex with cortactin is a general feature of WASP-family proteins, but that the potency of different WASP family proteins varies widely. Native N-WASP had the weakest synergistic activity, whether monomeric or dimerized. The weak synergy of native N-WASP is due to the presence of two V regions, since deletion of one V dramatically increased the potency of dimeric N-WASP in synergistic activation of Arp2/3 complex (Helgeson and Nolen 2013) (Figure 7A,B,G). How tandem actin monomer recruitment regions could influence synergy with cortactin can be understood in the context of the displacement mechanism. In this mechanism, the rate of WASP release from the nascent branch junction limits or partially limits the rate of branching nucleation (Helgeson and Nolen

2013; Smith, Padrick, et al. 2013). By displacing WASP from the nascent branch junction, cortactin increases branching rates. Therefore, the displacement mechanism predicts an inverse correlation between the intrinsic activity of WASP family proteins at saturation (which likely reflects the limiting release rate) and the fold increase in polymerization rate due to addition of cortactin. We previously observed this correlation for point mutations within the V-region of GST-N-WASP-VCA (Helgeson and Nolen 2013). Here we observe this correlation when comparing diverse WASP family proteins. For instance, GST-N-WASP-VVCA shows a much higher intrinsic NPF activity and a much lower synergy with cortactin compared to GST-N-WASP-VCA (Helgeson and Nolen 2013) (Figure 7A,B,G). These observations suggest that GST-N-WASP-VVCA shows decreased synergistic activation because it is released more rapidly from the nascent branch than GST-N-WASP-VCA. While we do not know how the number of V regions could influence the WASP release rate from nascent branches, one possibility is that recruitment of additional actin monomers helps stimulate a conformational change that accelerates WASP release and nucleation. Finally, we note that while we observed an inverse correlation between intrinsic NPF activity of WASP proteins to their synergy with cortactin, it was unexpected that the synergy of cortactin with GST-WAVE-VCA was not significantly greater than with GST-WASP-VCA. This observation may indicate that the intrinsic NPF activity at saturation is a relatively crude indicator of potential synergy with cortactin for reasons that we do not currently understand.

All WASP Family Proteins May Use a Similar Mechanism to Synergistically Activate Arp2/3 Complex with Cortactin

Our previous data indicate that release of dimeric but not monomeric N-WASP from the nascent branch junction is rate limiting, explaining why dimerization of WASP proteins is required for synergy with cortactin. Here we showed that multiple WASP family proteins synergize with cortactin to activate Arp2/3 complex, but that in each case potent synergy required dimerization of the WASP protein. These data suggest that all WASP family proteins use the displacement mechanism to synergize with cortactin. This finding has important implications for understanding the role of cortactin in assembling branched actin networks in diverse cellular structures. WASP, N-WASP and WAVE are frequently attached to cellular membranes, allowing them to initiate branched actin networks that provide pushing forces to move or remodel cellular membranes (Takenawa and Suetsugu 2007). WASP proteins are thought to provide a transient connection between membranes and the polymerizing actin networks by binding the barbed ends of polymerizing filaments, nascent branch junctions, or both (Co et al. 2007; Akin and Mullins 2008). Using the displacement mechanism to synergistically activate Arp2/3 complex with WASP family proteins, cortactin can not only increase rates of branching nucleation, but may also decrease the lifetime of WASP-mediated connections between the polymerizing network and the membrane (Siton et al. 2011). The importance of WASP-mediated connections to polymerizing actin networks has been demonstrated using *in vitro* bead motility assays (Co et al. 2007), and an important question to resolve will be the role of these connections in modulating actin network-membrane interactions *in vivo*.

EXPERIMENTAL PROCEDURES

Protein Purification

Rabbit skeletal muscle actin was purified and labeled with either Oregon-Green 488 or N-(1-pyrene)iodoacetamide (Molecular Probes, Eugene, OR) as previously described (Hetrick et al. 2013). Bovine Arp2/3 complex was purified as previously described (Hetrick et al. 2013). A-cortactin was generated by fusing residues 486-505 of bovine N-WASP to the N-terminus of residues 46-546 of cortactin. V-and VV-cortactin constructs were constructed by adding bovine N-WASP residues 428-457 and 399-457 (V and VV respectively) to the N-terminus of a 16 residue Gly-Ser linker attached to the N-terminus of full length cortactin. The Gly-Ser linker ensures that the number of residues separating the Arp2/3 complex binding tryptophan (DDWE motif) and the C-terminal V region residues corresponds to the shortest V to A distance of any WASP sequence. Alexa568-cortactin (residues 1-336) and Alexa546-NtA (residues 1-48), both with a C-terminal KCK (Lys-Cys-Lys) sequence, were labeled with malemide reactive Alexa fluorophore dyes (Molecular Probes, Eugene, OR) as previously described (Helgeson and Nolen 2013). All cortactin constructs are murine and were overexpressed and purified from *E. coli* as previously described (Helgeson and Nolen 2013). Human WAVE1 VCA (residues 485-559), human WASP VCA (residues 429-502), human WASP CA (residues 460-502), bovine N-WASP VCA (residues 428-505), bovine N-WASP VVCA (residues 392-505) and bovine N-WASP CA (residues 461-505) were purified as dimeric (GST-tagged) or monomeric proteins as previously described (Hetrick et al. 2013). Synthetic peptides of human WASP C (residues 464-484) and A (residues 497-502) are as previously described (Marchand et al. 2001).

Pyrene-actin Polymerization Assays

Pyrene-actin polymerization assays were performed as previously described (Liu et al. 2011). The influence of cortactin on polymerization rates of reactions containing Arp2/3 complex and a WASP family protein was quantified by dividing the maximum polymerization rate at each cortactin concentration by the maximum polymerization rate of an identical reaction without cortactin (Helgeson and Nolen 2013). These values were reported as fold activation and plotted versus cortactin concentration. Fold activation data were fit to the equation: $fold\ act. = \frac{max.\ synergy * X}{K_{syn}+X} + 1$, where X is the concentration of cortactin and K_{syn} is the concentration of cortactin at half maximal activity. The reaction lag phase lifetime was defined as the start of the reaction to the time at which the acceleration of the reaction was the greatest. This time point was found by taking the second derivative of the raw fluorescence data that had been filtered with a five point moving average.

Competition Binding Assays

The fluorescence anisotropy of 100 nM Alexa546-NtA (1-48) was measured in the presence of 750 nM Arp2/3 complex and 0.2–20 µM of cortactin NtA or cortactin NtA mutants. Fluorescence anisotropy was monitored through excitation at 530 nm and emission at 570 nm in a buffered solution of 10 mM Hepes pH 7.0, 50 mM KCl, 1 mM EGTA, 1 mM $MgCl_2$, 1 mM DTT and 0.2 mM ATP. Binding experiments were performed at least three times and the data from each experiment were fit individually as previously described (Wang 1995) with the probe affinity and receptor concentration held constant. The probe, Alexa546-NtA (1-48), affinity for the Arp2/3 complex was determined by measuring the fluorescence anisotropy under conditions described above and fitting the results with a previously described equation (Liu et al. 2013). The probe affinity was found to be 0.66 ± 0.13 µM, error is 95% confidence interval. Reported affinities are the mean of all individual fits.

TIRF Microscopy

Objective-based TIRF microscopy was performed on a Nikon TE2000-U microscopy body with a Nikon 100x 1.49 NA TIRF objective and a 1.5x auxiliary lens, as described previously (Helgeson and Nolen 2013). Laser light from an argon 488-nm (Dynamic Laser, Salt Lake City, UT) or solid-state 561-nm (Coherent, Santa Clara, CA) laser were filtered through dual-band excitation and dichroic filters (Chroma, Bellows Falls, VT) prior to striking the sample from which the resulting fluorescent emission was filtered through dual-band dichroic and emission filters before collection on an EM-CCD camera (iXon3, Andor or Image-EM, Hamamatsu). Actin polymerization was initiated by adding protein components to an oxygen-scavenging polymerization buffer composed of glucose-oxidase, catalase and Trolox. The polymerization reaction was imaged after wicking the reaction into a cleaned flow chamber where the cover slip surface was passivated with polyethylene glycol. Polymerizing actin filaments were tethered to the cover slip by N-ethyl-or biotin maleimide-inactivated myosin which was adhered to the cover slip through biotin-streptavidin interactions. The open source microscopy software, Micro-Manager (Edelstein et al. 2010), was used to acquire 488-channel images at rates of 0.2-1 s^{-1} and 561-channel images at 3.6 s^{-1} with exposure times of 25-100 ms. Individual reaction parameters are detailed in video figure legends. Images were processed in ImageJ by background subtraction with a rolling ball radius of 10 pixels then slightly blurred with a Gaussian filter of radius 0.6 pixels.

Image Analysis

Lifetime analysis of cortactin molecules was performed as previously described (Helgeson and Nolen 2013). Briefly, puncta in the 561 channel were automatically tracked using a nearest-neighbor algorithm to determine their lifetime. Tracks were rejected if: (1) they appeared in the first or last image of the acquisition, (2) their intensity did not correspond to single molecules or (3) their position did not correlate with actin filaments. Molecules from the tracks were manually viewed to classify them as binding to either single or bundled filaments. Molecule lifetimes were binned by 5 seconds and the cumulative frequency for all molecules was determined. 1-cumulative frequency as a function of binned lifetimes was fit to a single exponential decay equation to yield an off rate constant and accompanying standard error.

The number of cortactin molecules per micrometer of filament was determined by manually counting cortactin molecules along a filament and measuring the length of filaments using a previously published ImageJ plugin (Kuhn and Pollard 2005). The number of filaments in the bundles were manually determined and incorporated into the filament length measurements. Binding densities were analyzed at three separate time points (105, 140 and 174 seconds from the start of imaging). No time dependent difference was observed, so the average binding density reported contains measurements from all three time points.

The fraction of total filament bundled was calculated in Matlab (Mathworks Inc, Natick, MA) similar to a previously described procedure (Helgeson and Nolen 2013). Regions of interest were manually segmented to separate actin filaments from the background. Then extraneous pixels were removed using morphological opening to produce a binary image with filaments represented by positive pixels. The total length of all filaments was calculated by dividing the number of positive pixels by three (the average filament width due to the PSF) and then the summed pixel value was converted to micrometers using 1 pixel = 0.16 or 0.017 µm (depending upon magnification used). Pixels corresponding to bundled filaments were manually marked and analyzed with the assumption that bundles contain only two filaments. Manual tracking of bundles showed that a vast majority contained only two filaments at the time points measured. Multiple non-overlapping regions of interest were analyzed to calculate the reported fraction of total filament bundled.

Photobleaching data was collected by adhering 1 nM of NHS-biotin (Thermo-Pierce, Rockford, IL) conjugated Alexa568-cortactin (residues 1-336) to the surface of PEGylated cover slips and acquiring 100 ms exposures continuously for 3 minutes. Fluorescent puncta were identified in the first image frame and their positions were integrated across all images to produce an intensity time series for each puncta. The number of photobleaching steps was identified using a one-dimensional edge detection algorithm written in-house and implemented in Matlab.

Kinetic Modeling

Simulations were performed using previously described kinetic models (Helgeson and Nolen 2013). Briefly, time courses of actin polymerization for reactions containing GST-N-WASP-VCA, cortactin, and Arp2/3 complex were fit to a model in which cortactin can bind nascent branches and displace GST-N-WASP-VCA through an irreversible activation step (k_{dis}) allowing a new branched filament end to form. k_{dis} was the only parameter optimized during these fitting routines. Simulations of actin polymerization at increasing cortactin concentrations were performed using this optimized model and the corresponding lag phase lifetimes were calculated as described above.

BRIDGE TO CHAPTER IV

The work presented in this chapter has probed the methods by which cortactin and WASP family proteins interact with actin and Arp2/3 complex. We found that cortactin is uniquely suited to synergistically activate Arp2/3 complex with WASP family proteins. Additionally, the mechanism of synergy by cortactin mediated displacement is likely the same amongst the WASP family proteins. Furthermore, we have identified biochemical properties of cortactin which make it a weak Arp2/3 complex activator and a potent bundler of actin filaments. In the next chapter, we will investigate how a new set of biochemically distinct NPFs, WISH/DIP/SPIN90 proteins and WASP family proteins, coordinately activate Arp2/3 complex to regulate branched network initiation.

CHAPTER IV

DIP1 AND WSP1 CO-ACTIVATE ARP2/3 COMPLEX TO INITIATE BRANCHED NETWORK ASSEMBLY

This chapter contains unpublished co-authored material

Author contributions: Luke Helgeson and Brad Nolen designed research; Luke Helgeson performed research and analyzed data; Luke Helgeson and Brad Nolen wrote the manuscript.

INTRODUCTION

The assembly of branched actin networks is a highly regulated process that is critical for numerous cellular functions such as movement and endocytosis (Pollard and Cooper 2009). Branched actin filaments are nucleated by the actin-related protein 2/3 (Arp2/3) complex. The seven protein subunit Arp2/3 complex is the only known branch filament nucleator and is required for cellular processes that depend on branched actin networks (Rotty, Wu, and Bear 2013). The pathway to branched filament nucleation begins with activation of Arp2/3 complex by a special class of proteins known as nucleation promoting factors (NPFs) (Higgs, Blanchoin, and Pollard 1999; Goley and Welch 2006). Upon association with an NPF, the active NPF-Arp2/3 complex binds to the side of a pre-existing filament from which it nucleates a new branched filament

(Machesky and Insall 1998; Mullins, Heuser, and Pollard 1998). The newly nucleated branched filaments can serve as templates for further branching, resulting in an autocatalytic process that leads to the formation of dense, highly branched networks (Svitkina and Borisy 1999; Amann and Pollard 2001). Importantly, the *de novo* formation of branched networks requires an original pre-existing filament, called the seed filament, to initiate the first branching reaction. Genetic evidence suggests that seed filament generation is regulated and unlikely to the result of spontaneous nucleation (Q. Chen and Pollard 2013; Basu and Chang 2011). Identification of cellular seed filament sources is paramount to understanding the regulation of branched actin network initiation.

In vitro branched networks are seeded by spontaneously nucleated filaments, but in cells, spontaneous nucleation is blocked by actin monomer binding proteins (Pollard and Borisy 2003). This indicates that the filaments responsible to initiate cellular branched network assembly are unlikely to be generated through spontaneous nucleation. Cofilin is an actin filament binding protein that severs branched and linear filaments and is a critical component of the cellular actin assembly and disassembly cycle (Pollard and Borisy 2003). Recently, it was proposed that cofilin severed filaments diffuse through the cytoplasm to new sites of branched actin assembly and there, these cofilin severed filaments, seed branch filament nucleation by Arp2/3 complex (Q. Chen and Pollard 2013). In support of this model was the observation that a mutant of cofilin with a reduced severing rate was found to be defective in actin assembly at endocytic sites but this mutant did not disrupt NPF recruitment to these sites. Unfortunately, this mechanism still relies on the formation of an initial actin network and therefore does not completely address the origin of the seed filament. Furthermore, freely diffusing filaments are older and more likely to accumulate actin binding proteins, such as fimbrin, tropomyosin and coronin. All of these actin binding proteins inhibit Arp2/3 complex branch nucleation and are found at sites of branched network assembly (Blanchoin, Pollard, and Hitchcock-DeGregori 2001; Skau et al. 2011; Liu et al. 2011). Similarly, existing filaments from formin nucleated cellular networks, like stress fibers or actin cables, are also unlikely to prime branching nucleation because they are also coated with actin binding proteins that block Arp2/3 complex from binding (Tojkander et al. 2011). Another source of branched network seed filaments could be the tandem WH2 domain containing linear filament nucleators; spire, JMY and cordon-bleu (Campellone and Welch 2010). JMY has been implicated in cell motility but its ability to increase cell migration upon overexpression is dependent upon Arp2/3 complex binding and it has the potential to indirectly induce cell migration through transcription regulation roles or decreasing cell-cell adhesion (Zuchero et al. 2009; Coutts, Weston, and La Thangue 2009). It remains to be seen if the linear actin filament nucleation activity of JMY is critical for cell motility. Similarly, spire was recently identified to function in invadopodia but it was found to interact with the formin mDia1 suggesting spire is likely increasing formin activity, a common function of formin and spire interactions (Lagal et al. 2014; Breitsprecher et al. 2012). These data suggest that spontaneous nucleation, cofilin mediated severing, formins or tandem WH2 nucleators may not be able to explain seed filament generation. Detailed mechanisms of seed filament creation have yet to be determined.

Clathrin-mediated endocytosis in fission yeast (*S. pombe*) is a highly dynamic process that involves the synchronized assembly and function of numerous biochemically distinct proteins to internalize extracellular material (Sirotkin et al. 2010). Branched actin networks are essential for yeast endocytosis; possibly providing the forces for membrane invagination or endosome propulsion (Lee, Bezanilla, and Pollard 2001; Winter et al. 1997; Young, Cooper, and Bridgman 2004). Arp2/3 complex arrival at sites of endocytosis peaks at the onset of vesicle internalization, whereas the arrival of the *S. pombe* WASP family NPF, Wsp1, peaks ~3 seconds prior to Arp2/3 complex (Sirotkin et al. 2010). In Wsp1 deletion strains, the cortical accumulation of endocytic adaptors and actin dependent proteins is normal but endocytic vesicles fail to internalize (Basu and Chang 2011; Sirotkin et al. 2005). Independent deletion of another endocytic NPF, myosin-1, resulted in stalled endocytosis which occasionally failed to internalize (Sirotkin et al. 2005). However, the loss of myosin-1 is not as detrimental to endocytosis as Wsp1. These mutational studies suggest that Wsp1 is the primary activator of Arp2/3 complex during endocytosis and its role in regulating branched network assembly is critical for endocytosis.

S. pombe Dip1, a member of the WISH/DIP/SPIN90 family of proteins, is a recently discovered component of endocytosis (Basu and Chang 2011). Deletion of Dip1 decreased the number of endocytic sites, delayed vesicle internalization and disrupted actin filament network organization (Basu and Chang 2011). These phenotypes suggest that Dip1 is involved in endocytic branched network formation. Interestingly, biochemical characterization of Dip1 revealed that it activates Arp2/3 complex without the need of a pre-existing filament (Wagner et al. 2013). As a result of this novel activation method, Dip1 generates linear networks; unlike all other Arp2/3 complex activators, which promote branched networks. The mammalian ortholog of Dip1, Spin90, was also observed to activate Arp2/3 complex without a pre-formed filament (Wagner et al. 2013). Further analysis revealed that Dip1 does not bind to actin monomers or filaments. These results indicate that the WISH/DIP/SPIN90 family of proteins is a new class of NPFs that likely use a common mechanism of Arp2/3 complex activation that does not rely on a pre-existing filament. The details of this novel activation mechanism have yet to be discovered.

Based on the strong endocytic phenotypes and biochemical evidence, a new model was proposed whereby Dip1 and Wsp1 (or other canonical NPFs) coordinately activate Arp2/3 complex to regulate the formation of branched actin networks (Wagner et al. 2013). In this model, Dip1 initiates network formation by generating a linear seed filament through Arp2/3 complex activation. The newly created seed filament supports branched filament nucleation by Wsp1 activation of Arp2/3 complex. New branches can then serve as substrates for further branching as the dense network grows to perform the desired cellular function (Rotty, Wu, and Bear 2013). However, it remains unknown if Dip1 generated filaments can template Wsp1 mediated branching.

Here, we investigated the activities of Dip1 and Wsp1 during branched network formation. Using single-molecule TIRF microscopy, we observed that Dip1 generated filaments can template Wsp1 mediated branching. Interestingly, TIRF data along with kinetic modeling suggests that Wsp1 and Dip1 co-activate Arp2/3 complex and subsequent modeling has begun to dissect the mechanism of this co-activation. These results indicate a positive feedback pathway where Wsp1 modulates the activity of Dip1 to generate seed filaments which can serve as substrates for Wsp1 mediated branching. These multiple modes of regulation have the potential to rapidly generate branched networks by utilizing the same proteins in seed filament and branch filament nucleation.

RESULTS

Dip1 Activates Arp2/3 Complex and Remains Bound at the Pointed End of the Nucleated Filament

Arp2/3 complex binds to a pre-existing filament and nucleates a new filament that elongates away from the existing filament at an approximate 70° angle to create a branched filament structure (Blanchoin et al. 2000). After branched filament nucleation, Arp2/3 complex remains at the branch junction interacting with the existing filament side and the newly nucleated filament pointed end (Volkmann et al. 2001). Dip1 mediated activation of Arp2/3 complex was found to result in the formation of linear filaments demonstrating that Dip1 activates Arp2/3 complex through a novel mechanism that does not require pre-existing filaments (Wagner et al. 2013). This unique manner of nucleation, when activated by Dip1, makes it uncertain if Arp2/3 complex behaves similarly during branched and linear filament nucleation. To understand the mechanism of Arp2/3 complex activation by Dip1, we directly visualized Dip1 during Arp2/3 complex activation using single-molecule TIRF microscopy. Full-length Dip1 was labeled with a single Alexa-568 fluorescent dye (Dip1-568) and quantification of the labeled Dip1-568 activity revealed it has the same activity as wild type Dip1 (Figure 1A). Polymerization reactions with Oregon-Green 488 labeled actin monomers, Dip1-568 and Arp2/3 complex were initiated and visualized in real-time using a previously published single-molecule TIRF microscopy procedure (Helgeson and Nolen 2013). In the presence of Arp2/3 complex we observed Dip1-568 bound to the pointed end of a subpopulation of actin filaments which often entered the imaging plane after nucleation (Figure 1B, Video 1). We did not observe Dip1-568 binding to the sides of filaments or barbed ends.

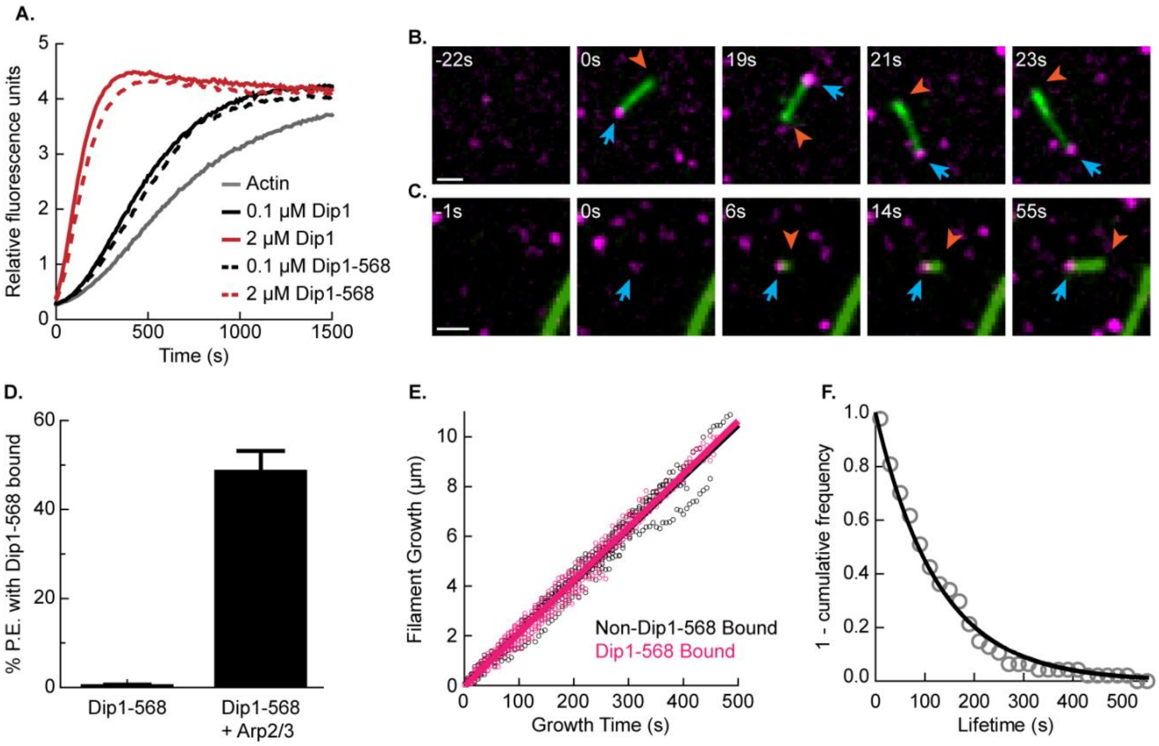

Figure 1. Dip1 Activates Arp2/3 Complex and Remains Bound at the Pointed End of the Nucleated Filament

A. Pyrene-actin polymerization time courses of 3 µM 15% pyrene-actin and 50 nM Arp2/3 complex activated by Dip1 (solid lines) and Dip1 labeled with Alexa-568 (Dip1-568, dashed lines) at two representative concentrations. **B.** TIRF microscopy images showing a representative Dip1-568 bound to a filament pointed-end from a reaction of 1 µM 33% Oregon-Green actin (green), 0.7 µM Arp2/3 complex and 2.5 nM Dip1-568 (magenta). 0s timestamp references the moment the Dip1-568 landed in the imaging plane. Cyan arrow indicates pointed end bound Dip1-568 and orange arrowhead indicates barbed end. Scale bar is 1 µm. **C.** TIRF microscopy images showing an example of a Dip1 mediated nucleation event from a reaction containing 1 µM 33% Oregon-Green actin (green), 0.5 µM Arp2/3 complex and 18 nM Dip1-568 (magenta). Arrows and timestamps reference same as in B. Scale bar is 1 µm. **D.** Percentage of visible filament pointed ends with Dip1-568 bound (Dip1 created filaments) with and without 0.5 µM Arp2/3 complex counted from TIRF microscopy images of reactions also containing 1 or 1.5 µM Oregon-Green actin, 0.25 µM Wsp1-GST-VCA and 6 or 8 nM Dip1-568. Error bars are S.E.M. **E.** Length of filament growth versus time of growth for 9 Dip1-568 bound filaments (pink dots) and 9 non-Dip1-568 bound filaments (black dots) measured from TIRF microscopy images of a reaction containing 1 µM Oregon-Green actin, 0.5 µM Arp2/3 complex and 18 nM Dip1-568. All data from each filament bound state was globally fit with a linear regression model (solid lines) to determine the growth rate: Dip1-568 bound filaments (pink line) = 0.0213 ± 0.0003 µm/s and non-Dip1-568 bound filaments (black line) = 0.0209 ± 0.0003 µm/s, errors are 95% confidence interval from fit. **F.** Frequency plot of Dip1-568 lifetimes bound to filament pointed ends (n = 47) and fit with a single exponential decay function to yield an off-rate of 0.0080 ± 0.0003 s^{-1}, errors are 95% confidence interval from fit.

Importantly, Dip1-568 did not bind to filaments in the absence of Arp2/3 complex and in the presence of Arp2/3 complex, Dip1-568 was rarely observed to capture the pointed-end of a pre-existing filament (Figure 1D). Filaments with Dip1-568 bound at their pointed ends elongated at the same rate as those created through spontaneous nucleation indicating that Dip1 does not affect filament elongation (Figure 1E).

The Dip1-568 bound filaments observed during these reactions were likely nucleated by Arp2/3 complex activated by Dip1-568. Capturing a nucleation event of a linear filament, spontaneous or Dip1-568 mediated, is rare because filaments are kept within the imaging TIRF plane through interactions with the surface bound myosin. Despite these difficulties, we observed some instances of Dip1-568 non-specifically associating with the surface and nucleating a linear actin filament which elongated away from the Dip1-568 puncta (Figure 1C and 2B, Video 2 and 4). These rare events clearly demonstrated that Dip1-568 activates Arp2/3 complex and remains bound to the complex after it nucleates the new filament. Our observations of nucleation events with Dip1-568 bound afterwards and the absence of pointed-end capture events, strongly suggests that Dip1-568 bound filaments that migrate into the imaging field were nucleated through Dip1-568 mediated activation of Arp2/3 complex. WASP family proteins must be released from Arp2/3 complex during branching nucleation but our visualization of Dip1 activated filament assembly demonstrates that Dip1 does not need to be released for new filament nucleation and elongation (Helgeson and Nolen 2013; Smith, Padrick, et al. 2013). These results highlight another important mechanistic distinction between Dip1 and WASP family protein activation of Arp2/3 complex.

Dip1 Remains Bound at the Pointed End after Nucleation

Our TIRF data show that Dip1 does not immediately release from Arp2/3 complex upon filament nucleation. Recently, it was found that the release rate of WASP from Arp2/3 complex during nucleation is correlated with the rate of branch filament nucleation (Helgeson and Nolen 2013; Smith, Padrick, et al. 2013). These findings demonstrate the importance of NPF release in regulating the assembly rate of branched networks. To understand if Dip1 release could modulate the rate of Arp2/3 complex activation, we measured the off-rate of Dip1-568 from our TIRF microscopy experiments. The off-rate was determined from a single-exponential decay fit to a one minus cumulative frequency plot of Dip1-568 lifetimes at the pointed end of actin filaments (Figure 1F). Lifetimes were measured by tracking individual Dip1-568 puncta bound to filaments from their appearance in the imaging field to their disappearance from the filament end. To correct for the time before Dip1-568 nucleated filaments migrated into the imaging field, we calculated the age of the Dip1-568 bound filament upon its first appearance by measuring the filament length and assuming a constant elongation of 0.031 μm/s. This allowed us to back calculate to the time of filament nucleation when Dip1-568 bound to and activated Arp2/3 complex, which is the true start of the Dip1-568 lifetime. We found that the rate of Dip1-568 signal disappearance from pointed ends was very slow with an average off-rate of 0.008 s^{-1}. It is not currently known if we are measuring dissociation or photobleaching in our reactions when we observe Dip1-568 disappearance. Therefore, our experimentally determined off-rate represents a minimum value whereas the maximum value could be infinite because we have yet to determine if Dip1 dissociates from Arp2/3 complex after activation. The lab will conduct follow-up studies with reduced image acquisition rates to more precisely measure if Dip1 releases from Arp2/3 complex. However, the current minimum average lifetime (125 s) suggests that activation of Arp2/3 complex by Dip1 could function as a single turnover reaction *in vivo* because the average endocytic pit lifetime is less than 20 s (Sirotkin et al. 2010). Restraining Dip1 to activate Arp2/3 complex once during network formation would drastically reduce the amount of Dip1 mediated nucleation. Explicit determination of the Dip1 off-rate will provide insight into how Dip1 regulates filament network assembly in cells.

Dip1 Generated Filaments Can Template WASP Mediated Branching

Based on genetic evidence and our biochemical dissection of Dip1, we hypothesized that Dip1 activation of Arp2/3 complex nucleates seed filaments which are necessary for WASP mediated branched network formation (Basu and Chang 2011; Wagner et al. 2013). Growing evidence suggests proteins bound to filament ends can allosterically affect the filament structure and directly influence the interactions of actin filament side binding proteins (Papp et al. 2006; Ujfalusi et al. 2009). Because Dip1 remains bound to Arp2/3 complex at the filament pointed end during elongation its presence could influence the ability of WASP mediated branching to occur from that filament. To determine if filaments nucleated through Dip1 activation can template WASP mediated branching, we added Wsp1-GST-VCA to our TIRF reactions with Oregon-Green 488 actin, Dip1-568 and Arp2/3 complex. We observed multiple instances of Dip1-568 bound filaments with branched filaments growing from their sides (Figure 2A,B; Video 3 and 4). These results clearly show that filaments nucleated through Dip1

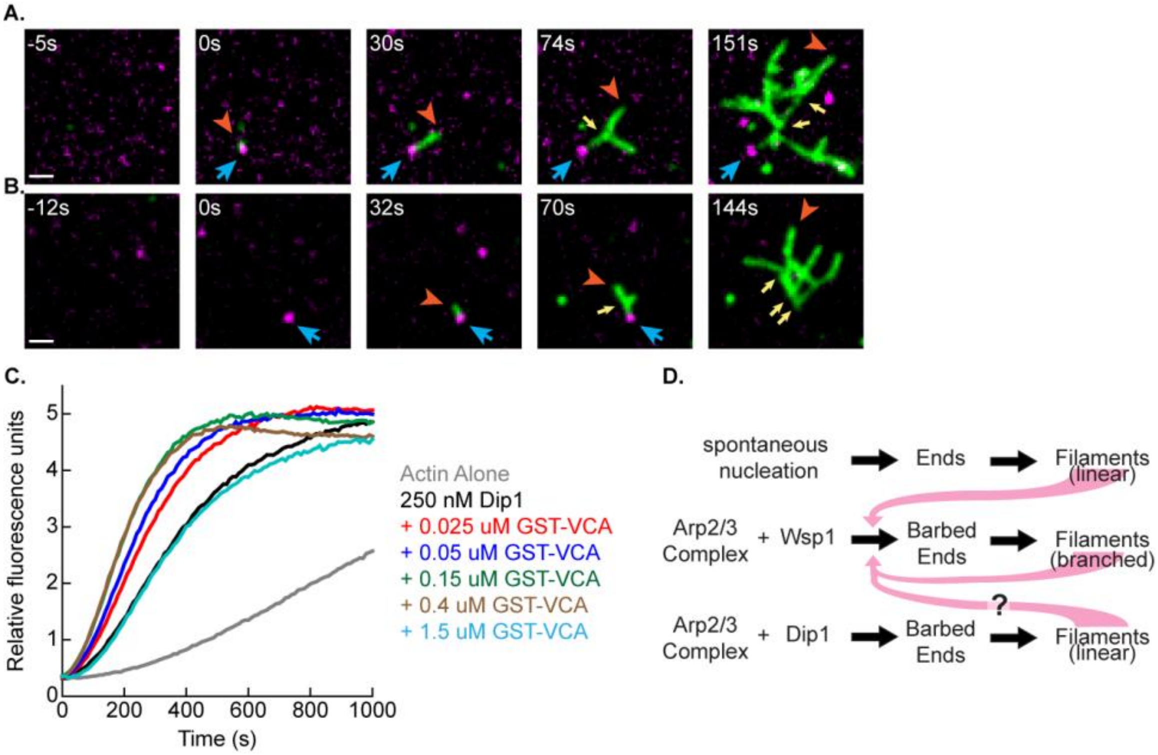

Figure 2. Dip1 Generated Filaments Serve as Templates for Branching
A. TIRF microscopy images showing a representative Dip1-568 generated filament supporting Wsp1 mediated branching from a reaction containing 1 µM 33% Oregon-Green actin (green), 0.5 µM Arp2/3 complex, 0.25 µM Wsp1-GST-VCA and 6 nM Dip1-568 (magenta). 0s timestamp references the moment Dip1-568 landed in the imaging plane. Cyan arrow indicates pointed end bound Dip1-568, orange arrowhead indicates barbed end and yellow arrows indicate branching events from the Dip1-568 generated filament. Scale bar is 1 µm. **B.** TIRF microscopy images showing a representative Dip1-568 (magenta) mediated nucleation event where the generated filament (green) supports Wsp1 branching. Reaction contains, arrows and timestamps reference same as in A. Scale bar is 1 µm. **C.** Pyrene-actin polymerization time courses of reactions containing 3 µM 15% pyrene-actin, 75 nM Arp2/3 complex and the indicated concentrations of Dip1 and Wsp1-GST-VCA. **D.** Schematic of nucleation pathways to actin network formation. Pink arrows indicate actin filaments that can template branching nucleation.

activation of Arp2/3 complex are substrates for WASP mediated branching.

Together, Dip1 and Wsp1 Accelerate Actin Network Formation

Our TIRF data demonstrates that Dip1-Arp2/3 complex nucleated and bound filaments can serve as templates for Wsp1-GST-VCA mediated branching. These results show that branched networks can be generated through coordinate activation of Arp2/3 complex by Dip1 and Wsp1-GST-VCA, meaning Dip1 activity can directly lead to Wsp1-GST-VCA activity. This mechanism of coordinate activation suggests that Dip1 can accelerate branched network assembly by seeding branching nucleation. To investigate the effect of Dip1 and Wsp1-GST-VCA on the rate of actin network formation we performed pyrene-actin polymerization assays with constant Arp2/3 complex and Dip1 and increasing concentration of Wsp1-GST-VCA (Figure 2C). Addition of Wsp1-GST-VCA up to 0.4 μM increased the rate of Dip1 and Arp2/3 complex network formation but at concentrations above 0.75 μM, Wsp1-GST-VCA reduced network formation due to spontaneous nucleation inhibition by the actin monomer binding V region. Despite our visualization of seed filament nucleation, our assays are unable to determine if coordinate activation of Arp2/3 complex by Dip1 and Wsp1-GST-VCA is the mechanism of the increased rate of branched network formation or if the increased rate could be due to independent activation by each NPF. In the latter mechanism, spontaneously nucleated filaments serve as the primary seed filaments for Wsp1-GST-VCA mediated branching while Dip1 filaments serve a minor role (Figure 2D). To identify the contribution of Dip1 created seed filaments to the rate of branched network formation we sought to build a kinetic model of coordinate activation of Arp2/3 complex by Dip1 and Wsp1-GST-VCA. Optimization of the model to our pyrene-actin polymerization data with both NPFs will allow us to track and quantify each reaction intermediate at high resolution to determine if Dip1 seeding branching nucleation accelerates network assembly.

Dip1 Activated Arp2/3 Complex Weakly Interacts with Actin Monomers Prior to Nucleation

Prior to modeling the coordinate activation by both NPFs, we constructed kinetic models of Arp2/3 complex activation by Dip1 and Wsp1-GST-VCA alone. We have previously published a model of branched actin formation by N-WASP GST-VCA activation of Arp2/3 complex (Helgeson and Nolen 2013). We replaced the N-WASP rate constants with those measured for Wsp1-GST-VCA and optimized the Arp2/3 complex nucleation rate against pyrene-actin fluorescent traces of 100 nM Arp2/3 complex with increasing Wsp1-GST-VCA concentrations (Figure 3A). Our model was able to accurately describe the increase in activity at low Wsp1-GST-VCA concentrations and the reduced activity at higher Wsp1-GST-VCA concentrations due to inhibition of spontaneous nucleation from the V region. These fits show that we constructed an accurate model of Wsp1 mediated branched network formation.

The detailed mechanism of Dip1 mediated activation of Arp2/3 complex remains unexplored. Therefore, we constructed our model of Dip1 filament assembly similar to WASP family mediated branching. WASP family proteins actively recruit two actin monomers to Arp2/3 complex during activation whereas Dip1 does not (Padrick et al. 2011; Boczkowska et al. 2014; Wagner et al. 2013). In accordance with WASP activation, we hypothesized that actin monomers bind to the Dip1-Arp2/3 complex prior to the irreversible formation of the new Arp2/3 nucleated filament. The final modeled pathway of Dip1 mediated filament assembly started with Dip1 binding to Arp2/3 complex, followed by two actin monomers binding to this complex and finally an irreversible nucleation reaction, similar to Wsp1-GST-VCA, to form a new filament that

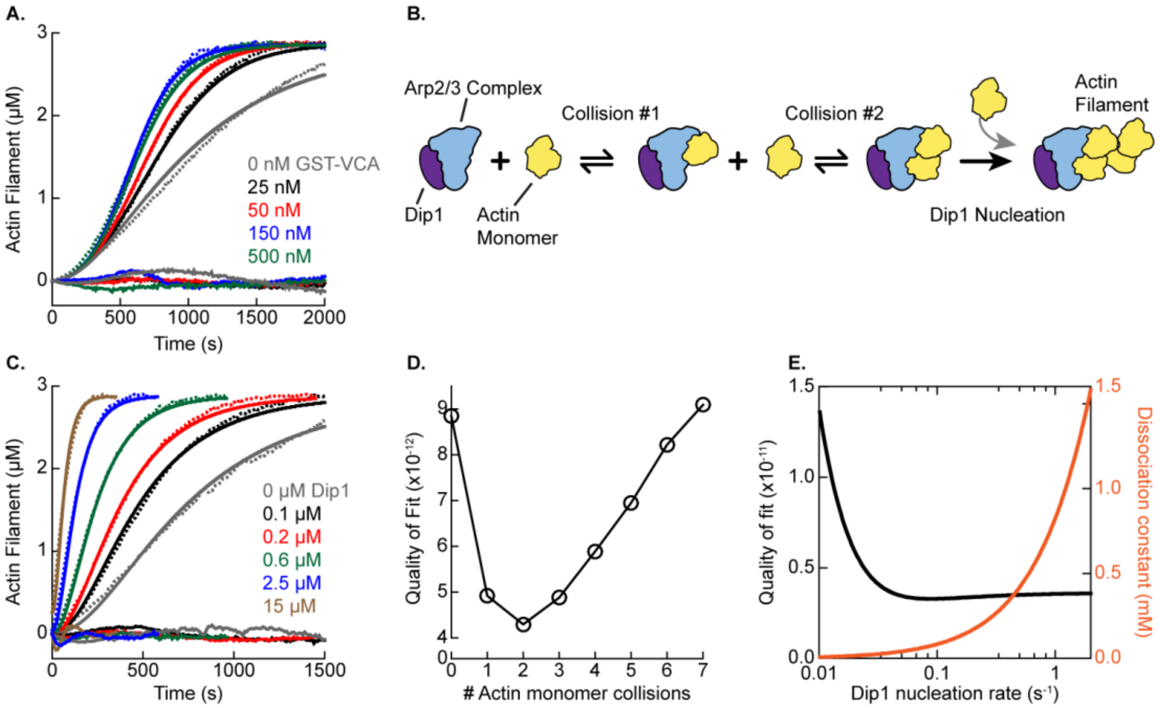

Figure 3. Dip1 Bound Arp2/3 Complex Weakly Interacts with Two Actin Monomers Prior to Nucleation

A. Pyrene-actin polymerization time courses of Arp2/3 complex activated by Wsp1-GST-VCA (dashed lines) with simulated fits (solid lines). Residuals are shown below as solid lines. Reactions contained 3 μM 15% pyrene-actin, 100 nM Arp2/3 complex and indicated concentrations of Wsp1-GST-VCA. **B.** Schematic of Dip1 activation of Arp2/3 complex pathway. Dip1 nucleation step irreversibly generates new filament. **C.** Pyrene-actin polymerization time courses of Arp2/3 complex activated by Dip1 (dashed lines) with simulated fits (solid lines). Residuals are shown below as solid lines. Reactions contain 3 μM 15% pyrene-actin, 75 nM Arp2/3 complex and indicated concentrations of Dip1. **D.** Quality of fit versus number of actin monomer collision steps prior to Dip1 nucleation for reactions described in C. **E.** Optimized dissociation constant (orange, right axis) and quality of fit (black line, left axis) from optimization routines of the Dip1 binding to Arp2/3 complex on- and off- rates at variable Dip1 activating nucleation rates. Dissociation constant calculated as off-rate divided by on-rate and simulations were optimized to pyrene-actin polymerization data from panel C.

elongates from its barbed end with Arp2/3 complex bound at its pointed end (Figure 3B). Our new model of Dip1 activation was optimized to pyrene-actin polymerization fluorescent traces of 75 nM Arp2/3 complex with increasing Dip1 concentrations (Figure 3C). We observed a range of Arp2/3 complex nucleation values which produced a similar quality of fit when Dip1 binding to Arp2/3 complex was also allowed to be optimized (Figure 3E). Without knowledge of the Dip1 to Arp2/3 complex on and off-rates we can only limit the Arp2/3 complex nucleation rate to a range of values with similar fits. Addition of an increasing number of actin monomer binding collision reactions to the Dip1-Arp2/3 complex, prior to nucleation, revealed that two actin monomer binding reactions with the complex resulted in the best fit (Figure 3C, D). Optimization of the new actin monomer binding rates indicate that they interact with the Dip1-Arp2/3 complex with a lower affinity than the barbed end of elongating filaments, 7 μM versus 0.12 μM respectively (Pollard 1986). Together, these results reveal that actin monomers associate with the Dip1-Arp2/3 complex more weakly than with filament barbed ends and this maybe a rate limiting step. Through our modeling of Dip1 mediated filament assembly we have found that actin monomers weakly associate with Dip1 bound Arp2/3 complex. These results have implications for other NPFs which do not recruit actin monomers during activation.

Dip1 Seeding Branching Nucleation Cannot Account for the Accelerated Rate of Actin Network Formation with Dip1 and Wsp1

Dip1 created seed filaments are hypothesized to increase the rate of Wsp1 mediated branched network formation. To identify the contribution of Dip1 created seed filaments to the rate of network assembly, we kinetically model Dip1 and Wsp1-GST-VCA coordinate activation of Arp2/3 complex. We combined the two independent NPF activation models developed above and allowed Wsp1-GST-VCA mediated branching to occur from Dip1 generated filaments at the same rate as spontaneously nucleated filaments. In this model, we kept Dip1 and Wsp1-GST-VCA binding to Arp2/3 complex mutually exclusive to test if the two NPFs compete for the complex (Figure 4A). Interestingly, simulations of a constant concentration of Dip1 and Arp2/3 complex with increasing concentrations of Wsp1-GST-VCA did not increase the rate of actin filament formation but potently inhibited network formation (Figure 4B). Examination of Arp2/3 complex associated species during the reaction revealed that Dip1 and Wsp1-GST-VCA do compete for Arp2/3 complex and this competition lead to the reduction in the polymerization rate (Figure 4C). Dip1 and Wsp1-GST-VCA are predicted to not share the same Arp2/3 complex binding sites suggesting that they may be able to simultaneously bind the complex (Ti et al. 2011; Wagner et al. 2013). To prevent competition, we adjusted our model to allow for Dip1 and Wsp1-GST-VCA to simultaneously bind the complex (Figure 4D). It is unknown if nucleation can occur when both NPFs are bound so we first performed our simulation with a model that restricted Arp2/3 complex nucleation to occur only when one NPF was bound. While Dip1 associated Arp2/3 complex did not significantly decrease, upon increasing Wsp1-GST-VCA in these simulations, there was still a decrease in the amount of Dip1 generated ends which lead to an overall reduction in the rate of network formation (Figure 4E, F). These simulations reveal that Dip1 and Wsp1-GST-VCA could simultaneously be bound to Arp2/3 complex during activation. Importantly, our modeling has revealed that the increased rate of network formation with Dip1 and Wsp1-GST-VCA is not predominantly caused by Dip1 alone seeding branching nucleation. Instead, these results suggest that these two NPFs may cooperatively activate Arp2/3 complex to accelerate the rate of network assembly.

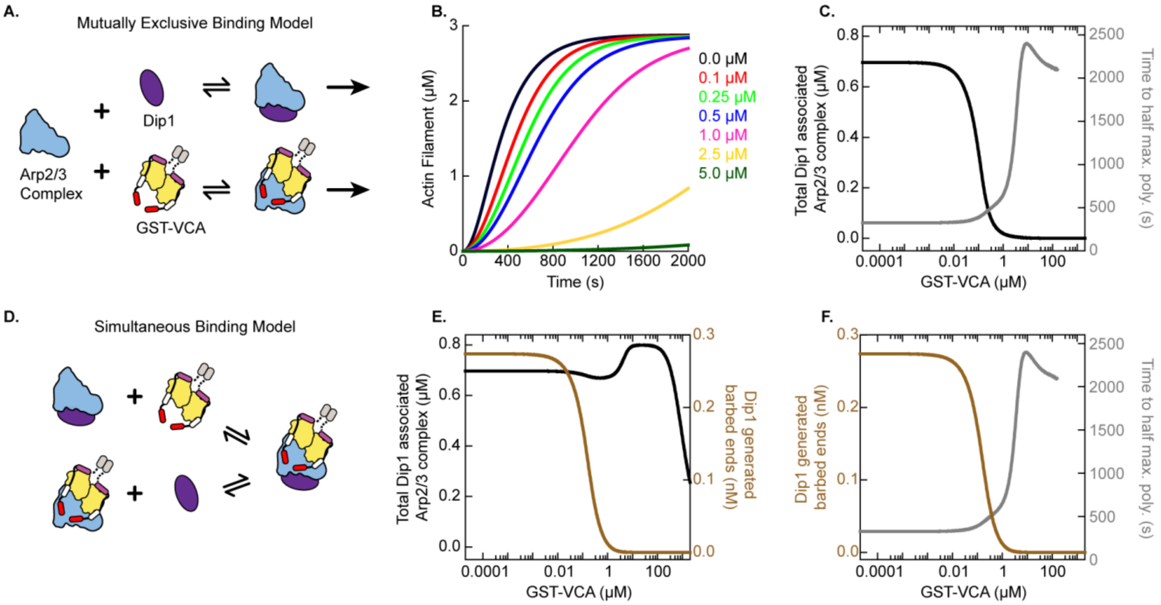

Figure 4. Dip1 and Wsp1 Compete for Arp2/3 Complex Activation
A. Cartoon of mutually exclusive binding of Arp2/3 complex by Dip1 and GST-VCA. Upon binding, each pathway can nucleate a new filament through an irreversible nucleation step (single black forward arrow). **B.** Simulated polymerization traces of 3 µM actin, 75 nM Arp2/3 complex, 250 nM Dip1 and indicated concentrations of GST-VCA using the mutually exclusive binding model. **C.** Total concentration of Dip1 associated Arp2/3 complex (black, left axis) and time to half maximum polymerization (gray, right axis) for mutually exclusive binding model simulations of 3 µM actin, 75 nM Arp2/3 complex, 250 nM Dip1 and increasing concentrations of GST-VCA. Total concentration of Dip1 associated Arp2/3 complex is calculated by integrating the concentration of all Dip1 bound Arp2/3 complex species at each time point across the entire time course. **D.** Cartoon of simultaneous binding of Arp2/3 complex by Dip1 and GST-VCA; dual bound species does not nucleate a new filament. **E.** Total concentration of Dip1 associated Arp2/3 complex (black, left axis) and concentration of Dip1 generated barbed ends (brown, right axis) for simultaneous binding model simulations of 3 µM actin, 75 nM Arp2/3 complex, 250 nM Dip1 and increasing concentrations of GST-VCA. **F.** Concentration of Dip1 generated barbed ends (brown, left axis) and time to half maximum polymerization (gray, right axis) for simultaneous binding model simulations of 3 µM actin, 75 nM Arp2/3 complex, 250 nM Dip1 and increasing concentrations of GST-VCA.

Dip1 and Wsp1 Co-activate Arp2/3 Complex to Increase the Rate of Filament Formation

Our simulations suggest that Dip1 and Wsp1-GST-VCA simultaneously bind and co-activate Arp2/3 complex to increase the rate of network formation (Figure 5A). Co-activation of Arp2/3 complex by Dip1 and Wsp1-GST-VCA would result in the formation of more linear filaments. To test this prediction, we analyzed the number of Dip1-568 generated filaments in our TIRF assays with and without Wsp1-GST-VCA. The reactions containing both Wsp1-GST-VCA and Dip1-568 showed a significant increase in the percentage of filament pointed ends bound by Dip1-568 (Figure 5B). These results indicate that the activity of Dip1 was increased upon addition of Wsp1-GST-VCA to the reaction. This demonstrates that Wsp1-GST-VCA may modulate the rate of seed filament formation by increasing the activity of Dip1. To further test this co-activation mechanism, we created a kinetic model of Dip1 and Wsp1-GST-VCA co-activation of Arp2/3 complex. We allowed irreversible Arp2/3 complex mediated actin nucleation to occur from an Arp2/3 complex simultaneously bound by 1 Dip1, 1 Wsp1-GST-VCA and 2 actin monomers (Figure 5A). Interestingly, addition of this single reaction to our model led to increased activity in our simulation of constant Dip1 and increasing Wsp1-GST-VCA (Figure 5C). Together, our kinetic modeling and TIRF data indicate that Dip1 and Wsp1-GST-VCA co-activate Arp2/3 complex to increase the rate of actin network construction.

The mechanism of co-activation of Arp2/3 complex by Dip1 and Wsp1 and how this activity contributes to increasing filament nucleation remains undetermined. Co-activation of Arp2/3 complex by Dip1 and Wsp1-GST-VCA requires both NPFs and

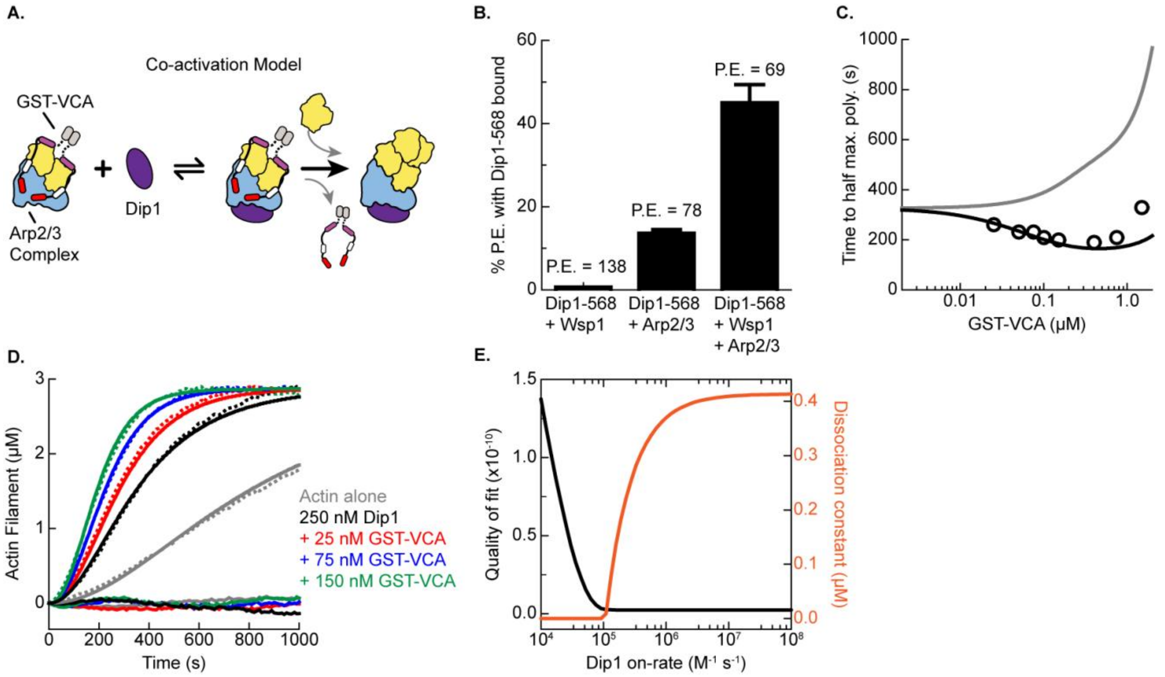

Figure 5. Dip1 and Wsp1 Co-activate Arp2/3 Complex

A. Cartoon of Dip1 and Wsp1-GST-VCA co-activation of Arp2/3 complex. The simultaneously bound Arp2/3 complex nucleates a new filament with an irreversible nucleation step (single black forward arrow). **B.** Percentage of visible filament pointed ends with Dip1-568 bound (Dip1 created filaments) from TIRF microscopy reactions of 1 or 1.5 μM Oregon-Green actin and either: 6 nM Dip1-568 + 0.25 μM Wsp1-GST-VCA, or 20 nM Dip1-568 + 0.7 μM Arp2/3 complex or 6 nM Dip1 + 0.25 μM Wsp1-GST-VCA + 0.5 μM Arp2/3 complex. Error bars are S.E.M. and P.E. is average number of pointed ends per reaction . **C.** Time to half maximum polymerization from pyrene-actin polymerization time courses (open circles) and simulations using either the mutually exclusive model (gray line) or the co-activation model (black line) at 3 μM 15% pyrene-actin, 75 nM Arp2/3 complex, 250 nM Dip1 and increasing concentrations of GST-VCA. **D.** Representative pyrene-actin polymerization time courses (dashed lines) and optimized fit time courses (solid lines) for reactions containing 3 μM 15% pyrene-actin, 75 nM Arp2/3 complex, 250 nM Dip1 and the indicated concentrations of Wsp1-GST-VCA. Residuals are shown below as solid lines. Model used for optimization was co-activation model depicted in panel A. **E.** Optimized dissociation constant (orange, right axis) and quality of fit (black line, left axis) from optimization routines of the Dip1 binding to Wsp1-GST-VCA bound Arp2/3 complex off- rate at variable on-rates of the same reaction. Dissociation constant calculated as off-rate divided by on-rate and simulations optimized to pyrene-actin polymerization data from panel D.

actin monomers to bind the complex prior to new filament nucleation. Using our kinetic models, we analyzed how these different reaction steps are involved in co-activation of Arp2/3 complex. Optimization of the new co-activation nucleation value from global fits to the pyrene-actin polymerization traces with constant Dip1 and increasing Wsp1-GST-VCA resulted in a good fit (Figure 5C, D). The optimized nucleation value was found to be 0.036 s^{-1}, which is 100x higher than Wsp1-GST-VCA alone nucleation but the same as Dip1 alone nucleation. Previously, we showed that the Dip1 mediated Arp2/3 complex nucleation reaction rate is coupled with the unknown rates at which Dip1 binds to the complex (Figure 3E). Therefore, the optimized nucleation rate from our co-activation modeling could instead be a function of an increased Dip1 affinity for Arp2/3 complex. We repeated our global fitting to the polymerization data by optimizing the on and off rates of Dip1 binding to the Wsp1-GST-VCA bound Arp2/3 complex while keeping the co-activation nucleation value fixed at the nucleation rate of Wsp1-GST-VCA. The slower Wsp1-GST-VCA nucleation value and not the Dip1 rate was used because Wsp1-GST-VCA must still be released from the complex for filament nucleation and elongation (Helgeson and Nolen 2013; Smith, Padrick, et al. 2013). Similar to Dip1 alone activation, a range of affinity values were found which had the same quality of fit (Figure 5E). Interestingly, the affinity range saturated at 0.4 μM which is 175 fold better than the modeled affinity of Dip1 for Arp2/3 complex alone. These data indicate that Wsp1-GST-VCA could be increasing the affinity of Dip1 for Arp2/3 complex to accelerate the rate of filament nucleation. Dip1 alone modeling suggested that actin monomer binding to the Dip1 bound Arp2/3 complex is slow and possibly rate limiting. The mechanism of co-activation could involve overcoming this rate limiting step by Wsp1-GST-VCA actively recruiting two actin monomers to the Dip1 bound Arp2/3 complex. Experiments to test this hypothesis are still on-going. According to our simulations the co-activation of Arp2/3 complex by Dip1 and Wsp1 is likely accomplished by both proteins simultaneously binding Arp2/3 complex to either increase: the Wsp1 nucleation rate, the affinity of Dip1 for Arp2/3 complex or interactions of Dip1-Arp2/3 complex with actin monomers.

Our data has revealed that Wsp1-GST-VCA can increase the rate of network formation through enhancing Dip1 mediated linear filament generation. The mechanisms proposed from our modeling are not mutually exclusive nor are they the only plausible mechanisms. Rigorous biochemically tested is being performed to identify the correct mechanism by which Wsp1 increases Dip1 activity. Accurate understanding of the co-activation mechanism will be critical for testing Wsp1 mediated enhancement of Dip1 seed filament generation in cellular branched network assembly.

DISCUSSION

Currently, cells possess three known ways to generate seed filaments: spontaneous nucleation, cofilin mediated severing and linear filament nucleators (Campellone and Welch 2010; Q. Chen and Pollard 2013; Krause and Gautreau 2014). We observed that Dip1 generated filaments can template Wsp1 mediated branching nucleation. This observation in conjunction with the *S. pombe* Dip1 deletion phenotype suggests that Dip1 primes branched network formation during *S. pombe* endocytosis (Basu and Chang 2011). Further studies will have to confirm these findings with the metazoan Arp2/3 complex activators, Spin90 and N-WASP or WAVE, in their respective structures (Kim et al. 2006). However, given the conserved Arp2/3 complex activation mechanism between Spin90 and Dip1, these results suggest that the general cellular role of WISH/DIP/SPIN90 proteins is to trigger branched network formation by nucleating the initial seed filaments (Wagner et al. 2013). Why this method of seed filament nucleation is utilized over other linear filament nucleators, formins and tandem WH2 nucleators, or cofilin based severing remains unexplored. One benefit of using Arp2/3 complex as the seed filament generator could be to ensure that Arp2/3 complex is pre-localized prior to the initiation of branched network formation. This mechanism of Arp2/3 complex pre-localization could reduce the lag time between seed filament and branching nucleation to allow for rapid branched network formation. Using separate filament nucleators to assemble seed and branched filaments could slow the rate of branched network creation. Additionally, our data suggest that the activity of WISH/DIP/SPIN90 proteins can be regulated by WASP family proteins through co-activation of Arp2/3 complex. Similar to WISH/DIP/SPIN90 activation of Arp2/3 complex, the use of WASP proteins to enhance WISH/DIP/SPIN90 activity could directly couple seed filament generation to branching nucleation. This model of regulation allows for rapid branched network construction from these multifunctional proteins without the need to recruit additional elements. Clarification of the biological role of WISH/DIP/SPIN90 mediated filament nucleation will require careful dissection of their activity in cells and how they function in concert with other NPFs. Establishing the cellular origin of seed filaments remains a fundamental piece to understanding how branched networks are regulated during dynamic biological functions.

Actin filament elongation is highly regulated through barbed end interactions with numerous actin binding proteins. During vesicle movement or cell motility, branched filaments are often kept short by capping their barbed ends with capping protein (Edwards et al. 2014). Maintaining short filament networks prevents filament buckling and is also suspected to funnel more actin monomers to new branch filament nucleation (Akin and Mullins 2008). Our TIRF microscopy data reveals that Dip1 does not bind to barbed ends or disrupt the elongation of newly nucleated filaments from their barbed ends. This mechanism maintains the new filament barbed ends are open to regulatory proteins such as capping protein. The capping of Dip1 generated filaments could control the rate of linear filament elongation during branched network assembly. This action would provide more actin monomers for branched filament nucleation and elongation or it would conserve the short, rigid structure of branched networks. Furthermore, formins can bind to existing barbed ends to enhance filament elongation (Goode and Eck 2007). Cooperative assembly of filaments by formin and tandem WH2 nucleators has recently been observed; opening the possibility that WISH/DIP/SPIN90 proteins could cooperatively generate linear networks with formins (Breitsprecher et al. 2012). Interestingly, Spin90 has been reported to bind to and modulate the activity of the formins mDia1 and mDia2 (Eisenmann et al. 2007). These finding suggest that WISH/DIP/SPIN90 proteins regulate formin elongation activity through direct interactions and by generating a filament with a free barbed end. By promoting nucleation through Arp2/3 complex interactions at the pointed end, WISH/DIP/SPIN90 mediated filaments are open to multiple modes of regulation at their barbed ends.

Vital to many cellular functions is the rapid disassembly of branched networks through the destabilization of branched filament interactions. Branch junction stability is a function of Arp2/3 complex interactions with both the actin filament template and the newly nucleated branched filament (Rouiller et al. 2008). Glial maturation factor (GMF) has been observed to specifically disassemble Arp2/3 complex nucleated branched filaments and a recent crystal structure of it bound to Arp2/3 complex indicates that GMF may induce debranching by disrupting the interactions between the complex and the filament it has nucleated (Gandhi et al. 2010; Luan and Nolen 2013). However, a comprehensive understanding of branch junction interactions and stability has yet to be achieved. Our visualization of Dip1 during filament assembly revealed that Dip1 remains stably bound to the filament pointed end through interactions with Arp2/3 complex. Clarification of whether or not Dip1 and Arp2/3 complex can release from the pointed end and if they release together or independently will provide insight into how Arp2/3 complex interacts with the template and branch nucleated filaments. Biochemical and structural details of how Dip1 either remains bound to Arp2/3 complex at pointed-ends or promotes interactions between Arp2/3 complex and filament pointed-ends will offer unique opportunities to study the stability of Arp2/3 complex at branch junction (Mullins, Heuser, and Pollard 1998; Volkmann et al. 2014). A fundamental understanding of Arp2/3 complex interactions after filament nucleation can be achieved through studying WISH/DIP/SPIN90 mediated activation of Arp2/3 complex. Knowledge gained from these investigations will directly aid in understanding the stability of branch junctions and, importantly, the mechanisms by which they are disassembled.

Proper control of branched network structure is critical for the function of many cellular processes. We observed that Dip1 remains bound to Arp2/3 complex at the filament pointed end it has helped to nucleate. These data suggest that sequestration of Dip1 at pointed ends may decrease its activity during branched network initiation. This reduced activity would limit the number of linear filaments generated, thereby preserving the branched network geometry. Our initial measurement of the Dip1 off-rate from pointed ends showed it releases slowly (lifetime = 125 s) or not at all. Given that the branched network dependent process of endocytic invagination occurs within ~ 10 s, this suggests that Dip1 activation of Arp2/3 complex is likely single-turnover *in vivo* (Sirotkin et al. 2010). Additionally, the number of Dip1 molecules found at endocytic sites is 7.5 and 17 fold less than the other Arp2/3 complex activators, Wsp1 and Myo1p, respectively (20 vs. 150 vs. 340 molecules/endocytic site, respectively) (Sirotkin et al. 2010; Basu and Chang 2011). Together the restriction of Dip1 activity, through reduced molecule numbers and slow or no release, could constrain the number of linear filaments generated to maintain the proper branched network architecture at sites of endocytosis (Haviv et al. 2006). Furthermore, restriction of Dip1 activity could preserve the branched network geometry by leaving more Arp2/3 complex to nucleate branched filaments instead of being sequestered at pointed ends. Additional methods of WISH/DIP/SPIN90 regulation should be perused in order to fully understand the role of WISH/DIP/SPIN90 proteins in the maintenance of branched networks that they have helped to initiate.

Our preliminary results strongly indicate that Dip1 and Wsp1 can simultaneously bind to and co-activate Arp2/3 complex. To date, all known NPFs use combinations of acidic regions and amphipathic helices to bind similar locations on Arp2/3 complex.

Because of these similar binding motifs, competition for Arp2/3 complex is readily observed amongst NPFs and exploited by Arp2/3 complex inhibitors (Dang et al. 2013; Ti et al. 2011; Marchand et al. 2001). This competitive binding is even utilized by the NPF cortactin to synergistically activate the complex with WASP family proteins, through a competitive displacement mechanism (Helgeson and Nolen 2013). Our models demonstrating that Dip1 and Wsp1 can simultaneously bind the complex provides further proof that WISH/DIP/SPIN90 proteins do not bind Arp2/3 complex through a canonical acidic region, as previously proposed. Instead, WISH/DIP/SPIN90 proteins may bind an opposite surface; such as the surface that interacts with filamentous actin (Goley et al. 2010). The proposed ability of Dip1 to interact with Arp2/3 complex in a similar manner as actin filaments could allow it to induce the conformational change(s) necessary for nucleation without an actin filament (Rouiller et al. 2008; Hetrick et al. 2013). Determining the specifics of Dip1 and Arp2/3 complex interactions will prove valuable in understanding not only how different biochemically distinct NPFs activate the complex but also details about the regulation of Arp2/3 complex alone.

The creation of an actin nucleus by Arp2/3 complex is poorly understood. While it is assumed that the two actin related subunits, Arp2 and Arp3, of Arp2/3 complex mimic the structure of a filament upon activation (Rouiller et al. 2008; Robinson et al. 2001). It is unknown how actin monomers interact with the complex to form or elongate from the new actin nucleus. WASP family proteins recruit actin monomers to Arp2/3 complex and that recruitment has been shown to increase an activating conformational change (Hetrick et al. 2013). Interestingly, actin monomer recruitment is not required for Arp2/3 complex activation because WISH/DIP/SPIN90 proteins and actin filament binding NPFs, like cortactin and coronin, activate Arp2/3 complex without the need to deliver monomers (Weed et al. 2000; Liu et al. 2011; Wagner et al. 2013). However, the activity of the actin filament binding NPF cortactin was greatly increased by allowing it to recruit actin monomers suggesting that actin interactions with Arp2/3 complex benefit from this recruitment (Kinley et al. 2003; Helgeson et al. 2014). While the ability of Dip1 to induce the Arp2/3 complex activating conformational change was shown to be unaffected by actin monomers (Wagner et al. 2013), our kinetic modeling has revealed that actin nucleus formation or filament elongation from Dip1 bound Arp2/3 complex maybe rate limiting. Overcoming this rate limiting step through Wsp1 mediated recruitment of actin monomers to a Dip1 bound Arp2/3 complex could be a mechanism of Arp2/3 complex co-activation by these two NPFs. Using WISH/DIP/SPIN90 proteins to help clarify the role of actin monomers during activation of Arp2/3 complex will be valuable to understanding how Arp2/3 complex forms an actin nucleus for filament nucleation.

MATERIALS AND METHODS

Protein Purification

Rabbit skeletal muscle actin was purified and labeled with either Oregon-Green 488 or N-(1-pyrene)iodoacetamide (pyrene) as previously described (Helgeson and Nolen 2013). *S. pombe* Arp2/3 complex, *S. pombe* WASP1 (Wsp1) GST-VCA (residues 497-574) and *S. pombe* full length Dip1 were purified as previously described (Liu et al. 2013; Nolen and Pollard 2008; Wagner et al. 2013). Purified Dip1 with all 6 endogenous cysteines mutated to serine and an N-terminus cysteine tag was reacted with Alexa Fluor

568 maleimide overnight at 4°C. The resulting Dip1 Alexa Fluor 568 labeled protein (Dip1-568) was separated from free dye using extensive dialysis and a HiTrap desalting column before flash freezing and storage at -80°C.

TIRF Microscopy

Single-molecule TIRF microscopy was performed as previously described with some minor modifications (Helgeson and Nolen 2013). A Nikon TE2000-E microscope equipped with a perfect focus unit, a 100x NA 1.49 Nikon TIRF objective with a 1.5x auxiliary lens and an Andor iXon3 EM-CCD were used for image collection. Solid-state 488 nM and 561 nM lasers were used to excite Oregon-Green 488 and Alexa Fluor 568 fluorophores, respectively. Excitation and emission light were filtered with triple band (488/561/641) emission, excitation and dichroic filters. Image frames were acquired at rates of 1-5 Hz with one 488-channel exposure taken for every 1-6 561-channel exposures. Images were background subtracted using a 10 pixel radius rolling ball subtraction algorithm in ImageJ and further smoothed by convolution with a two dimension gaussian kernel of radius 0.5-0.6 pixels.

Image Analysis

The lifetimes of Dip1-568 bound to Arp2/3 complex during nucleation were determined by visually tracking each filament pointed-end bound Dip1-568 molecule and its corresponding frame timestamps from the moment it entered the imaging plane to its disappearance. Dip1-568 bound filaments that entered the imaging plane were assumed to be generated by Dip1-568 and their lengths were measured and converted to age based on a filament growth rate of 11.6 subunits/s and filament dimensions of 370 subunits/µm (Pollard 1986; Kuhn and Pollard 2005). The filament age was added to the manually tracked lifetime to give the final Dip1-568 bound to Arp2/3 complex lifetime. Dip1-568 molecules that did not disappear before the end of the acquisition period were not included in the analysis. Lifetimes were binned into 20 s intervals and the total molecule cumulative frequency subtracted from 1 was calculated for each bin. 1 minus cumulative frequency as a function of bin lifetime was fit with a single-exponential decay model to determine the average off-rate of Dip1-568 from Arp2/3 complex.

Filament growth lengths were calculated as the difference between the initial filament length and the new filament length measured every 6.15 s. Filament lengths were measured using a previously described filament tracing and length measurement tool in ImageJ (Kuhn and Pollard 2005). Global growth rates for Dip1-568 and non-Dip1-568 bound filaments were determined by a linear regression fit to all measured growth data from each filament bound state (non-Dip1 and Dip1 bound states).

Kinetic Modeling

Model optimization routines and simulations were performed in the kinetic modeling software, COPASI, as previously described (Helgeson and Nolen 2013). Rate constants for Wsp1 GST-VCA binding to Arp2/3 complex and actin filaments were input into the model based on experimentally determined values but Dip1 rate constants were optimized as described in the text. Actin alone rate constants were determined by simultaneous optimization to actin polymerization time courses at 2, 3, 4 and 5 μM 15% pyrene-actin. Dissociation constants were calculated as the off-rate divided by the on-rate. Total Dip1 associated Arp2/3 complex was calculated by summing the concentrations of all Dip1 bound Arp2/3 complex species at each time point and integrating those values over the entire time series. This analysis yields the time independent total amount of Dip1 bound to Arp2/3 complex for the entire time course and was chosen because of the dynamic nature of Arp2/3 complex bound species throughout the simulations.

BRIDGE TO CHAPTER V

In this chapter, we established that Dip1 generated filaments can template branching nucleation by Wsp1 mediated activation of Arp2/3 complex. We discovered that Wsp1 and Dip1 co-activate Arp2/3 complex to generate linear filaments and began to dissect the mechanism of this co-activation. We have now classified how two distinct sets of NPFs coordinately and individually activate Arp2/3 complex. In the next chapter, we will synthesize the implications of all these findings. Specifically we will discuss how multiple biochemically distinct NPFs coordinately activate Arp2/3 complex to regulate the formation of branched actin networks.

CHAPTER V

DISCUSSION

Comprehensive regulation of actin based biological processes utilizes multiple biochemically distinct NPFs to fine-tune the nucleation, architecture and assembly rate of cellular branched networks. While NPFs are characterized by their ability to activate Arp2/3 complex, we found that not all NPFs individually activate the complex in a similar manner nor do they form the same network structures. WISH/DIP/SPIN90 proteins generate linear networks while cortactin mediated networks are significantly bundled and have less higher-order branching than WASP family activated networks. Importantly, we have established functional interactions between multiple NPFs which strongly regulate the formation of branched networks. We found that cortactin and WASP family proteins synergistically activate Arp2/3 complex through a mechanism by which cortactin increases WASP protein release from the nascent branch junction, a newly determined rate limiting step. Furthermore, cortactin appears to be uniquely designed to displace WASP family proteins. Fission yeast Wsp1 was found to regulate the activity of Dip1, suggesting these pairs of NPFs also co-activate Arp2/3 complex. Additionally, we directly observed Dip1 generated filaments initiating Wsp1 mediated branched network assembly. Together, our results suggest that multiple NPFs regulate the formation of branched networks through coordinated activation of Arp2/3 complex; both individually and cooperatively.

Actin nucleators, capping proteins, filament bundlers and filament cross-linkers regulate the structure of actin networks (Pollard and Cooper 2009). Branched networks are used in numerous force generating processes because they are mechanically more rigid than linear filament networks (Blanchoin et al. 2014). Maintaining a proper branch density is critical for the function of branched networks (Bernheim-Groswasser et al. 2002). The work presented here indicates that NPFs could provide another mechanism of controlling branched network architecture and function. We identified that activation of Arp2/3 complex by cortactin lead to bundled, branched networks that are much less dense than WASP family created networks. Branched networks tailored for specific biological functions could be nucleated through precise control of which NPF activates Arp2/3 complex. Ridged bundled filaments which are important for invadopodia formation and growth could originate from cortactin activation of Arp2/3 complex; both proteins are required to interact for proper invadopodia function (A. Li et al. 2010; Ayala et al. 2008). Verification of cortactin as the primary Arp2/3 complex activator in invadopodia would establish a functional link between NPF activation and the cellular specificity of branched network structure. Alternatively, WISH/DIP/SPIN90 mediated formation of linear filaments would contaminate branched networks leading to a reduced branch density which could compromise the rigidity of branched networks (Blanchoin et al. 2014). Little is known about the mechanics and cellular use of mixed, linear and branched, networks but WISH/DIP/SPIN90 activity could fine-tune the stiffness of the networks through linear filament generation (Haviv et al. 2006; Vignjevic et al. 2003). The coupling of NPF activity to biological function and their required filament network mechanical properties is fundamental to understanding the cellular specification of the primary Arp2/3 complex activators.

Coordinate activation of Arp2/3 complex was found to be a robust determinant of branched network regulation. We identified that coordinate activation of Arp2/3 complex can be broken down into; synergistic and temporal NPF coordination. In the former condition, the individual filament nucleation rate with both NPFs is greater than each NPF individually; whereas the latter condition is defined as an increase in the overall rate of branched network formation through individual activation. These coordination events do not have to be mutually exclusive as found in the case of Dip1 and Wsp1 branched network assembly; where Wsp1 and Dip1 synergistically activate Arp2/3 complex to quickly generate seed filaments for subsequent branching nucleation mediated by Wsp1. These findings demonstrate the complexity of branched network assembly and establish the necessity of diverse NPF properties for comprehensive control of branched networks, from initiation through functional mechanics.

Our data suggests that previously proposed models of branched network assembly by Arp2/3 complex have over-simplified the role of NPFs. Based on our findings, we propose a new model of branched network formation by multiple NPFs which emphasizes the coordinate activation of Arp2/3 complex. Our model highlights branched network assembly in lamellipodia which is dependent upon three biochemically distinct NPFs: WAVE, cortactin and Spin90 (Suetsugu et al. 2003; Bryce et al. 2005; Kim et al. 2006). The model can be applied to other NPF rich cellular structures, but must be adjusted to account for the specific activation properties of each NPF, alone and cooperatively.

Lamellipodia formation starts with intracellular signaling events to activate and localize Spin90 and WAVE to the leading edge of the cell along with Arp2/3 complex (Kim et al. 2006; Miki, Suetsugu, and Takenawa 1998). Once activated and localized, Spin90 and WAVE simultaneously bind and co-activate Arp2/3 complex to nucleate the seed filaments, which will initiate branched network assembly. The pre-emptive recruitment of WAVE and Arp2/3 complex to the site of seed filament formation reduces any delay in WAVE and Arp2/3 complex association, which promotes rapid branching nucleation upon seed filament creation. Two membrane connected WAVE molecules bind Arp2/3 complex and together this active complex associates with the newly formed seed filament to form a nascent branch junction (Padrick et al. 2011; Ti et al. 2011). Cortactin directly targets the stalled nascent branch junction and actively displaces the WAVE molecules from Arp2/3 complex to finish nucleation of the new branched filament. Cortactin mediated release of the membrane bound WAVE molecules from the nascent branch junction disconnects the membrane from the actin cytoskeleton and allows for elongation of the new filament against the membrane (Akin and Mullins 2008). The newly nucleated branched filament templates further rounds of branching nucleation by synergistic activation of Arp2/3 complex by WAVE and cortactin to rapidly generate a dense, dendritic network that begins to protrude the membrane. During the rapid formation of branches, Spin90 remains stably bound to Arp2/3 complex at the pointed end of the seed filament. Sequestration of Spin90 ensures that few linear filaments are nucleated which would weaken the pushing force produced by the branched network (Haviv et al. 2006). Similarly, cortactin alone activation of Arp2/3 complex is kept at minimum to maintain dendritic unbundled networks required for the lamellipodia structure (Svitkina and Borisy 1999). After Arp2/3 complex activation, cortactin directly targets branch junctions with a high affinity and stabilizes them to maintain the integrity of the branched network (Weaver et al. 2001). Additionally, membrane bound WAVE binds free barbed ends and filament bound Arp2/3 complex to modulate interactions between the membrane and the actin cytoskeleton which are important for mechanical pressure on the membrane (Co et al. 2007). Once established, the branched network is further regulated by a plethora of specialized non-NPF actin binding proteins which cap, bundle and disassemble filaments.

In-depth dissection of NPF function within the cell will be required to fully elucidate their role in cellular branched network regulation. Our examination of NPF activation mechanisms, both individually and cooperatively, will provide the specific knowledge needed to correctly identify the observed cellular NPF functions. The widespread use of branched networks across many distinct cellular processes with different molecular compositions suggests that not all branched networks are structurally and functionally the same. Fundamental understanding of how branched networks are assembled and regulated will offer valuable insight into the biological functions that rely on them.

APPENDIX A

SUPPLEMENTAL FIGURES AND VIDEO LEGENDS FOR CHAPTER II

Supplemental Figure 1. Mathematical Modeling of Actin Polymerization in the Presence or Absence of GST-VCA, Arp2/3 Complex and Cortactin

(A) Cartoon pathway of mathematical models used to fit four independent sets of pyrene-actin polymerization assays. The conditions of each reaction set and its associated model are described in table 2. (B and C) Pyrene-actin polymerization time courses run at different initial actin concentrations (B) or at 3 µM 15% pyrene-actin and varying GST-VCA concentrations (C). Dashed lines show experimental data and solid lines show simulated fits after optimization of the floating parameters indicated in Table 2. Residuals are shown below as solid lines. All reactions used 15% pyrene-labeled actin. Indicated GST-VCA concentrations are monomeric.

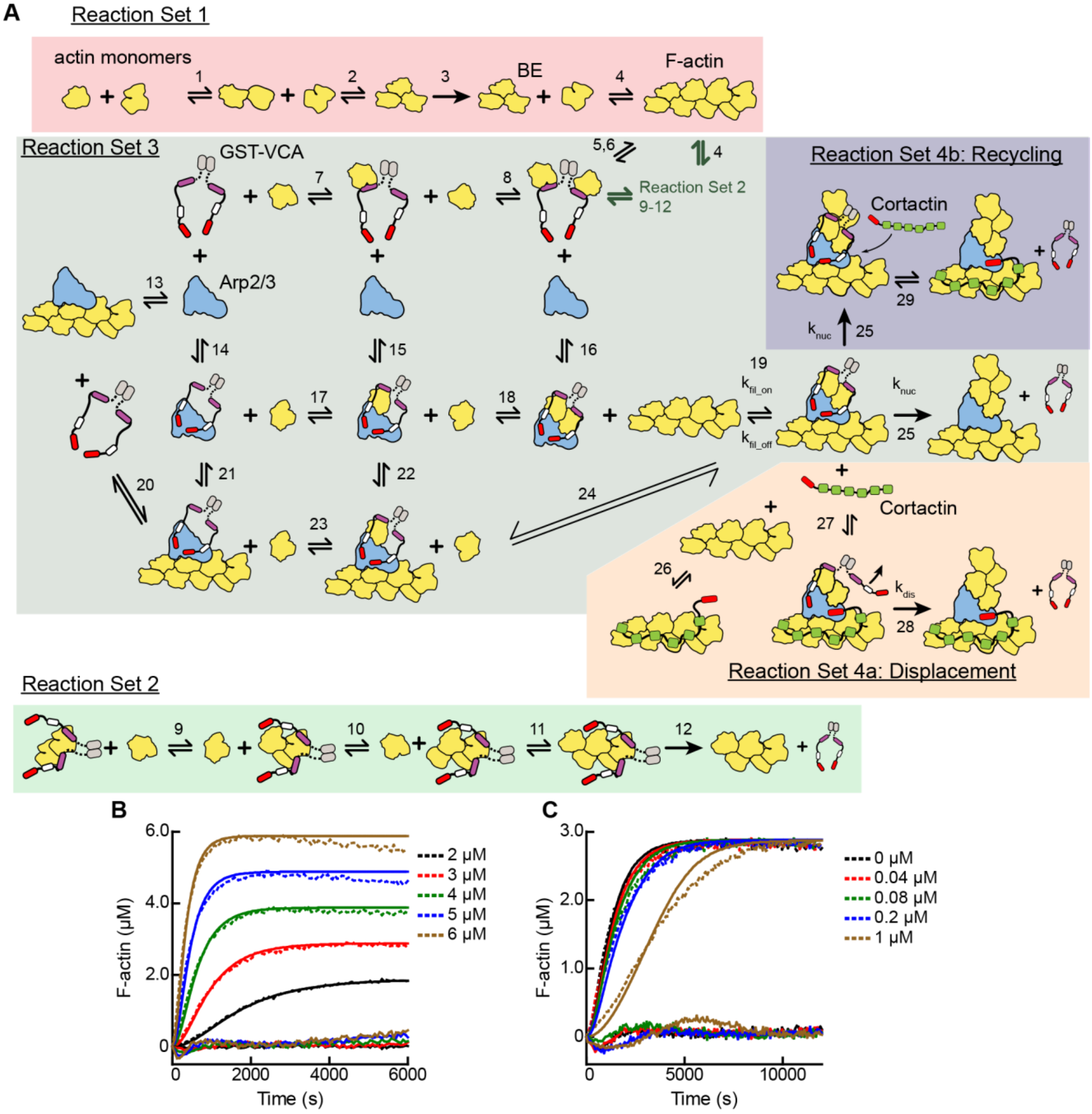
A
Reaction Set 1
actin monomers
1
2
3
BE
4
F-actin
Reaction Set 3
GST-VCA
5,6
4
7
8
Reaction Set 2
9-12
Reaction Set 4b: Recycling
Cortactin
13
Arp2/3
29
k_{nuc}
25
14
15
16
19
k_{fil_on}
k_{fil_off}
k_{nuc}
25
17
18
20
21
22
23
24
Cortactin
27
26
k_{dis}
28
Reaction Set 4a: Displacement
Reaction Set 2
9
10
11
12
B
6.0
4.0
2.0
0
F-actin (µM)
0
2000
4000
6000
Time (s)
2 µM
3 µM
4 µM
5 µM
6 µM
C
3.0
2.0
1.0
0
F-actin (µM)
0
5000
10000
Time (s)
0 µM
0.04 µM
0.08 µM
0.2 µM
1 µM

Supplemental Figure 2. The Level of Synergy is the same at Saturating and Subsaturating Concentrations of the type I NPF
Plot of fold activation versus cortactin concentration for reactions containing 2 µM 15% pyrene-actin, 20 nM Arp2/3 complex and subsaturating (open symbols and dotted fit line) or saturating (closed symbols and solid fit line) concentrations of the indicated VCA constructs. Saturating data is the same as figure 4A and fits were performed as described in methods. The concentration of each construct required to saturate Arp2/3 complex activity is based on data in figure 5A.

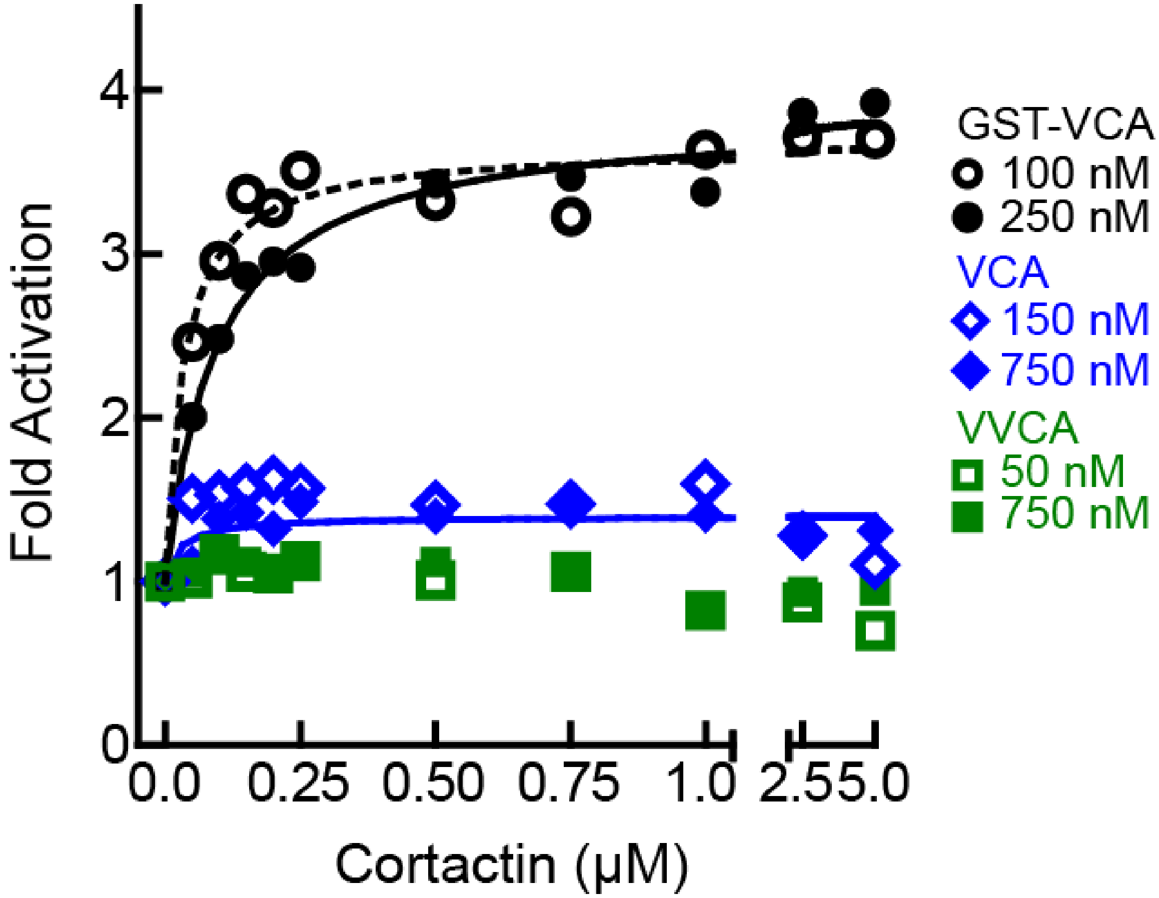

Supplemental Figure 3. The E455R Mutation in N-WASP is Predicted to Provide Additional Favorable Electrostatic Interactions with Actin Monomers
(A) Alignment of WH2/V sequences (sequence accession numbers): Tβ4 (NP_001106702.1), Ciboulot isoform D (NP_001245516.1), MIM (O43312.2), WIP (O43516.3), N-WASP (Q95107.1) and WASP (P42768.4). Residue E455 in N-WASP and homologous residues in other V regions are colored based on charge conservation. (B) Structural alignment (RMSD = 0.458 Å) of WIP-V (orange – 2A41.pdb) and N-WASP-V (green – 2VCP.pdb) bound to an actin monomer showing the 5th residue beyond the LKKT in WIP, Arg54, interacts with an acidic pocket of actin that includes Glu93. Electrostatic surface representation shows acidic (red) and basic (blue) regions on actin.

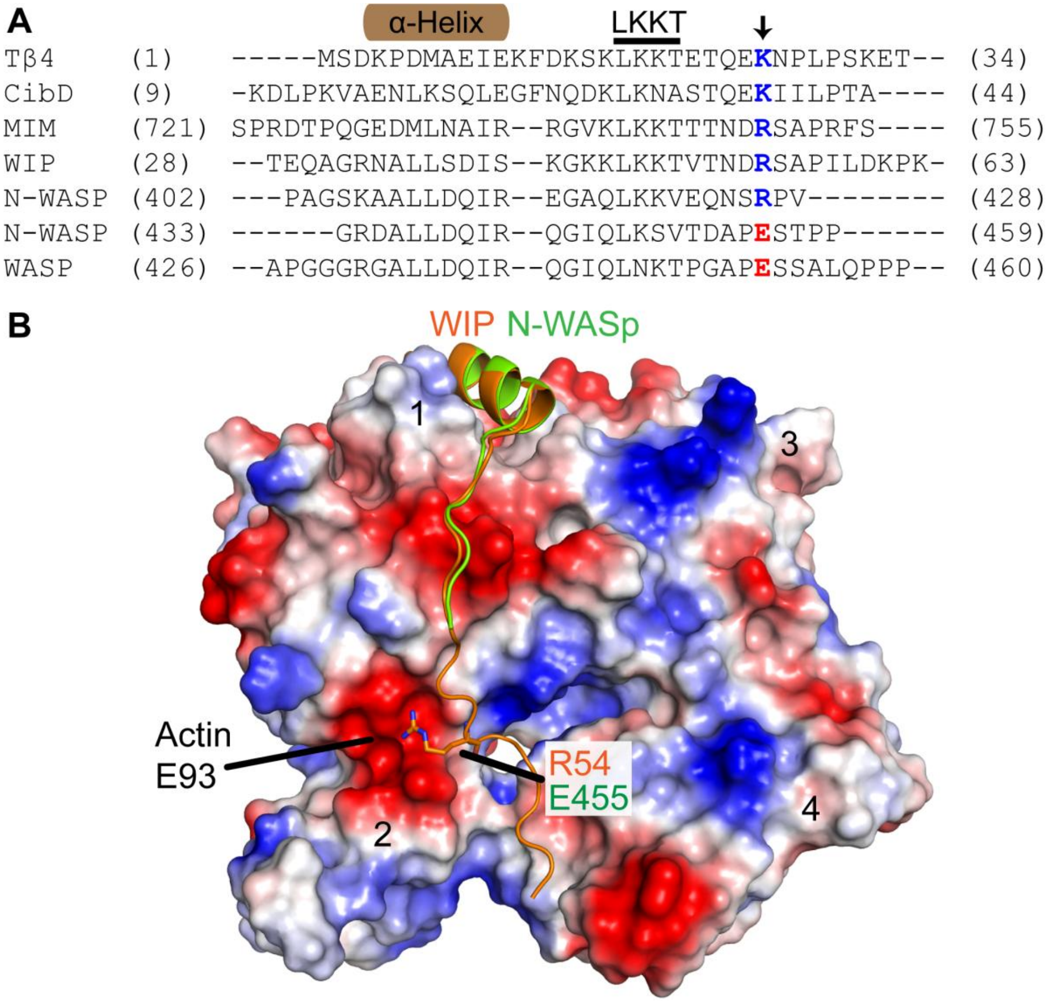

```
Tβ4    (1)   -----MSDKPDMAEIEKFDKSKLKKTETQEKNPLPSKET-- (34)
CibD   (9)   -KDLPKVAENLKSQLEGFNQDKLKNASTQEKIILPTA---- (44)
MIM    (721) SPRDTPQGEDMLNAIR--RGVKLKKTTTNDRSAPRFS---- (755)
WIP    (28)  --TEQAGRNALLSDIS--KGKKLKKTVTNDRSAPILDKPK- (63)
N-WASP (402) ---PAGSKAALLDQIR--EGAQLKKVEQNSRPV-------- (428)
N-WASP (433) ------GRDALLDQIR--QGIQLKSVTDAPESTPP------ (459)
WASP   (426) --APGGGRGALLDQIR--QGIQLNKTPGAPESSALQPPP-- (460)
```

Supplemental Figure 4. Validation of Single Molecule Data
(A) Plot of fold activation versus cortactin concentration for reactions containing 20 nM Arp2/3 complex and 250 nM GST-VCA and either full length cortactin (circle) or Alexa568-cortactin residues 1-336 (square). (B) Plot of fluorescence intensity versus frame number (left) plus still images (right) for two representative spots in the 561 channel. Biotinylated Alexa568-cortactin (1-336) at 1 nM was flowed into a streptavidin-PEG reaction chamber and imaged at 5.5 frames per second. Scale bar = 1 µm. Single-step photobleaching indicates that both signals tracked are single molecules of cortactin. (C) Lifetime plots of single cortactin molecules bound to the sides of polymerizing actin filaments, with data collected at two different laser intensities (measured at laser head). Data were fit with a single exponential to determine the binding lifetime (τ). The lifetime does not decrease at higher laser intensity, indicating that photobleaching does not significantly influence the measurements. Data for all other figures were collected (only) at 25 mW.

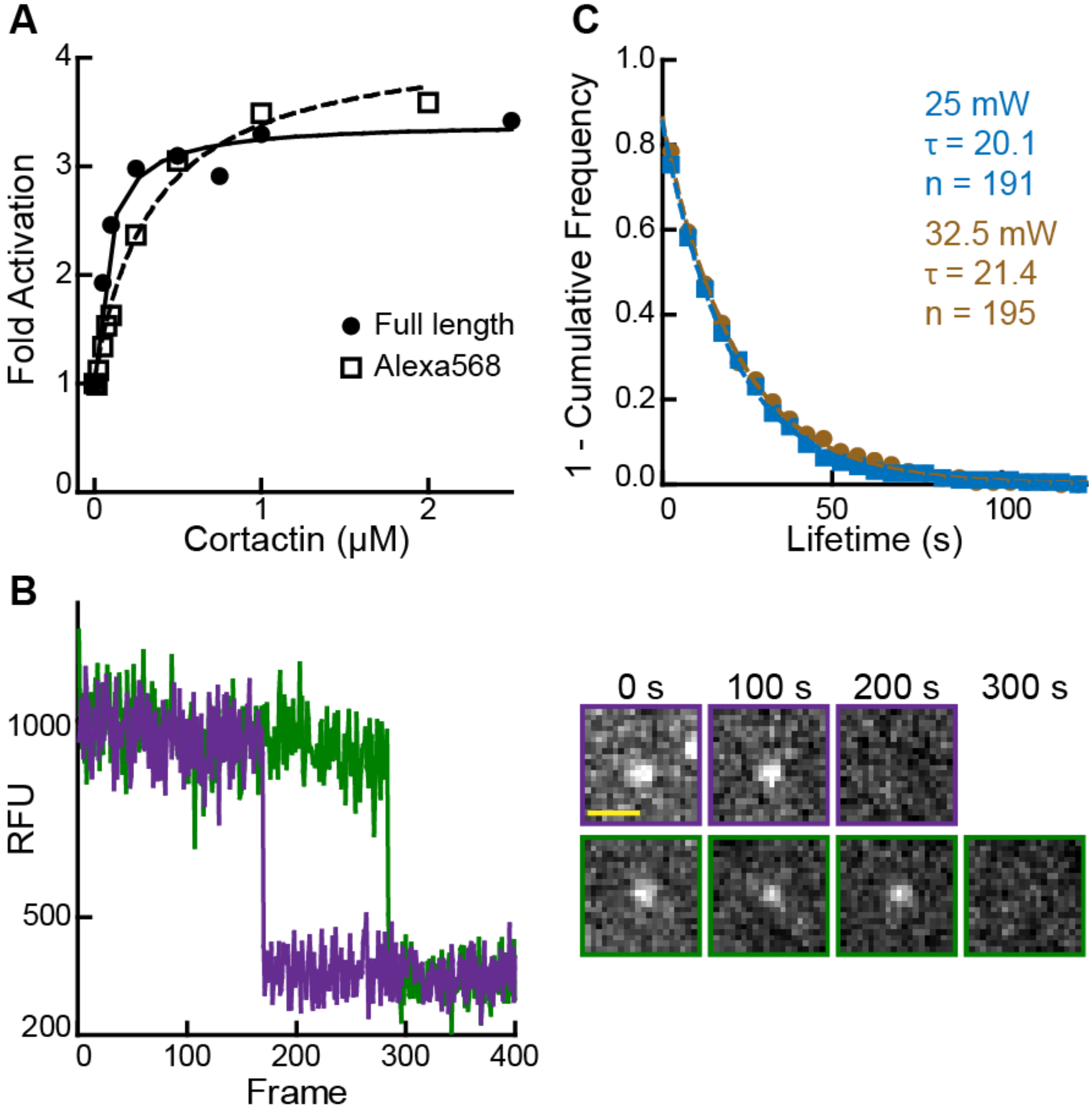

Video 1: Synergistic Activation of Arp2/3 Complex by GST-VCA and high Concentrations of Cortactin

Video corresponds to images in figure 2C. Reaction contains 1 µM 33% Oregon-Green actin, 10 nM Arp2/3 complex, 50 nM GST-VCA and 1 µM cortactin. Single-wavelength (488 nm) images were acquired at a final magnification of 100x with an exposure time of 100 ms and a frame rate of 1 fps (frames per second).

Video 2: Polymerizing Actin Filaments with Single Molecules of Cortactin Binding

Reaction contains 1 µM 33% Oregon-Green actin (green) and 2 nM Alexa568-cortactin (red). Images from both laser channels were acquired using a 50 ms exposure at a ratio of 5 561-channel images per 1 488-channel image (5:1) and a frame rate of 3.7 frames per second (fps) for the 561-channel and 1.6 fps for the 488-channel.

Video 3: Single Molecules of Cortactin Binding to Preformed Branch Junctions and Filament Sides

Preformed branched filament networks were created by polymerizing 1 µM 33% Oregon-Green actin (green), 5 nM Arp2/3 complex and 30 nM VCA for 6.4 minutes, then flowing into the reaction chamber buffer containing 1.5 nM Alexa568-cortactin (red) and 0.1 µM actin monomers. Out of focus frames (at ~1 s in video) represents when cortactin was flowed into the chamber. Each image from both channels was exposed for 50 ms at a 561:488 image ratio of 6:1. The calculated frame rate was 5 561-channel fps (3.3 when a 488-channel image was taken).

Video 4: Single Molecules of Cortactin Binding to Branching Networks

Reaction contains 1 µM 33% Oregon-green actin (green), 5 nM Arp2/3 complex, 50 nM VCA and 2 nM Alexa568-cortactin (red). 561- and 488-channel images were exposed for 50 ms and 30 ms, respectively, at a 561:488 image ratio of 8:1, with a frame rate of 5 fps for the 561-channel and 2.6 fps for the 488 channel.

Video 5: Single Molecule of Cortactin Binding to a Nascent Branch Junction

Visible in the video are nascent branch (left-center at 3 s), branch junction and filament side binding cortactin molecules. Reaction contents are the same as video 4.

Video 6: Single Molecule of NtA Binding to a Nascent Branch Junction

Reaction contains 1 µM 33% Oregon-Green actin (green), 10 nM Arp2/3 complex, 350 nM VCA and 10 nM Alexa568-NtA(1-48) (red). 561- and 488-channel images were exposed for 50 ms and 30 ms, respectively, at a 561:488 image ratio of 15:1, with a frame rate was 11 fps for the 561 channel and 1.7 fps for the 488-channel.

APPENDIX B

VIDEO LEGENDS FOR CHAPTER III

Video 1: TIRF microscopy video showing polymerization of 1.5 µM 33% Oregon-Green actin with 100 nM GST-N-WASP-VCA and 20 nM Arp2/3 complex. Images were acquired from 100 ms exposures every 5 seconds. Video playback is 20 frames per second (fps) corresponding to 100x real time and time stamps reference the start of the reaction.

Video 2: TIRF microscopy video showing polymerization of 1 µM 33% Oregon-Green actin, 500 nM Arp2/3 complex and 500 nM cortactin (residues 1-336). Images were acquired from 25 ms exposures every 1.4 seconds. Video playback is 20 fps corresponding to 28x real time and time stamps reference the start of the reaction.

Video 3: TIRF microscopy video with reaction conditions identical to video 2.

Video 4: TIRF microscopy video showing polymerization of 1 µM 33% Oregon-Green actin in the presence of 10 nM Arp2/3 complex, 50 nM GST-VCA and 1 µM cortactin. Images were acquired from 50 ms exposures every second. Video playback is 50 fps corresponding to 50x real time and time stamps reference the start of the reaction.

Video 5: TIRF microscopy video showing cortactin bundling parallel actin filaments. Reaction contains 1.5 µM 33% Oregon-Green actin (green, 488 nm channel) and 10 nM Alexa568-cortactin (magenta, 561 channel). Reactions were exposed for 50 ms at a ratio of 5 561-channel images per 1 488-channel image (5:1) at a rate of 3.6 images per second for the 561 and 0.6 images per second for the 488-channel. Video playback is 50 fps corresponding to 14x real time. The apparent frame offset comparing the movement of the Alexa-568 and Oregon-green 488 signals is due to the sequential acquisition of the two channels and the slower frame rate in the 488 channel.

Video 6: TIRF microscopy video showing cortactin bundling anti-parallel actin filaments. Reaction and image acquisition parameters are the same as video 5. Video playback is 20 fps corresponding to 5x real time. Orange and cyan arrowheads point to the two bundling filament barbed ends.

Video 7: TIRF microscopy video showing cortactin bundling filaments which have elongated into each other. Reaction and image acquisition parameters are the same as video 5. Video playback is 25 fps corresponding to 7x real time.

APPENDIX C

VIDEO LEGENDS FOR CHAPTER IV

Video 1: TIRF microscopy video showing Dip1-568 bound to an actin filament pointed end. Reaction contains 1 μM 33% Oregon-Green actin (green, 488 nm channel), 0.7 μM Arp2/3 complex and 2.5 nM Dip1-568 (magenta, 561 nm channel). Reactions were exposed for 50 ms at a ratio of 5 561-channel images per 488-channel image at a rate of 4 images per second for the 561-channel and 0.8 per second for the 488-channel.

Video 2: TIRF microscopy video showing Dip1-568 mediated nucleation of a linear filament. Reaction contains 1 μM 33% Oregon-Green actin (green, 488 nm channel), 0.5 μM Arp2/3 complex and 18 nM Dip1-568 (magenta, 561 nm channel). Reactions were exposed for 50 ms at a ratio of 6 561-channel images per 488-channel image at a rate of 5 images per second for the 561-channel and 0.8 per second for the 488-channel.

Video 3: TIRF microscopy video showing a Dip1-568 generated filament serving as a template for Wsp1-GST-VCA mediated branching. Reaction contains 1 μM 33% Oregon-Green actin (green, 488 nm channel), 0.5 μM Arp2/3 complex, 0.25 μM Wsp1-GST-VCA and 6 nM Dip1-568 (magenta, 561 nm channel). Reactions were exposed for 50 ms at a ratio of 6 561-channel images per 488-channel image at a rate of 5 images per second for the 561-channel and 1 per second for the 488-channel.

Video 4: TIRF microscopy video showing Dip1-568 mediated nucleation of a filament that serves as a template for branch nucleation by Wsp1-GST-VCA. Reaction contains 1 μM 33% Oregon-Green actin (green, 488 nm channel), 0.5 μM Arp2/3 complex, 0.25 μM Wsp1-GST-VCA and 6 nM Dip1-568 (magenta, 561 nm channel). Reactions were exposed for 50 ms at a ratio of 6 561-channel images per 488-channel image at a rate of 5 images per second for the 561-channel and 1 per second for the 488-channel.

REFERENCES CITED

Achard, Vérane, Jean-louis Martiel, Alphée Michelot, Christophe Guérin, Anne-Cécile Reymann, Laurent Blanchoin, and Rajaa Boujemaa-Paterski. 2010. “A ‘Primer’-Based Mechanism Underlies Branched Actin Filament Network Formation and Motility.” *Current Biology* 20 (5) (March): 423–8. doi:10.1016/j.cub.2009.12.056.

Akin, Orkun, and R Dyche Mullins. 2008. “Capping Protein Increases the Rate of Actin-Based Motility by Promoting Filament Nucleation by the Arp2/3 Complex.” *Cell* 133 (5) (May 30): 841–51. doi:10.1016/j.cell.2008.04.011.

Amann, Kurt J, and Thomas D Pollard. 2001. “Direct Real-Time Observation of Actin Filament Branching Mediated by Arp2/3 Complex Using Total Internal Reflection Fluorescence Microscopy.” *Proceedings of the National Academy of Sciences of the United States of America* 98 (26) (December): 15009–13. doi:10.1073/pnas.211556398.

Artym, Vira V, Ying Zhang, Françoise Seillier-Moiseiwitsch, Kenneth M Yamada, and Susette C Mueller. 2006. “Dynamic Interactions of Cortactin and Membrane Type 1 Matrix Metalloproteinase at Invadopodia: Defining the Stages of Invadopodia Formation and Function.” *Cancer Research* 66 (6) (March 15): 3034–43. doi:10.1158/0008-5472.CAN-05-2177.

Ayala, Inmaculada, Massimiliano Baldassarre, Giada Giacchetti, Giusi Caldieri, Stefano Tetè, Alberto Luini, and Roberto Buccione. 2008. “Multiple Regulatory Inputs Converge on Cortactin to Control Invadopodia Biogenesis and Extracellular Matrix Degradation.” *Journal of Cell Science* 121 (Pt 3) (February): 369–78. doi:10.1242/jcs.008037.

Basu, Roshni, and Fred Chang. 2011. “Characterization of dip1p Reveals a Switch in Arp2/3-Dependent Actin Assembly for Fission Yeast Endocytosis.” *Current Biology* 21 (11) (June 7): 905–16. doi:10.1016/j.cub.2011.04.047.

Beltzner, Christopher C, and Thomas D Pollard. 2008. “Pathway of Actin Filament Branch Formation by Arp2/3 Complex.” *The Journal of Biological Chemistry* 283 (11) (March): 7135–44. doi:10.1074/jbc.M705894200.

Bernheim-Groswasser, Anne, Sebastian Wiesner, Roy M Golsteyn, Marie-France Carlier, and Cécile Sykes. 2002. “The Dynamics of Actin-Based Motility Depend on Surface Parameters.” *Nature* 417 (6886) (May 16): 308–11. doi:10.1038/417308a.

Blanchoin, Laurent, Kurt J Amann, Henry N Higgs, Jean-Baptiste Marchand, Donald A Kaiser, and Thomas D Pollard. 2000. “Direct Observation of Dendritic Actin Filament Networks Nucleated by Arp2/3 Complex and WASP/Scar Proteins.” *Nature* 171 (1994): 1007–1011.

Blanchoin, Laurent, Rajaa Boujemaa-Paterski, Cécile Sykes, and Julie Plastino. 2014. “Actin Dynamics, Architecture, and Mechanics in Cell Motility.” *Physiological Reviews* 94 (1) (January): 235–63. doi:10.1152/physrev.00018.2013.

Blanchoin, Laurent, Thomas D Pollard, and S E Hitchcock-DeGregori. 2001. “Inhibition of the Arp2/3 Complex-Nucleated Actin Polymerization and Branch Formation by Tropomyosin.” *Current Biology : CB* 11 (16) (August 21): 1300–4.

Blanchoin, Laurent, Thomas D Pollard, and R Dyche Mullins. 2000. “Interactions of ADF/cofilin, Arp2/3 Complex, Capping Protein and Profilin in Remodeling of Branched Actin Filament Networks.” *Current Biology* 10 (20) (October 19): 1273–82.

Boczkowska, Malgorzata, Grzegorz Rebowski, David J. Kast, and Roberto Dominguez. 2014. “Structural Analysis of the Transitional State of Arp2/3 Complex Activation by Two Actin-Bound WCAs.” *Nature Communications* 5 (3308).

Boczkowska, Malgorzata, Grzegorz Rebowski, Maxim V Petoukhov, David B Hayes, Dmitri I Svergun, and Roberto Dominguez. 2008. “X-Ray Scattering Study of Activated Arp2/3 Complex with Bound Actin-WCA.” *Structure* 16 (5) (May): 695–704. doi:10.1016/j.str.2008.02.013.

Bowden, Emma T, Mara Barth, Dianne Thomas, Robert I Glazer, and Susette C Mueller. 1999. “An Invasion-Related Complex of Cortactin, Paxillin and PKCmu Associates with Invadopodia at Sites of Extracellular Matrix Degradation.” *Oncogene* 18 (31) (August 5): 4440–9. doi:10.1038/sj.onc.1202827.

Breitsprecher, Dennis, Richa Jaiswal, Jeffery P Bombardier, Christopher J Gould, Jeff Gelles, and Bruce L Goode. 2012. “Rocket Launcher Mechanism of Collaborative Actin Assembly Defined by Single-Molecule Imaging.” *Science* 336 (6085) (May 31): 1164–1168. doi:10.1126/science.1218062.

Bryce, Nicole S, Emily S Clark, Ja’Mes L Leysath, Joshua D Currie, Donna J Webb, and Alissa M Weaver. 2005. “Cortactin Promotes Cell Motility by Enhancing Lamellipodial Persistence.” *Current Biology* 15 (14) (July 26): 1276–85. doi:10.1016/j.cub.2005.06.043.

Cai, Liang, Alexander M Makhov, Dorothy a Schafer, and James E Bear. 2008. “Coronin 1B Antagonizes Cortactin and Remodels Arp2/3-Containing Actin Branches in Lamellipodia.” *Cell* 134 (5) (September): 828–42. doi:10.1016/j.cell.2008.06.054.

Campellone, Kenneth G, and Matthew D Welch. 2010. “A Nucleator Arms Race: Cellular Control of Actin Assembly.” *Nature Reviews Molecular Cell Biology* 11 (4) (April): 237–51. doi:10.1038/nrm2867.

Cao, Hong, James D Orth, Jing Chen, Weller Shaun, John E Heuser, and Mark A. McNiven. 2003. “Cortactin Is a Component of Clathrin-Coated Pits and Participates in Receptor-Mediated Endocytosis.” *Molecular and Cellular Biology* 23 (6): 2162–70. doi:10.1128/MCB.23.6.2162.

Chen, Qian, and Thomas D Pollard. 2013. “Actin Filament Severing by Cofilin Dismantles Actin Patches and Produces Mother Filaments for New Patches.” *Current Biology : CB* (May 29): 1–9. doi:10.1016/j.cub.2013.05.005.

Chen, Zhucheng, Dominika Borek, Shae B Padrick, Timothy S. Gomez, Zoltan Metlagel, Ayman M Ismail, Junko Umetani, Daniel D. Billadeau, Zbyszek Otwinowski, and Michael K Rosen. 2010. “Structure and Control of the Actin Regulatory WAVE Complex.” *Nature* 468 (7323) (November): 533–538. doi:10.1038/nature09623.

Chereau, David, Frederic Kerff, Philip Graceffa, Zenon Grabarek, Langsetmo Knut, and Roberto Dominguez. 2005. “Actin-Bound Structures of Wiskott–Aldrich Syndrome Protein (WASP)-Homology Domain 2 and the Implications for Filament Assembly.” *Proceedings of the National Academy of Sciences of the United States of America* 102 (46): 16644–49.

Chhabra, Ekta Seth, and Henry N Higgs. 2007. “The Many Faces of Actin: Matching Assembly Factors with Cellular Structures.” *Nature Cell Biology* 9 (10) (October): 1110–21. doi:10.1038/ncb1007-1110.

Co, Carl, Derek T Wong, Sarah Gierke, Vicky Chang, and Jack Taunton. 2007. “Mechanism of Actin Network Attachment to Moving Membranes: Barbed End Capture by N-WASP WH2 Domains.” *Cell* 128 (5) (March): 901–13. doi:10.1016/j.cell.2006.12.049.

Collins, Agnieszka, Anthony Warrington, Kenneth A Taylor, and Tatyana M Svitkina. 2011. “Structural Organization of the Actin Cytoskeleton at Sites of Clathrin-Mediated Endocytosis.” *Current Biology : CB* 21 (14) (July 26): 1167–75. doi:10.1016/j.cub.2011.05.048.

Cordes, Thorben, Jan Vogelsang, and Philip Tinnefeld. 2009. “On the Mechanism of Trolox as Antiblinking and Antibleaching Reagent.” *Journal of the American Chemical Society* 131 (14) (April 15): 5018–9. doi:10.1021/ja809117z.

Coutts, Amanda S, Louise Weston, and Nicholas B La Thangue. 2009. “A Transcription Co-Factor Integrates Cell Adhesion and Motility with the p53 Response.” *Proceedings of the National Academy of Sciences of the United States of America* 106 (47) (November 24): 19872–7. doi:10.1073/pnas.0906785106.

Cowieson, Nathan P, Gordon King, David Cookson, Ian Ross, Thomas Huber, David a Hume, Bostjan Kobe, and Jennifer L Martin. 2008. "Cortactin Adopts a Globular Conformation and Bundles Actin into Sheets." *The Journal of Biological Chemistry* 283 (23) (June): 16187–93. doi:10.1074/jbc.M708917200.

Dang, Irene, Roman Gorelik, Carla Sousa-Blin, Emmanuel Derivery, Christophe Guérin, Joern Linkner, Maria Nemethova, et al. 2013. "Inhibitory Signalling to the Arp2/3 Complex Steers Cell Migration." *Nature* 503 (7475) (November 14): 281–4. doi:10.1038/nature12611.

De La Cruz, Enrique M, Amber L Wells, Steven S Rosenfeld, E. Michael Ostap, and H Lee Sweeney. 1999. "The Kinetic Mechanism of Myosin V." *Proceedings of the National Academy of Sciences of the United States of America* 96 (24): 13726–13731.

Desmarais, Vera, Hideki Yamaguchi, Matthew Oser, Lilian Soon, Ghassan Mouneimne, Corina Sarmiento, Robert Eddy, and John Condeelis. 2009. "N-WASP and Cortactin Are Involved in Invadopodium-Dependent Chemotaxis to EGF in Breast Tumor Cells." *Cell Motility and the Cytoskeleton* 66 (6) (June): 303–16. doi:10.1002/cm.20361.

Destaing, Olivier, Frederic Saltel, Jean-christophe Geminard, Pierre Jurdic, and Frederic Bard. 2003. "Podosomes Display Actin Turnover and Dynamic Self- Organization in Osteoclasts Expressing Actin-Green Fluorescent Protein." *Molecular Biology of the Cell* 14 (February): 407–16. doi:10.1091/mbc.E02.

Didry, Dominique, Francois-Xavier Cantrelle, Clotilde Husson, Pierre Roblin, Anna M Eswara Moorthy, Javier Perez, Christophe Le Clainche, et al. 2011. "How a Single Residue in Individual Β-thymosin/WH2 Domains Controls Their Functions in Actin Assembly." *The EMBO Journal* 31 (4) (December 23): 1000–3013. doi:10.1038/emboj.2011.461.

Edelstein, Arthur, Nenad Amodaj, Karl Hoover, Ron Vale, and Nico Stuurman. 2010. "Computer Control of Microscopes Using µManager." *Current Protocols in Molecular Biology* Chapter 14 (October) (October): Unit14.20. doi:10.1002/0471142727.mb1420s92.

Eden, Sharon, Rajat Rohatgi, Alexandre V Podtelejnikov, Matthias Mann, and Marc W Kirschner. 2002. "Mechanism of Regulation of WAVE1-Induced Actin Nucleation by Rac1 and Nck." *Nature* 418 (August): 1–4.

Edwards, Marc, Adam Zwolak, Dorothy a Schafer, David Sept, Roberto Dominguez, and John a Cooper. 2014. "Capping Protein Regulators Fine-Tune Actin Assembly Dynamics." *Nature Reviews Molecular Cell Biology* (September) (September 10). doi:10.1038/nrm3869.

Egile, Coumaran, Isabelle Rouiller, Xiao-Ping Xu, Niels Volkmann, Rong Li, and Dorit Hanein. 2005. “Mechanism of Filament Nucleation and Branch Stability Revealed by the Structure of the Arp2/3 Complex at Actin Branch Junctions.” *PLoS Biology* 3 (11) (November): e383. doi:10.1371/journal.pbio.0030383.

Eisenmann, Kathryn M, Elizabeth S Harris, Susan M Kitchen, Holly a Holman, Henry N Higgs, and Arthur S Alberts. 2007. “Dia-Interacting Protein Modulates Formin-Mediated Actin Assembly at the Cell Cortex.” *Current Biology : CB* 17 (7) (April 3): 579–91. doi:10.1016/j.cub.2007.03.024.

Footer, Matthew J, John K Lyo, and Julie A Theriot. 2008. “Close Packing of Listeria Monocytogenes ActA, a Natively Unfolded Protein, Enhances F-Actin Assembly without Dimerization.” *The Journal of Biological Chemistry* 283 (35) (August 29): 23852–62. doi:10.1074/jbc.M803448200.

Galkin, Vitold E, Albina Orlova, William Brieher, Hao Yuan Kueh, Timothy J Mitchison, and Edward H Egelman. 2008. “Coronin-1A Stabilizes F-Actin by Bridging Adjacent Actin Protomers and Stapling Opposite Strands of the Actin Filament.” *Journal of Molecular Biology* 376 (3) (February): 607–13. doi:10.1016/j.jmb.2007.12.007.

Galletta, Brian J, Dennis Y Chuang, and John A Cooper. 2008. “Distinct Roles for Arp2/3 Regulators in Actin Assembly and Endocytosis.” *PLoS Biology* 6 (1) (January): e1. doi:10.1371/journal.pbio.0060001.

Gandhi, Meghal, Benjamin A Smith, Miia Bovellan, Ville Paavilainen, Karen Daugherty-Clarke, Jeff Gelles, Pekka Lappalainen, and Bruce L Goode. 2010. “GMF Is a Cofilin Homolog That Binds Arp2/3 Complex to Stimulate Filament Debranching and Inhibit Actin Nucleation.” *Current Biology* 20 (9) (May 11): 861–7. doi:10.1016/j.cub.2010.03.026.

Gaucher, Jean-Francois, Chloe Mauge, Dominique Didry, Bérengère Guichard, Louis Renault, and Marie-France Carlier. 2012. “Interactions of Isolated C-Terminal Fragments of Neural Wiskott-Aldrich Syndrome Protein (N-WASP) with Actin and Arp2/3 Complex.” *The Journal of Biological Chemistry* 287 (July 30): 34646–59. doi:10.1074/jbc.M112.394361.

Gohl, Christina, Daniel Banovic, Astrid Grevelhörster, and Sven Bogdan. 2010. “WAVE Forms Hetero- and Homo-Oligomeric Complexes at Integrin Junctions in Drosophila Visualized by Bimolecular Fluorescence Complementation.” *The Journal of Biological Chemistry* 285 (51) (December 17): 40171–9. doi:10.1074/jbc.M110.139337.

Goley, Erin D, Aravind Rammohan, Elizabeth A Znameroski, Elif Nur Firat-Karalar, David Sept, and Matthew D Welch. 2010. “An Actin-Filament-Binding Interface on the Arp2/3 Complex Is Critical for Nucleation and Branch Stability.” *Proceedings of the National Academy of Sciences of the United States of America* 107 (18) (May): 8159–64. doi:10.1073/pnas.0911668107.

Goley, Erin D, Stacia E Rodenbusch, Adam C Martin, and Matthew D Welch. 2004. “Critical Conformational Changes in the Arp2/3 Complex Are Induced by Nucleotide and Nucleation Promoting Factor.” *Molecular Cell* 16 (2) (October): 269–79. doi:10.1016/j.molcel.2004.09.018.

Goley, Erin D, and Matthew D Welch. 2006. “The ARP2/3 Complex: An Actin Nucleator Comes of Age.” *Nature Reviews Molecular Cell Biology* 7 (10): 713–726.

Goode, Bruce L, and Michael J Eck. 2007. “Mechanism and Function of Formins in the Control of Actin Assembly.” *Annual Review of Biochemistry* 76 (January): 593–627. doi:10.1146/annurev.biochem.75.103004.142647.

Goode, Bruce L, Avital A Rodal, Georjana Barnes, and David G Drubin. 2001. “Activation of the Arp2/3 Complex by the Actin Filament Binding Protein Abp1p.” *The Journal of Cell Biology* 153 (3) (April 30): 627–34.

Grassart, Alexandre, Vannary Meas-Yedid, Alexandre Dufour, Jean-Christophe Olivo-Marin, Alice Dautry-Varsat, and Nathalie Sauvonnet. 2010. “Pak1 Phosphorylation Enhances Cortactin-N-WASP Interaction in Clathrin-Caveolin-Independent Endocytosis.” *Traffic* 11 (8) (August): 1079–91. doi:10.1111/j.1600-0854.2010.01075.x.

Hansen, Scott D, and R Dyche Mullins. 2010. “VASP Is a Processive Actin Polymerase That Requires Monomeric Actin for Barbed End Association.” *The Journal of Cell Biology* 191 (3) (November 1): 571–84. doi:10.1083/jcb.201003014.

Haviv, Lior, Yifat Brill-karniely, Rachel Mahaffy, Frederic Backouche, Avinoam Ben-shaul, Thomas D Pollard, and Anne Bernheim-groswasser. 2006. “Reconstitution of the Transition from Lamellipodium to Filopodium in a Membrane-Free System.” *Proceedings of the National Academy of Sciences* 103 (13): 4906–4911.

Helgeson, Luke A, and Brad J Nolen. 2013. “Mechanism of Synergistic Activation of Arp2/3 Complex by Cortactin and N-WASP.” *eLife* 2 (September 3): e00884. doi:10.7554/eLife.00884.

Helgeson, Luke A, Julianna G Prendergast, Andrew R Wagner, Max Rodnick-Smith, and Brad J Nolen. 2014. “Interactions with Actin Monomers, Actin Filaments and Arp2/3 Complex Define the Roles of WASP Family Proteins and Cortactin in Coordinately Regulating Branched Actin Networks.” *The Journal of Biological Chemistry* 289 (42) (August 26): 28856–28869. doi:10.1074/jbc.M114.587527.

Hetrick, Byron, Min Suk Han, Luke A Helgeson, and Brad J Nolen. 2013. “Small Molecules CK-666 and CK-869 Inhibit Actin-Related Protein 2/3 Complex by Blocking an Activating Conformational Change.” *Chemistry & Biology* 20 (5) (April): 701–12. doi:10.1016/j.chembiol.2013.03.019.

Higgs, Henry N, Laurent Blanchoin, and Thomas D Pollard. 1999. “Influence of the C Terminus of Wiskott-Aldrich Syndrome Protein (WASp) and the Arp2/3 Complex on Actin Polymerization.” *Biochemistry* 38 (46) (November): 15212–22.

Higgs, Henry N, and Thomas D Pollard. 2000. “Activation by Cdc42 and PIP2 of Wiskott-Aldrich Syndrome Protein (WASp) Stimulates Actin Nucleation by Arp2/3 Complex.” *The Journal of Cell Biology* 150 (6): 1311–1320.

Higgs, Henry N, and Thomas D Pollard. 2001. “Regulation of Actin Filament Network Formation through ARP2/3 Complex: Activation by a Diverse Array of Proteins.” *Annual Review of Biochemistry* 70 (January): 649–76. doi:10.1146/annurev.biochem.70.1.649.

Hoops, Stefan, Sven Sahle, Ralph Gauges, Christine Lee, Jürgen Pahle, Natalia Simus, Mudita Singhal, Liang Xu, Pedro Mendes, and Ursula Kummer. 2006. “COPASI--a COmplex PAthway SImulator.” *Bioinformatics (Oxford, England)* 22 (24) (December 15): 3067–74. doi:10.1093/bioinformatics/btl485.

Huang, Cai, Yansong Ni, Tony Wang, Yamei Gao, Christian C. Haudenschild, and Xi Zhan. 1997. “Down-Regulation of the Filamentous Actin Cross-Linking Activity of Cortactin by Src-Mediated Tyrosine Phosphorylation.” *The Journal of Biological Chemistry* 272 (21) (May 23): 13911–5.

Hüfner, Katharina, Henry N Higgs, Thomas D Pollard, Christoph Jacobi, Martin Aepfelbacher, and Stefan Linder. 2001. “The Verprolin-like Central (vc) Region of Wiskott-Aldrich Syndrome Protein Induces Arp2/3 Complex-Dependent Actin Nucleation.” *Journal of Biological Chemistry* 276 (38): 35761–67. doi:10.1074/jbc.M106520200.

Kaksonen, Marko, H B Peng, and H Rauvala. 2000. “Association of Cortactin with Dynamic Actin in Lamellipodia and on Endosomal Vesicles.” *Journal of Cell Science* 113 (24) (December): 4421–6.

Kaksonen, Marko, Christopher P Toret, and David G Drubin. 2006. “Harnessing Actin Dynamics for Clathrin-Mediated Endocytosis.” *Nature Reviews. Molecular Cell Biology* 7 (6) (June): 404–14. doi:10.1038/nrm1940.

Katsube, Takanori, Shin Togashi, Naoko Hashimoto, Toshiaki Ogiu, and Hideo Tsuji. 2004. “Filamentous Actin Binding Ability of Cortactin Isoforms Is Responsible for Their Cell-Cell Junctional Localization in Epithelial Cells.” *Archives of Biochemistry and Biophysics* 427 (1) (July 1): 79–90. doi:10.1016/j.abb.2004.04.015.

Kelly, Alexander E, Heather Kranitz, Volker Dötsch, and R Dyche Mullins. 2006. “Actin Binding to the Central Domain of WASP/Scar Proteins Plays a Critical Role in the Activation of the Arp2/3 Complex.” *The Journal of Biological Chemistry* 281 (15) (April): 10589–97. doi:10.1074/jbc.M507470200.

Kim, Dae Joong, Sung Hyun Kim, Chol Seung, Kyu Yeong Choi, Chun Shik Park, Hwan Sung, Myeong Gu Yeo, Jin-kyu Kim, Woo Keun Song, and Sunghoe Chang. 2006. “Interaction of SPIN90 with the Arp2 / 3 Complex Mediates Lamellipodia and Actin Comet Tail Formation.” *The Journal of Biological Chemistry* 281 (1): 617–625. doi:10.1074/jbc.M504450200.

Kinley, Andrew W, Scott A Weed, Alissa M Weaver, Andrei V Karginov, Eric Bissonette, John A Cooper, and J Thomas Parsons. 2003. “Cortactin Interacts with WIP in Regulating Arp2/3 Activation and Membrane Protrusion.” *Current Biology* 13 (5) (March): 384–93.

Kirkbride, Kellye C, Bong Hwan Sung, Seema Sinha, and Alissa M Weaver. 2011. “Cortactin: A Multifunctional Regulator of Cellular Invasiveness.” *Cell Adhesion & Migration* 5 (2) (March 1): 187–198. doi:10.4161/cam.5.2.14773.

Kovács, Mihály, Judit Tóth, Csaba Hetényi, András Málnási-Csizmadia, and James R Sellers. 2004. “Mechanism of Blebbistatin Inhibition of Myosin II.” *The Journal of Biological Chemistry* 279 (34) (August 20): 35557–63. doi:10.1074/jbc.M405319200.

Kowalski, Jennifer R, Coumaran Egile, Susana Gil, Scott B Snapper, Rong Li, and Sheila M Thomas. 2005. “Cortactin Regulates Cell Migration through Activation of N-WASP.” *Journal of Cell Science* 118 (1) (January): 79–87. doi:10.1242/jcs.01586.

Krause, Matthias, and Alexis Gautreau. 2014. “Steering Cell Migration: Lamellipodium Dynamics and the Regulation of Directional Persistence.” *Nature Reviews Molecular Cell Biology* 15 (9) (August 22): 577–590. doi:10.1038/nrm3861.

Kuhn, Jeffrey R, and Thomas D Pollard. 2005. “Real-Time Measurements of Actin Filament Polymerization by Total Internal Reflection Fluorescence Microscopy.” *Biophysical Journal* 88 (2) (February): 1387–402. doi:10.1529/biophysj.104.047399.

Lagal, Vanessa, Marie Abrivard, Virginie Gonzalez, Audrey Perazzi, Sonam Popli, Elodie Verzeroli, and Isabelle Tardieux. 2014. “Spire-1 Contributes to the Invadosome and Its Associated Invasive Properties.” *Journal of Cell Science* 127 (Pt 2) (January 15): 328–40. doi:10.1242/jcs.130161.

Lai, Frank PL, Malgorzata Szczodrak, Jennifer Block, Jan Faix, Dennis Breitsprecher, Hans G Mannherz, Theresia EB Stradal, Graham A Dunn, J Victor Small, and Klemens Rottner. 2008. “Arp2/3 Complex Interactions and Actin Network Turnover in Lamellipodia.” *The EMBO Journal* 27 (7) (April 9): 982–92. doi:10.1038/emboj.2008.34.

Lee, Wei-lih, Magdalena Bezanilla, and Thomas D Pollard. 2001. “Fission Yeast Myosin-I , Myo1p , Stimulates Actin Assembly by Arp2/3 Complex and Shares Functions with WASp.” *The Journal of Cell Biology* 151 (4): 789–799.

Li, Ang, John C Dawson, Manuel Forero-Vargas, Heather J Spence, Xinzi Yu, Ireen König, Kurt Anderson, and Laura M Machesky. 2010. “The Actin-Bundling Protein Fascin Stabilizes Actin in Invadopodia and Potentiates Protrusive Invasion.” *Current Biology : CB* 20 (4) (February 23): 339–45. doi:10.1016/j.cub.2009.12.035.

Li, Pilong, Sudeep Banjade, Hui-Chun Cheng, Soyeon Kim, Baoyu Chen, Liang Guo, Marc Llaguno, et al. 2012. “Phase Transitions in the Assembly of Multivalent Signalling Proteins.” *Nature* 483 (7389) (March 7): 336–40. doi:10.1038/nature10879.

Liu, Su-Ling, Jordan R May, Luke A Helgeson, and Brad J Nolen. 2013. “Insertions within the Actin Core of Actin-Related Protein 3 (Arp3) Modulate Branching Nucleation by Arp2/3 Complex.” *The Journal of Biological Chemistry* 288 (1) (January 4): 487–97. doi:10.1074/jbc.M112.406744.

Liu, Su-Ling, Karen M Needham, Jordan R May, and Brad J Nolen. 2011. “Mechanism of a Concentration-Dependent Switch between Activation and Inhibition of Arp2/3 Complex by Coronin.” *The Journal of Biological Chemistry* 286 (19) (May 13): 17039–46. doi:10.1074/jbc.M111.219964.

Lorenz, Mike, Hideki Yamaguchi, Yarong Wang, Robert H Singer, and John Condeelis. 2004. “Imaging Sites of N-WASP Activity in Lamellipodia and Invadopodia of Carcinoma Cells.” *Current Biology* 14: 697–703. doi:10.1016/j.

Luan, Qing, and Brad J Nolen. 2013. “Structural Basis for Regulation of Arp2/3 Complex by GMF.” *Nature Structural & Molecular Biology* (July 28). doi:10.1038/nsmb.2628.

MacGrath, Stacey M, and Anthony J Koleske. 2012. “Arg/Abl2 Modulates the Affinity and Stoichiometry of Binding of Cortactin to F-Actin.” *Biochemistry* 51 (33): 6644–53. doi:10.1021/bi300722t.

Machesky, Laura M, and Robert H Insall. 1998. “Scar1 and the Related Wiskott-Aldrich Syndrome Protein, WASP, Regulate the Actin Cytoskeleton through the Arp2/3 Complex.” *Current Biology : CB* 8 (25): 1347–56.

Machesky, Laura M, R Dyche Mullins, Henry N Higgs, Donald A Kaiser, Laurent Blanchoin, R C May, M E Hall, and Thomas D Pollard. 1999. “Scar, a WASp-Related Protein, Activates Nucleation of Actin Filaments by the Arp2/3 Complex.” *Proceedings of the National Academy of Sciences of the United States of America* 96 (7) (March): 3739–44.

Mahaffy, Rachel E, and Thomas D Pollard. 2006. “Kinetics of the Formation and Dissociation of Actin Filament Branches Mediated by Arp2/3 Complex.” *Biophysical Journal* 91 (9) (November): 3519–28. doi:10.1529/biophysj.106.080937.

Marchand, Jean-Baptiste, Donald A Kaiser, Thomas D Pollard, and Henry N Higgs. 2001. “Interaction of WASP/Scar Proteins with Actin and Vertebrate Arp2/3 Complex.” *Nature Cell Biology* 3 (1) (January): 76–82. doi:10.1038/35050590.

Maritzen, Tanja, Tobias Zech, Michael R Schmidt, Eberhard Krause, Laura M Machesky, and Volker Haucke. 2012. “Gadkin Negatively Regulates Cell Spreading and Motility via Sequestration of the Actin-Nucleating ARP2/3 Complex.” *Proceedings of the National Academy of Sciences of the United States of America* 109 (26) (July 26): 10382–7. doi:10.1073/pnas.1206468109.

Martin, Adam C, Matthew D Welch, and David G Drubin. 2006. “Arp2/3 ATP Hydrolysis-Catalysed Branch Dissociation Is Critical for Endocytic Force Generation.” *Nature Cell Biology* 8 (8) (August): 826–33. doi:10.1038/ncb1443.

Martinez-Quiles, Narcisa, Hsin-Yi H Ho, Marc W Kirschner, Narayanaswamy Ramesh, and Raif S Geha. 2004. “Erk/Src Phosphorylation of Cortactin Acts as a Switch on-Switch off Mechanism That Controls Its Ability to Activate N-WASP.” *Molecular and Cellular Biology* 24 (12): 5269–80. doi:10.1128/MCB.24.12.5269.

Merrifield, Christien J, Britta Qualmann, Michael M Kessels, and Wolfhard Almers. 2004. “Neural Wiskott Aldrich Syndrome Protein (N-WASP) and the Arp2/3 Complex Are Recruited to Sites of Clathrin-Mediated Endocytosis in Cultured Fibroblasts.” *European Journal of Cell Biology* 83: 13–18.

Miki, Hiroaki, Shiro Suetsugu, and Tadaomi Takenawa. 1998. “WAVE, a Novel WASP-Family Protein Involved in Actin Reorganization Induced by Rac.” *The EMBO Journal* 17 (23) (December 1): 6932–41. doi:10.1093/emboj/17.23.6932.

Mizutani, Kiyohito, Hiroaki Miki, Hong He, Hiroshi Maruta, and Tadaomi Takenawa. 2002. “Essential Role of Neural Wiskott-Aldrich Syndrome Protein in Podosome Formation and Degradation of Extracellular Matrix in Src-Transformed Fibroblasts.” *Cancer Research* 62 (3) (February): 669–74.

Mooren, Olivia L, Brian J Galletta, and John A Cooper. 2012. “Roles for Actin Assembly in Endocytosis.” *Annual Review of Biochemistry* 81 (January): 661–86. doi:10.1146/annurev-biochem-060910-094416.

Mooren, Olivia L, Tatyana I Kotova, Andrew J Moore, and Dorothy A Schafer. 2009. “Dynamin2 GTPase and Cortactin Remodel Actin Filaments.” *The Journal of Biological Chemistry* 284 (36) (September): 23995–4005. doi:10.1074/jbc.M109.024398.

Mullins, R Dyche, John E Heuser, and Thomas D Pollard. 1998. “The Interaction of Arp2/3 Complex with Actin: Nucleation, High Affinity Pointed End Capping, and Formation of Branching Networks of Filaments.” *Proceedings of the National Academy of Sciences of the United States of America* 95 (11) (May 26): 6181–6.

Murphy, Danielle A, and Sara A Courtneidge. 2011. “The ‘Ins’ and ‘Outs’ of Podosomes and Invadopodia: Characteristics, Formation and Function.” *Nature Reviews Molecular Cell Biology* 12 (7) (June 23): 413–26. doi:10.1038/nrm3141.

Nolen, Brad J, and Thomas D Pollard. 2008. “Structure and Biochemical Properties of Fission Yeast ARP2/3 Complex Lacking the ARP2 Subunit.” *Journal of Biological Chemistry* 283 (39) (September 26): 26490. doi:10.1074/jbc.M802607200.

Nürnberg, Alexander, Thomas Kitzing, and Robert Grosse. 2011. “Nucleating Actin for Invasion.” *Nature Reviews Cancer* (February): 1–11. doi:10.1038/nrc3003.

Oser, Matthew, Hideki Yamaguchi, Christopher C Mader, J J Bravo-Cordero, Marianela Arias, Xiaoming Chen, Vera Desmarais, Jacco van Rheenen, Anthony J Koleske, and John Condeelis. 2009. “Cortactin Regulates Cofilin and N-WASp Activities to Control the Stages of Invadopodium Assembly and Maturation.” *The Journal of Cell Biology* 186 (4) (August): 571–87. doi:10.1083/jcb.200812176.

Padrick, Shae B, Hui-Chun Cheng, Ayman M Ismail, Sanjay C Panchal, Lynda K Doolittle, Soyeon Kim, Brian M Skehan, et al. 2008. “Hierarchical Regulation of WASP/WAVE Proteins.” *Molecular Cell* 32 (3) (November 7): 426–38. doi:10.1016/j.molcel.2008.10.012.

Padrick, Shae B, Lynda K Doolittle, Chad a Brautigam, David S King, and Michael K Rosen. 2011. “Arp2/3 Complex Is Bound and Activated by Two WASP Proteins.” *Proceedings of the National Academy of Sciences of the United States of America* 108 (33) (June 15): E472–E479. doi:10.1073/pnas.1100236108.

Padrick, Shae B, and Michael K Rosen. 2010. “Physical Mechanisms of Signal Integration by WASP Family Proteins.” *Annual Review of Biochemistry* 79 (January): 707–35. doi:10.1146/annurev.biochem.77.060407.135452.

Panchal, Sanjay C, Donald A Kaiser, Eduardo Torres, Thomas D Pollard, and Michael K Rosen. 2003. “A Conserved Amphipathic Helix in WASP/Scar Proteins Is Essential for Activation of Arp2/3 Complex.” *Nature Structural & Molecular Biology* 10 (8) (August): 591–8. doi:10.1038/nsb952.

Pant, Kiran, David Chereau, Victoria Hatch, Roberto Dominguez, and William Lehman. 2006. “Cortactin Binding to F-Actin Revealed by Electron Microscopy and 3D Reconstruction.” *Journal of Molecular Biology* 359 (4) (June): 840–7. doi:10.1016/j.jmb.2006.03.065.

Papp, Gábor, Beáta Bugyi, Zoltán Ujfalusi, Szilvia Barkó, Gábor Hild, Béla Somogyi, and Miklós Nyitrai. 2006. “Conformational Changes in Actin Filaments Induced by Formin Binding to the Barbed End.” *Biophysical Journal* 91 (7) (October 1): 2564–72. doi:10.1529/biophysj.106.087775.

Pollard, Thomas D. 1986. “Rate Constants for the Reactions of ATP- and ADP-Actin with the Ends of Actin Filaments.” *The Journal of Cell Biology* 103 (6 Pt 2) (December): 2747–54.

Pollard, Thomas D. 2007. “Regulation of Actin Filament Assembly by Arp2/3 Complex and Formins.” *Annual Review of Biophysics and Biomolecular Structure* 36 (January): 451–77. doi:10.1146/annurev.biophys.35.040405.101936.

Pollard, Thomas D, and Gary G Borisy. 2003. “Cellular Motility Driven by Assembly and Disassembly of Actin Filaments.” *Cell* 112 (4) (February): 453–65.

Pollard, Thomas D, and John A Cooper. 2009. “Actin, a Central Player in Cell Shape and Movement.” *Science* 326 (5957) (November): 1208–12. doi:10.1126/science.1175862.

Prehoda, Kenneth E, Jessica A Scott, R Dyche Mullins, and Wendell A Lim. 2000. “Integration of Multiple Signals Through Cooperative Regulation of the N-WASP-Arp2/3 Complex.” *Science* 290 (5492) (October 27): 801–806. doi:10.1126/science.290.5492.801.

Rebowski, Grzegorz, Suk Namgoong, Malgorzata Boczkowska, Paul C Leavis, Jorge Navaza, and Roberto Dominguez. 2010. “Structure of a Longitudinal Actin Dimer Assembled by Tandem W Domains - Implications for Actin Filament Nucleation.” *Journal of Molecular Biology* 403 (1) (August): 11–23. doi:10.1016/j.jmb.2010.08.040.

Robinson, Robert C, Kirsi Turbedsky, Donald A Kaiser, Jean-Baptiste Marchand, Henry N Higgs, Senyon Choe, and Thomas D Pollard. 2001. “Crystal Structure of Arp2/3 Complex.” *Science* 294 (5547) (November 23): 1679–84. doi:10.1126/science.1066333.

Rocca, Daniel L, Stéphane Martin, Emma L Jenkins, and Jonathan G Hanley. 2008. “Inhibition of Arp2/3-Mediated Actin Polymerization by PICK1 Regulates Neuronal Morphology and AMPA Receptor Endocytosis.” *Nature Cell Biology* 10 (3) (March): 259–71. doi:10.1038/ncb1688.

Rodal, Avital A, Lukasz Kozubowski, Bruce L Goode, David G Drubin, and John H Hartwig. 2005. “Actin and Septin Ultrastructures at the Budding Yeast Cell Cortex.” *Molecular Biology of the Cell* 16 (January): 372–384. doi:10.1091/mbc.E04.

Rogers, Stephen L, Ursula Wiedemann, Nico Stuurman, and Ronald D Vale. 2003. “Molecular Requirements for Actin-Based Lamella Formation in Drosophila S2 Cells.” *The Journal of Cell Biology* 162 (6) (September 15): 1079–88. doi:10.1083/jcb.200303023.

Rohatgi, Rajat, Le Ma, Hiroaki Miki, Marco Lopez, Tomas Kirchhausen, Tadaomi Takenawa, and Marc W Kirschner. 1999. “The Interaction between N-WASP and the Arp2/3 Complex Links Cdc42-Dependent Signals to Actin Assembly.” *Cell* 97 (2) (April 16): 221–31.

Rohatgi, Rajat, Peter Nollau, Hsin-Yi H Ho, Marc W Kirschner, and Bruce J Mayer. 2001. “Nck and Phosphatidylinositol 4,5-Bisphosphate Synergistically Activate Actin Polymerization through the N-WASP-Arp2/3 Pathway.” *The Journal of Biological Chemistry* 276 (28) (July 13): 26448–52. doi:10.1074/jbc.M103856200.

Rotty, Jeremy D, Congying Wu, and James E Bear. 2013. “New Insights into the Regulation and Cellular Functions of the ARP2/3 Complex.” *Nature Reviews. Molecular Cell Biology* 14 (1) (January 5): 7–12. doi:10.1038/nrm3492.

Rouiller, Isabelle, Xiao-Ping Xu, Kurt J Amann, Coumaran Egile, Stephan Nickell, Daniela Nicastro, Rong Li, Thomas D Pollard, Niels Volkmann, and Dorit Hanein. 2008. “The Structural Basis of Actin Filament Branching by the Arp2/3 Complex.” *The Journal of Cell Biology* 180 (5) (March): 887–95. doi:10.1083/jcb.200709092.

Sept, David, and J Andrew McCammon. 2001. “Thermodynamics and Kinetics of Actin Filament Nucleation.” *Biophysical Journal* 81 (2) (August): 667–74. doi:10.1016/S0006-3495(01)75731-1.

Shvetsov, Alexander, Emir Berkane, David Chereau, Roberto Dominguez, and Emil Reisler. 2009. “The Actin-Binding Domain of Cortactin Is Dynamic and Unstructured and Affects Lateral and Longitudinal Contacts in F-Actin.” *Cell Motility and the Cytoskeleton* 66 (2) (February): 90–8. doi:10.1002/cm.20328.

Sirotkin, Vladimir, Christopher C Beltzner, Jean-Baptiste Marchand, and Thomas D Pollard. 2005. “Interactions of WASp, Myosin-I, and Verprolin with Arp2/3 Complex during Actin Patch Assembly in Fission Yeast.” *The Journal of Cell Biology* 170 (4) (August 15): 637–48. doi:10.1083/jcb.200502053.

Sirotkin, Vladimir, Julien Berro, Keely Macmillan, Lindsey Zhao, and Thomas D Pollard. 2010. “Quantitative Analysis of the Mechanism of Endocytic Actin Patch Assembly and Disassembly in Fission Yeast.” *Molecular Biology of the Cell* 21 (16): 2894. doi:10.1091/mbc.E10.

Siton, Orit, Yaron Ideses, Shira Albeck, Tamar Unger, Alexander D Bershadsky, Nir S Gov, and Anne Bernheim-Groswasser. 2011. “Cortactin Releases the Brakes in Actin- Based Motility by Enhancing WASP-VCA Detachment from Arp2/3 Branches.” *Current Biology* 21 (24) (December): 2092–7. doi:10.1016/j.cub.2011.11.010.

Skau, Colleen T, David S Courson, Andrew J Bestul, Jonathan D Winkelman, Ronald S Rock, Vladimir Sirotkin, and David R Kovar. 2011. “Actin Filament Bundling by Fimbrin Is Important for Endocytosis, Cytokinesis, and Polarization in Fission Yeast.” *The Journal of Biological Chemistry* 286 (30) (July 29): 26964–77. doi:10.1074/jbc.M111.239004.

Smith, Benjamin A, Karen Daugherty-Clarke, Bruce L Goode, and Jeff Gelles. 2013. “Pathway of Actin Filament Branch Formation by Arp2/3 Complex Revealed by Single-Molecule Imaging.” *Proceedings of the National Academy of Sciences of the United States of America* 110 (4) (January 4): 1285–1290. doi:10.1073/pnas.1211164110.

Smith, Benjamin A, Shae B Padrick, Lynda K Doolittle, Karen Daugherty-Clarke, Ivan R Correa, Ming-Quan Xu, Bruce L Goode, Michael K Rosen, and Jeff Gelles. 2013. “Three-Color Single Molecule Imaging Shows WASP Detachment from Arp2/3 Complex Triggers Actin Filament Branch Formation.” *eLife* 2 (September 3): e01008. doi:10.7554/eLife.01008.

Stradal, Theresia E B, Klemens Rottner, Andrea Disanza, Stefano Confalonieri, Metello Innocenti, and Giorgio Scita. 2004. “Regulation of Actin Dynamics by WASP and WAVE Family Proteins.” *Trends in Cell Biology* 14 (6) (June): 303–11. doi:10.1016/j.tcb.2004.04.007.

Suetsugu, Shiro. 2013. “Activation of Nucleation Promoting Factors for Directional Actin Filament Elongation: Allosteric Regulation and Multimerization on the Membrane.” *Seminars in Cell & Developmental Biology* (February 1): 1–5. doi:10.1016/j.semcdb.2013.01.006.

Suetsugu, Shiro, Daisuke Yamazaki, Shusaku Kurisu, and Tadaomi Takenawa. 2003. “Differential Roles of WAVE1 and WAVE2 in Dorsal and Peripheral Ruffle Formation for Fibroblast Cell Migration.” *Developmental Cell* 5 (4) (October): 595–609. doi:10.1016/S1534-5807(03)00297-1.

Suraneni, Praveen, Boris Rubinstein, Jay R. Unruh, Michael Durnin, Dorit Hanein, and Rong Li. 2012. “The Arp2/3 Complex Is Required for Lamellipodia Extension and Directional Fibroblast Cell Migration.” *The Journal of Cell Biology* 197 (2) (April 9): 239–51. doi:10.1083/jcb.201112113.

Svitkina, Tatyana M, and Gary G Borisy. 1999. “Organization and Treadmilling of Actin Filament Array in Lamellipodia.” *The Journal of Cell Biology* 145 (5): 1009–26.

Takenawa, Tadaomi, and Shiro Suetsugu. 2007. “The WASP-WAVE Protein Network: Connecting the Membrane to the Cytoskeleton.” *Nature Reviews Molecular Cell Biology* 8 (1) (January): 37–48. doi:10.1038/nrm2069.

Taylor, Marcus J, David Perrais, and Christien J Merrifield. 2011. “A High Precision Survey of the Molecular Dynamics of Mammalian Clathrin-Mediated Endocytosis.” Edited by Sandra L. Schmid. *PLoS Biology* 9 (3) (March): e1000604. doi:10.1371/journal.pbio.1000604.

Tehrani, Shandiz, Roberta Faccio, Indra Chandrasekar, F Patrick Ross, and John A Cooper. 2006. “Cortactin Has an Essential and Specific Role in Osteoclast Actin Assembly.” *Molecular Biology of the Cell* 17 (July): 2882–95. doi:10.1091/mbc.E06.

Tehrani, Shandiz, Nenad Tomasevic, Scott A Weed, Roman Sakowicz, and John A Cooper. 2007. “Src Phosphorylation of Cortactin Enhances Actin Assembly.” *Proceedings of the National Academy of Sciences of the United States of America* 104: 11933–11938.

Ti, Shih-Chieh, Christopher T Jurgenson, Brad J Nolen, and Thomas D Pollard. 2011. “Structural and Biochemical Characterization of Two Binding Sites for Nucleation-Promoting Factor WASp-VCA on Arp2/3 Complex.” *Proceedings of the National Academy of Sciences of the United States of America* 108 (33) (June 15): E472–E479. doi:10.1073/pnas.1100125108.

Tojkander, Sari, Gergana Gateva, Galina Schevzov, Pirta Hotulainen, Perttu Naumanen, Claire Martin, Peter W Gunning, and Pekka Lappalainen. 2011. “A Molecular Pathway for Myosin II Recruitment to Stress Fibers.” *Current Biology : CB* 21 (7) (April 12): 539–50. doi:10.1016/j.cub.2011.03.007.

Ujfalusi, Zoltán, Andrea Vig, Gábor Hild, and Miklós Nyitrai. 2009. “Effect of Tropomyosin on Formin-Bound Actin Filaments.” *Biophysical Journal* 96 (1) (January): 162–8. doi:10.1529/biophysj.108.138420.

Uruno, Takehito, Jiali Liu, Yansong Li, Nicole Smith, and Xi Zhan. 2003. "Sequential Interaction of Actin-Related Proteins 2 and 3 (Arp2/3) Complex with Neural Wiscott-Aldrich Syndrome Protein (N-WASP) and Cortactin during Branched Actin Filament Network Formation." *The Journal of Biological Chemistry* 278 (28) (July): 26086–93. doi:10.1074/jbc.M301997200.

Uruno, Takehito, Jiali Liu, Peijun Zhang, Ying-xin Fan, Coumaran Egile, Rong Li, Susette C Mueller, and Xi Zhan. 2001. "Activation of Arp2/3 Complex-Mediated Actin Polymerization by Cortactin." *Nature Cell Biology* 3 (3): 259–266.

Van Oijen, Antoine M. 2011. "Single-Molecule Approaches to Characterizing Kinetics of Biomolecular Interactions." *Current Opinion in Biotechnology* 22 (1) (February): 75–80. doi:10.1016/j.copbio.2010.10.002.

Vignjevic, Danijela, Defne Yarar, Matthew D Welch, John Peloquin, Tatyana M Svitkina, and Gary G Borisy. 2003. "Formation of Filopodia-like Bundles in Vitro from a Dendritic Network." *The Journal of Cell Biology* 160 (6) (March 17): 951–62. doi:10.1083/jcb.200208059.

Volkmann, Niels, Kurt J Amann, Svetla Stoilova-McPhie, Coumaran Egile, Dirk C Winter, Larnele Hazelwood, John E Heuser, Rong Li, Thomas D Pollard, and Dorit Hanein. 2001. "Structure of Arp2/3 Complex in Its Activated State and in Actin Filament Branch Junctions." *Science* 293 (5539) (September 28): 2456–9. doi:10.1126/science.1063025.

Volkmann, Niels, Christopher Page, Rong Li, and Dorit Hanein. 2014. "Three-Dimensional Reconstructions of Actin Filaments Capped by Arp2/3 Complex." *European Journal of Cell Biology* (January 25): 1–5. doi:10.1016/j.ejcb.2014.01.003.

Wagner, Andrew R, Qing Luan, Su-Ling Liu, and Brad J Nolen. 2013. "Dip1 Defines a Class of Arp2/3 Complex Activators That Function without Preformed Actin Filaments." *Current Biology : CB* (October 8): 1–9. doi:10.1016/j.cub.2013.08.029.

Wang, Zhi-xin. 1995. "An Exact Mathematical Expression for Describing Competitive Binding of Two Different Ligands to a Protein Molecule." *FEBS Letters* 360: 111–14.

Weaver, Alissa M, John E Heuser, Andrei V Karginov, Wei-lih Lee, J Thomas Parsons, and John a Cooper. 2002. "Interaction of Cortactin and N-WASp with Arp2/3 Complex." *Current Biology* 12 (15): 1270–1278.

Weaver, Alissa M, Andrei V Karginov, Andrew W Kinley, Scott A Weed, Yan Li, J Thomas Parsons, and John A Cooper. 2001. "Cortactin Promotes and Stabilizes Arp2/3-Induced Actin Filament Network Formation." *Current Biology* 11 (5): 370–4.

Weed, Scott A, Andrei V Karginov, Dorothy A Schafer, Alissa M Weaver, Andrew W Kinley, John A Cooper, and J Thomas Parsons. 2000. "Cortactin Localization to Sites of Actin Assembly in Lamellipodia Requires Interactions with F-Actin and the Arp2/3 Complex." *The Journal of Cell Biology* 151 (1) (October): 29–40.

Wegner, Albrecht, and Klaus Ruhnau. 1988. "Rate of Binding of Tropomyosin to Actin Filaments." *Biochemistry* 27 (18) (September 6): 6994–7000.

Welch, Matthew D, Akihiro Iwamatsu, and Timothy J Mitchison. 1997. "Actin Polymerization Is Induced by Arp2/3 Protein Complex at the Surface of Listeria Monocytogenes." *Nature* 385: 265–268.

Winter, Dirk, Alexandre V. Podtelejnikov, Matthias Mann, and Rong Li. 1997. "The Complex Containing Actin-Related Proteins Arp2 and Arp3 Is Required for the Motility and Integrity of Yeast Actin Patches." *Current Biology* 7 (7) (July): 519–529. doi:10.1016/S0960-9822(06)00223-5.

Wu, Hong, and J Thomas Parsons. 1993. "Cortactin, an 80/85-Kilodalton pp60src Substrate, Is a Filamentous Actin-Binding Protein Enriched in the Cell Cortex." *The Journal of Cell Biology* 120 (6) (March): 1417–26.

Xu, Jingyuan, James F Casella, and Thomas D Pollard. 1999. "Effect of Capping Protein, CapZ, on the Length of Actin Filaments and Mechanical Properties of Actin Filament Networks." *Cell Motility and the Cytoskeleton* 42 (1) (January): 73–81. doi:10.1002/(SICI)1097-0169(1999)42:1<73::AID-CM7>3.0.CO;2-Z.

Xu, Xiao-Ping, Isabelle Rouiller, Brian D Slaughter, Coumaran Egile, Eldar Kim, Jay R Unruh, Xiaoxue Fan, et al. 2011. "Three-Dimensional Reconstructions of Arp2/3 Complex with Bound Nucleation Promoting Factors." *The EMBO Journal* 31 (September 20): 1–12. doi:10.1038/emboj.2011.343.

Yamada, Hiroshi, Tadashi Abe, Ayano Satoh, Nana Okazaki, Shota Tago, Kinue Kobayashi, Yumi Yoshida, et al. 2013. "Stabilization of Actin Bundles by a Dynamin 1/Cortactin Ring Complex Is Necessary for Growth Cone Filopodia." *Journal of Neuroscience* 33 (10) (March 6): 4514–26. doi:10.1523/JNEUROSCI.2762-12.2013.

Yamaguchi, Hideki, Mike Lorenz, Stephan Kempiak, Corina Sarmiento, Salvatore Coniglio, Marc Symons, Jeffrey Segall, et al. 2005. "Molecular Mechanisms of Invadopodium Formation: The Role of the N-WASP-Arp2/3 Complex Pathway and Cofilin." *The Journal of Cell Biology* 168 (3) (January 31): 441–52. doi:10.1083/jcb.200407076.

Yamaguchi, Hideki, Hiroaki Miki, S Suetsugu, L Ma, M W Kirschner, and Tadaomi Takenawa. 2000. “Two Tandem Verprolin Homology Domains Are Necessary for a Strong Activation of Arp2/3 Complex-Induced Actin Polymerization and Induction of Microspike Formation by N-WASP.” *Proceedings of the National Academy of Sciences of the United States of America* 97 (23) (November): 12631–6. doi:10.1073/pnas.190351397.

Young, Michael E, John a Cooper, and Paul C Bridgman. 2004. “Yeast Actin Patches Are Networks of Branched Actin Filaments.” *The Journal of Cell Biology* 166 (5) (August 30): 629–35. doi:10.1083/jcb.200404159.

Zuchero, J Bradley, Amanda S Coutts, Margot E Quinlan, Nicholas B La Thangue, and R Dyche Mullins. 2009. “p53-Cofactor JMY Is a Multifunctional Actin Nucleation Factor.” *Nature Cell Biology* 11 (4) (April): 451–9. doi:10.1038/ncb1852.